



Rational and Statistical Approaches in Enhancing Yield Of Ethylene Carbonate in Urea Transesterification with Ethylene Glycol

Dina Fakhrnasova

ADVERTIMENT. L'accés als continguts d'aquesta tesi doctoral i la seva utilització ha de respectar els drets de la persona autora. Pot ser utilitzada per a consulta o estudi personal, així com en activitats o materials d'investigació i docència en els termes establerts a l'art. 32 del Text Refós de la Llei de Propietat Intel·lectual (RDL 1/1996). Per altres utilitzacions es requereix l'autorització prèvia i expressa de la persona autora. En qualsevol cas, en la utilització dels seus continguts caldrà indicar de forma clara el nom i cognoms de la persona autora i el títol de la tesi doctoral. No s'autoritza la seva reproducció o altres formes d'explotació efectuades amb finalitats de lucre ni la seva comunicació pública des d'un lloc aliè al servei TDX. Tampoc s'autoritza la presentació del seu contingut en una finestra o marc aliè a TDX (framing). Aquesta reserva de drets afecta tant als continguts de la tesi com als seus resums i índexs.

ADVERTENCIA. El acceso a los contenidos de esta tesis doctoral y su utilización debe respetar los derechos de la persona autora. Puede ser utilizada para consulta o estudio personal, así como en actividades o materiales de investigación y docencia en los términos establecidos en el art. 32 del Texto Refundido de la Ley de Propiedad Intelectual (RDL 1/1996). Para otros usos se requiere la autorización previa y expresa de la persona autora. En cualquier caso, en la utilización de sus contenidos se deberá indicar de forma clara el nombre y apellidos de la persona autora y el título de la tesis doctoral. No se autoriza su reproducción u otras formas de explotación efectuadas con fines lucrativos ni su comunicación pública desde un sitio ajeno al servicio TDR. Tampoco se autoriza la presentación de su contenido en una ventana o marco ajeno a TDR (framing). Esta reserva de derechos afecta tanto al contenido de la tesis como a sus resúmenes e índices.

WARNING. Access to the contents of this doctoral thesis and its use must respect the rights of the author. It can be used for reference or private study, as well as research and learning activities or materials in the terms established by the 32nd article of the Spanish Consolidated Copyright Act (RDL 1/1996). Express and previous authorization of the author is required for any other uses. In any case, when using its content, full name of the author and title of the thesis must be clearly indicated. Reproduction or other forms of for profit use or public communication from outside TDX service is not allowed. Presentation of its content in a window or frame external to TDX (framing) is not authorized either. These rights affect both the content of the thesis and its abstracts and indexes.

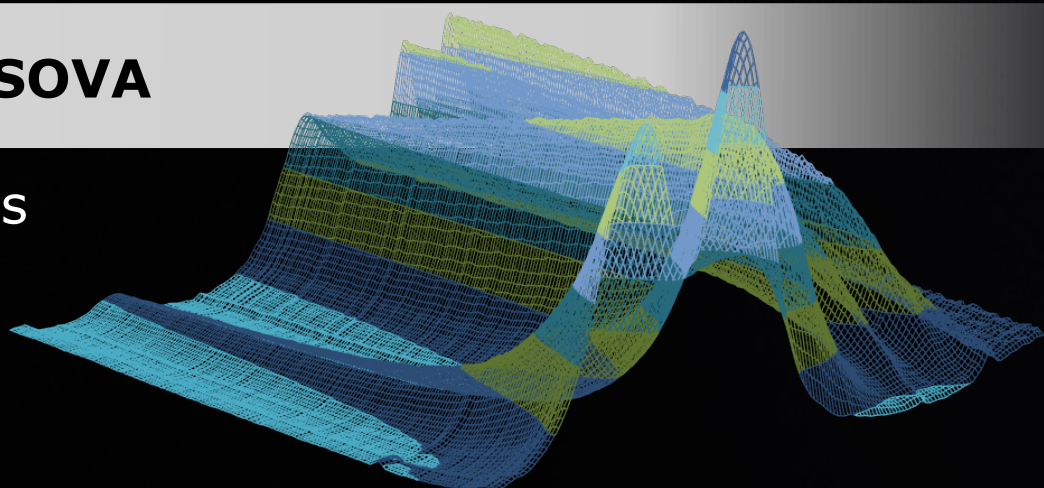
Rational and Statistical Approaches in Enhancing Yield of Ethylene Carbonate in Urea Transesterification with Ethylene Glycol



**UNIVERSITAT
ROVIRA I VIRGILI**

DINA FAKHRNASOVA

Doctoral Thesis
2016



DOCTORAL THESIS

**Rational and Statistical Approaches in Enhancing Yield of
Ethylene Carbonate in Urea Transesterification with Ethylene
Glycol**

DINA FAKHRNASOVA

Supervised by:

Dr. Atsushi Urakawa

ICIQ-URV

Dr. Ricardo J. Chimentão

URV

Prof. Francisco Medina

URV



Tarragona

2016

UNIVERSITAT ROVIRA I VIRGILI
Rational and Statistical Approaches in Enhancing Yield
Of Ethylene Carbonate in Urea Transesterification with Ethylene Glycol
Dina Fakhrnasova



UNIVERSITAT ROVIRA I VIRGILI



I STATE that the present study, entitled “Rational and statistical approaches in enhancing yield of ethylene carbonate in urea transesterification with ethylene glycol”, presented by Dina Fakhrnasova for the award of the degree of Doctor, has been carried out under my supervision at the Department of Chemical Engineering (DEQ) of this university and at the group of Dr. Urakawa of ICIQ.

Tarragona, 11th January 2016

Doctoral Thesis Supervisors

Dr. Atsushi Urakawa

Dr. Ricardo J. Chimentão

Prof. Francisco Medina

Acknowledgement

First of all I would like to acknowledge my main thesis supervisor, Prof. Francisco Medina, for the opportunity to join his research group CATHETER where I made my first steps in doctoral study. I would like to express my sincere gratitude to the former CATHETER member Dr. Ricardo Chimentão accompanying and guiding me in my research journey. I am deeply grateful for his support and care not only in my professional but also in the personal life. The greatest acknowledge I would like to express to Dr. Atsushi Urakawa who gave me opportunity to continue my doctoral study in collaboration with his research group in ICIQ and has been supervising me by providing research guidance over four years. I will always remain thankful for his immense support, motivation, demanding a high quality of work in all my endeavours, expert knowledge and patience. Without his supervision and constant help this thesis work would not have been possible.

I am very grateful to all the scientific and non-scientific staff from ICIQ for facilitating my research work. I am indebted to members of Chemical Reaction Technologies Unit and especially to Dr. Marta Giménez for her support and help with very sensitive and sometimes naughty equipment that I was dealing with. I am also thankful to Dr. Miguel Gonzalez from Heterogeneous Catalysis Unit for his expertise and help with analytical equipment of his lab. I would like to acknowledge Jose Luis Leon from the Mechanical Workshop for making my research experiments happen. Special thanks to Aurora for her assistance in administrative tasks during my stay and visits of Tarragona.

I would like to express my gratitude to all the members of CATHETER group who welcomed me and greatly supported my initial stage of doctoral study. I am sincerely grateful to people in Urakawa research group, who created

incredible atmosphere in the lab and made me believe that research can be fun. Greatest thanks to pioneers of the group: Atul, Antonio and Jordi. Thank you for taking care of your “little sister”, helping to survive in the lab and making me smile in tough situations. I am also very grateful to colleagues who joined the group later: Dragos, Sergio, Rohit, Marta, Muralidhar, Yi, Andrea and many other former members and visiting students. Thanks to your assistance and friendship I will always keep warm memories of my PhD life.

I must thank my friends from Russian community in Tarragona: Andrei, Sasha, Maria, Evgeny and many others for their priceless support and encouragement during my PhD time. Thanks for believing in me and for unforgettable times in Tarragona.

Me gustaría agradecer a mis amigos de En Dantza y la escuela de idiomas por acompañarme en mi vida social aparte del doctorado.

Ich bedanke mich bei meinen Kollegen von Dow für die Unterstützung und der Hilfe bei meiner Dissertation.

Отдельные слова благодарности моим русскоговорящим друзьям во всех уголках мира за поддержку и мотивацию, а так же моим родителям и брату за веру в меня.

I would like to acknowledge ICIQ and URV for supporting this doctoral work in the form of ICIQ-URV fellowship and Ministry of Economy and Competitiveness (MINECO) for financial support (CTQ2012-34153) and support through Severo Ochoa Excellence Accreditation 2014-2018 (SEV-2013-0319).



UNIVERSITAT ROVIRA I VIRGILI



UNIVERSITAT ROVIRA I VIRGILI
Rational and Statistical Approaches in Enhancing Yield
Of Ethylene Carbonate in Urea Transesterification with Ethylene Glycol
Dina Fakhrnasova

Table of Contents

1 Introduction	1
1.1 Linear and cyclic organic carbonates	2
1.1.1 DMC – highly demanded linear organic carbonate	2
1.1.2 Cyclic carbonates: A building block for DMC production	4
1.2 Transesterification of urea with EG: State of the art	8
1.2.1 Reaction products and pathway	8
1.2.2 Reaction conditions	9
1.2.2.1 Time	10
1.2.2.2 Temperature	10
1.2.2.3 Pressure	10
1.2.2.4 Feed composition and catalyst loading	11
1.2.3 Catalysts and active sites	11
1.2.4 Reaction mechanism	13
1.3 Acid-base catalysis: choice of the materials and precursors	14
1.3.1 LDH structure of precursors	14
1.3.2 Metal cations in the layers	15
1.3.3 Interlamellar anions	16
1.4 Rational and statistical approaches in enhancing EC synthesis	17
1.4.1 <i>In situ</i> reaction monitoring by attenuated total reflection (ATR)-IR dip-in probe	18
1.4.2 <i>In situ</i> ATR-IR study of catalytic solid-liquid interfaces	20
1.4.3 Multivariate Curve Resolution (MCR)	22
1.4.4 Design of Experiments (DoE)	24

1.5 Aim and overview of the thesis: enhance of EC synthesis	26
References	28
2 Methods.....	33
2.1 Catalyst preparation	34
2.2 <i>In situ</i> reaction monitoring by ATR-IR spectroscopy.....	35
2.2.1 Reaction setup	35
2.2.2 Time-resolved spectra.....	37
2.3 Multivariate Curve Resolution (MCR) analysis	39
2.3.1 Basic theory of MCR	39
2.3.2 Component spectra and component concentrations	41
2.4 Kinetic study	42
References	44
3. Catalyst Characterization.....	45
3.1 Introduction.....	46
3.2 Experimental section	47
3.3 Results and discussion.....	48
3.3.1 XRD.....	48
3.3.1.1 Hydrotalcite precursors for mixed metal oxides.....	48
3.3.1.2 Single metal oxides and hydrotalcite-derived mixed metal oxides.....	49
3.3.2 Textural property	51
3.3.3 CO ₂ - and NH ₃ -TPD.....	52

3.3.4 DRIFTS characterization of surface acidity and basicity	54
3.3.4.1 Pyridine adsorption	54
3.3.4.2 CO ₂ adsorption.....	58
3.4 Conclusions.....	60
References	61
4 Understanding the Role of Acidic and Basic Sites	63
4.1 Introduction.....	64
4.2 Experimenta section.....	64
4.3 Results and discussion.....	65
4.3.1 Catalytic test of overall reaction.....	65
4.3.2 Separate study of reaction paths.....	69
4.3.2.1 Reaction of urea with EG	69
4.3.2.2 Reaction of EC with EG	72
4.3.2.3 Reaction of 2-Ox with EG.....	76
4.3.2.4 Reaction of 2-HC with EG	80
4.3.3 Role of acidic and basic sites in urea transesterification of EG	84
4.4 Conclusions.....	88
References	91
5 Catalyst Tuning and New Materilas	93
5.1 Introduction.....	94
5.2 Experimental section	95
5.2.1 Catalyst synthesis	95
5.2.2 Catalyst characterization	96

5.2.3 Catalytic test.....	96
5.3 Results and discussion.....	97
5.3.1 Mixed metal oxides.....	97
5.3.1.1 Catalyst characterization.....	97
5.3.1.2 Catalytic test.....	101
5.3.2 Y-zeolites.....	104
5.3.2.1 Catalyst characterization.....	104
5.3.2.2 Catalytic test.....	106
5.3.3 Na-Y zeolite supported ZnO.....	107
5.3.3.1 Catalyst characterization.....	107
5.3.3.2 Catalytic test.....	109
5.4 Conclusions.....	110
References.....	111
6 Design of Experiments (DoE).....	113
6.1 Introduction.....	114
6.2 Methods.....	114
6.2.1 Screening experimental design.....	114
6.2.2 Optimization experimental design.....	116
6.3 Results and discussion.....	117
6.3.1 Screening experimental designs.....	117

6.3.2 Optimization experimental design	120
6.4 Conclusions.....	124
References	126
7 Static and Transient <i>In situ</i> ATR-IR Study of Activation	
Mechanism.....	127
7.1 Introduction.....	128
7.2 Experimental section	129
7.2.1 Catalyst and experimental setup	129
7.2.2 <i>In situ</i> static experiment.....	131
7.2.3 <i>In situ</i> transient experiment	131
7.2.4 Data treatment.....	131
7.3 Results and discussion.....	132
7.3.1 Urea activation	132
7.3.1.1 <i>In situ</i> static experiment: Urea adsorption over single and mixed metal oxides	132
7.3.1.2 <i>In situ</i> transient experiment: Urea activation over single and mixed metal oxides	136
7.3.1.3 Mechanism of urea activation.....	141
7.3.2 2-HC activation.....	143
7.3.2.1 <i>In situ</i> static experiment: 2-HC adsorption over mixed and metal oxides.....	143
7.3.2.2 <i>In situ</i> transient experiment: 2-HC active species and intermediates	145
7.3.2.3 Mechanism of 2-HC activation and correlation with acid- base properties of catalyst	148

7.4 Conclusions.....	150
References.....	152
8 Summary and Outlook.....	155
8.1 Summary.....	156
8.2 Outlook.....	158
References.....	163
Appendix A Supplementary Information of Chapter 4.....	165
Figure A1. Concentration profiles of urea transesterification in the presence of Zn-Fe.....	166
Table A1. Reaction rate constant k values.....	168
Figure A2. Concentration profiles of urea transesterification after fitting procedure.....	169
Publications and Conference Contributions.....	171
Curriculum Vitae.....	173

Chapter 1

Introduction

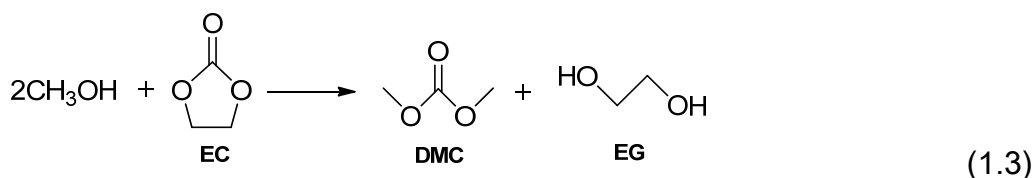
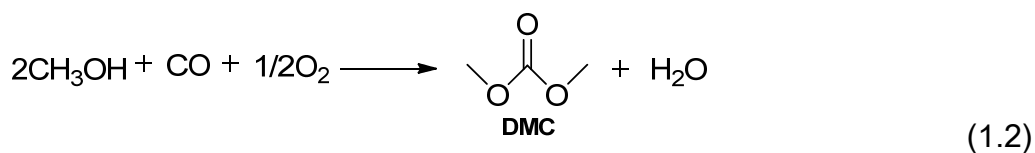
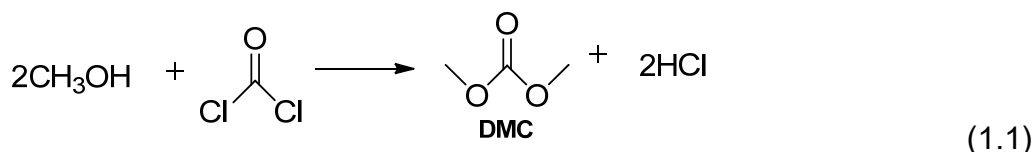
1.1 Linear and cyclic organic carbonates

Recently organic carbonates are widely used in various fields. As final products, organic carbonates are commonly used as solvents for coating [1], varnish [2] and chemical reactions [3] and also as lubricants [4] and electrolytes in lithium-ion batteries [5]. As intermediates, organic carbonates find their application in the production of pharmaceuticals [6], agrochemicals and polymers [7]. The use of organic carbonates for the production of polymers is expected to expand in the near future, resulting in a recent large increase in their demand in the world market [8]. In the energy sector, marked expansion of demands is also expected as fuel additives since fuels can give better combustion performance and reduction in soot emissions upon blending with organic carbonates [9]. For such global applications, the demands are estimated in the range of several tons to megatons per year.

1.1.1 DMC – highly demanded linear organic carbonate

Dimethyl carbonate (DMC) is one of the most produced organic carbonates. DMC exhibits environmentally and ecologically favourable chemical properties such as low toxicity, an absence of any irritant or mutagenic effects, and high biodegradability [10]. Demand of DMC is continuously rising; in 2005 the worldwide consumption of DMC was about 100,000 tons, with production concentrated mainly in the United States, Europe and Japan. Nowadays, DMC manufacturing is expanding rapidly in other countries, mainly in China exceeding a production capacity of 250,000 tons per year [11].

Traditionally DMC is produced by the reaction of phosgene with methanol (Equation 1.1), however this route is currently being replaced by alternative non-phosgene technologies such as oxidative carbonylation of methanol and transesterification of cyclic carbonates, assisting to increase DMC production volume (Equations 1.2-1.3).



The oxidative carbonylation of methanol (Equation 1.2) was introduced on an industrial scale during the early 1980s by EniChem [12]. Later, during the 1990s, Ube Industries Ltd (Japan) developed a variation on the basis of two-stage process. Both processes present several drawbacks due to the procedure and reactants used. The EniChem process is based on the liquid-phase oxidative carbonylation of methanol in the presence of CuCl_2 as catalyst. Even though DMC selectivity is higher than 95%, the by-product water may deactivate the catalyst. Additional constraints are the use of homogeneous catalyst and related corrosion problems. On the other hand, the gas-phase reactor technology implemented by Ube Industries utilizes a heterogeneous catalyst based on PdCl_2 supported on active carbon. The selectivity to DMC is in the range of 90–95%. Nonetheless both processes require handling of toxic and hazardous reactants.

The latter process (Equation 1.3), which was introduced by Asahi Kasei [13] in the early 2000s, is based on the transesterification between methanol and ethylene carbonate. Using proper reactor design, thermodynamic equilibrium can be shifted and complete conversion of ethylene carbonate achieved, resulting in 99.5% yield of DMC and ethylene glycol (EG). The process is capable of supplying DMC as well as EG to the market. This multistep technology brings additional demand for cyclic organic carbonates (e.g. EC) as they are required for DMC synthesis, pushing further development of new technologies for cyclic organic carbonates production.

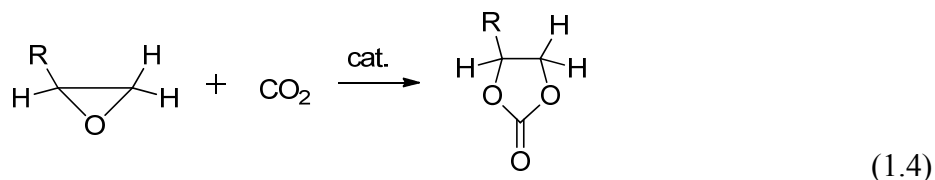
1.1.2 Cyclic carbonates: A building block for DMC production

Cyclic carbonates such as ethylene carbonate (EC), propylene carbonate (PC) have been commercially available for over 40 years [14]. Since their commercialization in the mid-1950s, they have found numerous applications as both are reactive intermediates [15] and inert solvents [16]. Current production of cyclic carbonates (excluding their use as unisolated intermediates) is around 100,000 tons per year. New plants are currently being constructed to meet increasing demands [17].

Similarly to linear carbonates, cyclic carbonates can be synthesized from diols with phosgene [18]. However, a substitute for phosgene is highly sought after because of its highly toxic and corrosive nature. On the other hand, CO₂ is safe (non-toxic and non-flammable), economical and abundant reagent. Therefore more attractive methods of organic carbonate synthesis involve the use of CO₂ and offer a way to utilize the latter [8]. Such reactions are, for example, direct carboxylation of epoxides, oxidative carboxylation of olefins, and reaction of carbon dioxide with diols and transesterification of diols using urea as an indirect source of CO₂ as described below more in detail.

Carboxylation of epoxides

The conventional method to produce cyclic carbonates nowadays is carboxylation of epoxides (Equation 1.4) [19].

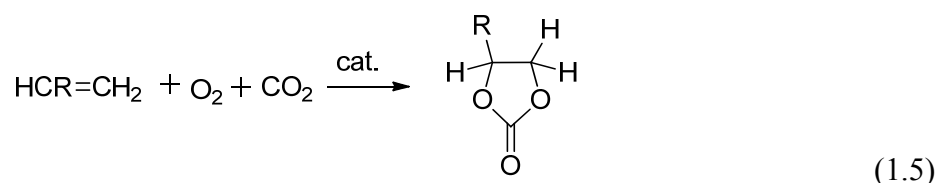


A large number of catalyst systems have been developed for this reaction, including alkali metal salts, ammonium salts, ionic liquids, metal oxides, transition metal and main group complexes [20]. However, these catalysts typically suffer from drawbacks such as the need of high concentration of the catalyst, co-solvent (amides: DMF, DAA), or the requirement of high pressure (up to 5 MPa of CO₂)

and/or high temperature (up to 370-400 K). Moreover, homogeneous catalysts are disadvantageous in terms of catalyst separation. The exploration of highly efficient heterogeneous catalysts under the conditions of low temperature and low carbon dioxide pressure remains a great challenge.

Oxidative carboxylation of olefins

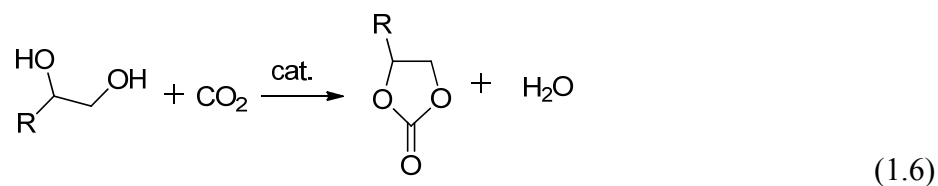
As an alternative to direct utilization of carbon dioxide the oxidative carboxylation of olefins (Equation 1.5) appears as very interesting approach to synthesize cyclic carbonates starting from cheap and easily available reagents [21].



The direct oxidative carboxylation of olefins has a great potential and has many advantages. First, it does not require carbon dioxide free of oxygen. This feature makes it attractive because of the high purification cost of carbon dioxide, which may discourage its use. Above all, the main advantage is that the reaction couples two reaction processes, the epoxidation of the olefins and the carbonation of the epoxides. This approach also avoids the isolation of the (often toxic) epoxide. However, the method faces several technological challenges such as short lifetime (1-3 h) of catalysts, low turnover number (TON) and low reaction selectivity (max. 50%) [21b, 22].

Reaction between carbon dioxide and diols

Another route for synthesis of cyclic carbonates was recently reported from diols and carbon dioxide (Equation 1.6) [23].



Ceria-based catalysts [24] and $\text{CeO}_2\text{-ZrO}_2$ [25] solid solution catalysts have been reported to be very efficient for the synthesis of EC and PC by the reaction of CO_2 with EG and propylene glycol (PG), respectively.

However, great challenges remain; the thermodynamics of this reaction is not favorable and coproduced water may induce modification or deactivation of the catalyst with negative effects on the conversion rate. Different metallic acetates [26] have been used in acetonitrile, which acts not only as solvent but also as dehydrating agent to eliminate the effect of the water produced during the reaction. In this way, the thermodynamic equilibrium is shifted and the yield of cyclic carbonates was improved; however, reaction with addition of acetonitrile cannot be considered as low-toxic process.

Reaction of urea and diols (transesterification)

A thermodynamically favorable approach for the synthesis of cyclic carbonates is to convert CO_2 into urea and use the latter for the reaction with diols (transesterification). This process is advantageous since it allows not only producing valuable cyclic carbonate by the indirect CO_2 utilization but also DMC can be obtained by further reaction of those with methanol in a more economically beneficial way (Figure 1.1).

Moreover, if urea production plant and a DMC plant are integrated, then the whole facility takes mainly CO_2 and methanol as feeds and produces DMC and cyclic carbonates as intermediates via the process (Figure 1.1).

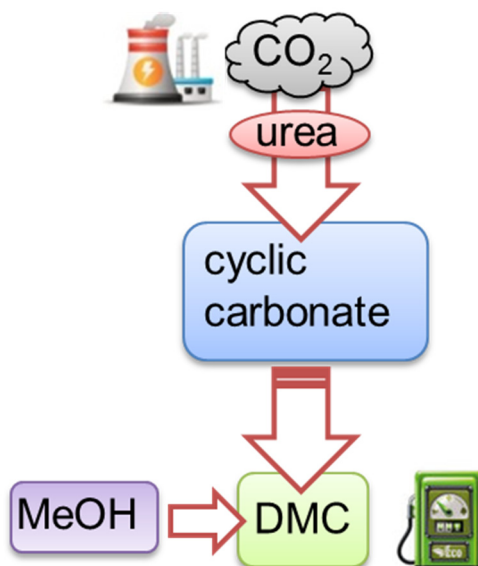
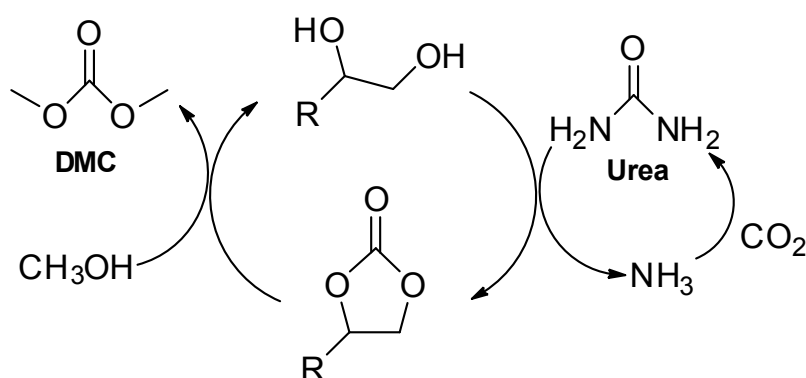


Figure 1.1. Synthesis of DMC by indirect CO₂ utilization.

Detailed reaction network of DMC production through cyclic organic carbonate synthesized by reaction of urea transesterification with diols is shown on the Scheme 1.1. The advantage of the process is that the by-product, e.g. EG or PG, may be further reacted with urea to produce cyclic organic carbonate which is used as starting material for the synthesis of DMC. As the demand of DMC is rising greater than the demand of diols, utilization of the latter has positive economic impact on the production of DMC. Another advantage mentioned previously is that released ammonia can be recycled to produce urea by reaction with CO₂ (typically at 112-207 atm and 433-513 K [27]) so that the overall process forms a greener chemical cycle.



Scheme 1.1. Urea transesterification with diols as a way to produce DMC.

For the DMC synthesis in this route, any cyclic carbonate can be used in principle. Among them, EC is the most attractive due to the market consideration of corresponding diol (EG) and to the fact that production and demands of EG are higher than those of PG and other diols. As of 2013, the global PG production exceeded 2.18 million tons [28], whereas the global market volume for EG was 16.51 million tons. Moreover, market of EG expands rapidly and is expected to reach 22.81 million tons by 2020, estimated with a Compound Annual Growth Rate (CAGR) of 4.7% from 2014 to 2020 [29].

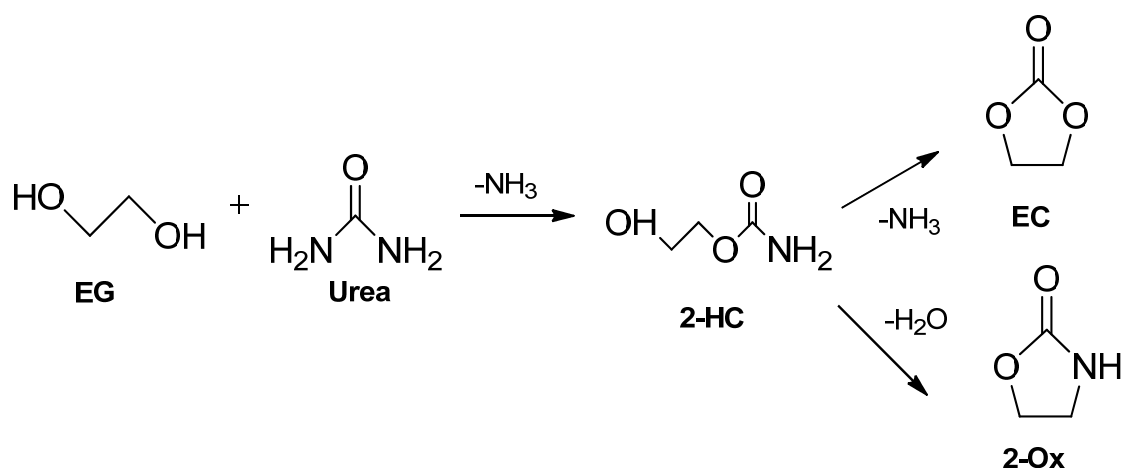
Therefore we have selected EG as an abundant and easily available diol to produce corresponding cyclic organic carbonate, EC, in the aim to be used for further processing such as DMC synthesis. Also due to the advantages shown above, this work focuses on the reaction path of urea transesterification with EG to produce EC.

1.2 Transesterification of urea with EG: State of the art

Knowledge from literature on critical parameters influencing EC synthesis via transesterification of urea with EG such as time, temperature, amount of catalyst and feed composition as well as reaction products and proposed reaction mechanisms is described below.

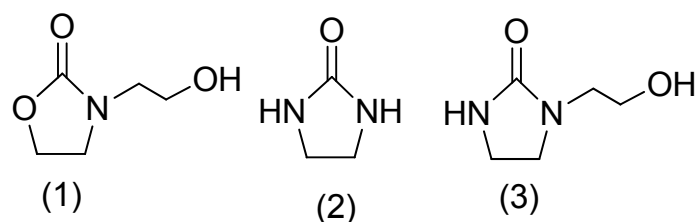
1.2.1 Reaction products and pathway

Transesterification of urea is known to proceed in a consecutive two-step reaction which involves rapid conversion of urea into an intermediate product, 2-hydroxyethyl carbamate (2-HC), with further formation of EC by release of ammonia from 2-HC (Scheme 1.2). The side reaction occurs via a dehydration reaction of 2-HC to form 2-oxazolidone (2-Ox) (Scheme 1.2) [30].



Scheme 1.2. Urea transesterification with EG.

Besides these products, Bhanage et al. [31] reported the formation of (1) *N*-(2-hydroxyethyl)-2-oxazolidone and (2) ethyleneurea. Moreover, if the reaction mixture contains EC, 2-Ox and EG in sufficient amount another side product (3) *N*-(2-hydroxyethyl)-2-imidazolidone can be formed [31].



Insights into the reaction pathway were brought by Zhao et al [30]. Applying *in situ* ATR-IR monitoring of liquid solution during EC synthesis they concluded that the synthesis of 2-HC from EG and urea is a fast reaction, and the rate-limiting step of EC synthesis is the elimination of an ammonia molecule from 2-HC to give EC. Still, chemical components present in the reaction mixture, their evolution with the time, and the role of catalytic sites remain unclarified.

1.2.2 Reaction conditions

Factors known to have significant impacts on the catalytic performance (time, temperature, pressure, feed composition and catalyst loading) are summarized below.

1.2.2.1 Time

Earlier it was described that the synthesis of EC via urea transesterification with EG is not a simple direct reaction, and undergoes an intermediate step (2-HC, Scheme 1.2). For this consecutive nature of the reaction, residence time is an important factor influencing EC selectivity and yield.

The conversion of urea as well as EC yield increase with the prolonged reaction time, but the change was not significant after about 3 h [30, 32]. Even it may affect negatively, as proposed by some authors due to the hydrolysis of EC to EG and carbon dioxide [33].

1.2.2.2 Temperature

From the reported reaction pathways (Scheme 1.2) it is also obvious that EC is not the only product and a certain reaction temperature may favour one pathway to the others.

When the temperature was raised up to 423 K, the urea conversion and EC selectivity were improved. However, the EC yield decreased when the reaction temperature was further raised as the result of fast decomposition of urea to ammonia and CO₂ [32, 34]. The transformation of 2-HC as well as 2-Ox selectivity were also promoted by increased temperature. Therefore, it is very important to optimize reaction temperature to reach good conversion rates at high EC selectivity and avoid side products formation.

1.2.2.3 Pressure

From thermodynamic point of view the reaction between urea and EG is limited by equilibrium, and produced ammonia should be removed in order to shift the equilibrium towards the products. For this reason, the reaction is commonly performed either under reduced pressure [31-32, 34-35] or in the continuous flow of inert gas [30].

1.2.2.4 Feed composition and catalyst loading

Other important aspects are feed composition and catalyst loading. For example, the highest yield of EC was achieved when EG was in large excess (urea/EG molar ratio around 1:8) [30]. Some authors also investigated the influence of catalyst amount on EC synthesis [30, 34]. It was found that increase in the catalyst amount can enhance EG conversion but only up to a certain degree. The optimum catalyst loading in the reaction system has been reported to be 1.5 wt%. A higher catalyst loading resulted in a lower EC yield possibly owing to the hydrolysis of EC.

Optimal reaction conditions according to literature are summarized in Table 1.1.

Table 1.1. Reported optimal reaction conditions for EC synthesis via urea transesterification of EG.

	Reaction condition			Reference
	Temperature / K	Time / min	Urea/EG Pressure / kPa	
423	180	1/1.5	11	[32]
423	150	1/6	atm., N ₂ flow	[30]
423	180	1/1.35	3	[31]
423	120	1/1.5	Vacuum	[34]
423	180	1/1.5	8	[35]

1.2.3 Catalysts and active sites

Various catalysts, mainly metal oxides, have been tested in urea transesterification, however it is important to note that the reaction can proceed in the absence of the catalyst, giving low EG conversion and EC yield [32].

First catalytic materials for urea transesterification with glycols were reported by Su and Speranza [36]. They found out that in the presence of Sn-

based catalyst conversion of PG was 43% with the PC yield and selectivity of 36 and 84%, respectively. However, decomposition of urea was severe. Doya et al. [37] have described a synthesis method of alkylene carbonates from alkylene glycols and urea under reduced pressure using zinc, magnesium and lead oxides, or their mixtures as catalysts and reported EC yield as high as 92.6%. Ball et al. [38] concluded that the combination of a weak Lewis acid and a Lewis base could improve the carbonate formation. Later Li et al. [32, 39] examined a series of metal oxide catalysts such as CaO, La₂O₃, MgO, ZnO, ZrO₂, and Al₂O₃ and found that amphoteric ZnO showed the highest catalytic activity and the yield of EC reached 93.1%. The catalytic performance was deteriorated for basic oxides with stronger basic sites whereas acidic oxides did not show reasonable activity. An identical conclusion was drawn by Bhanage [31]. Bhadauria [34] studied Cr-containing zinc oxide materials while Zhao [30] investigated Fe-containing ones. In both studies the formation of the spinel phases (ZnCr₂O₄ and ZnFe₂O₄) was found to be important, promoting EC yield. Table 1.2 summarizes catalysts with excellent catalytic performance for EC synthesis via urea transesterification with EG. All the previous works hinted that a proper balance in the amount and nature of acidic and basic sites is important; however, their roles in each reaction step and in the overall reaction performance, i.e. yield of EC, have been unclarified to date.

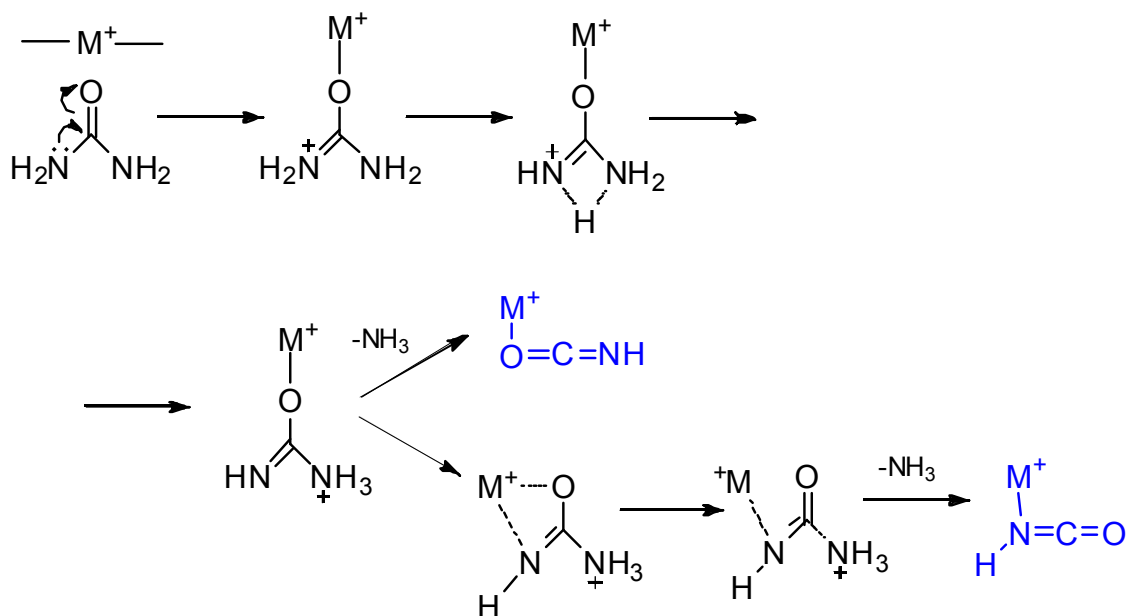
Table 1.2. Reported remarkable catalytic performance for EC synthesis via urea transesterification with EG.

Catalyst	Y(EC) / %	S(EC) / %	X(urea) / %	Reference
ZnO	31.1	97.1	97.8	[32]
Zn/Fe	66.1	-	-	[30]
ZnO	-	98	100	[31]
ZnO·Cr ₂ O ₃	59.9	-	-	[34]
Zn _N /Y	-	98	96	[35]

1.2.4 Reaction mechanism

Some attempts have been made to investigate how urea reacts with active sites of the catalysts and types of active species produced as a result of this interaction, proposing the mechanism of transesterification.

Li [32] studied interaction of solid urea with metal oxides and observed formation of isocyanate species ($\text{N}=\text{C}=\text{O}$) over some metal oxides and concluded that the formation of active species was promoted by the catalysts with appropriate density and strength of acid sites. Later, focusing on reaction between urea and PG, a reaction mechanism (Scheme 1.3) was proposed with urea activation through carbonyl group with further transformation into intermediate and PC [39]. Other researchers investigated glycerol-urea system [40] and have drawn a similar conclusion that Lewis acid sites activate the carbonyl group of urea, so that it will become more prone to the nucleophilic attack of the glycerol adsorbed on the Lewis basic site.



Scheme 1.3. Mechanism of urea activation via formation of isocyanate species proposed by Li [39].

1.3 Acid-base catalysis: Choice of the materials and precursors

As described above, the previous studies indicated that a catalyst with balanced acid-base sites is important for the EC synthesis via urea transesterification with EG. The proper balance could be achieved by mixing metal oxides with distinct acid-base properties, such as oxides containing metals Zn, Mg, Al, Fe, La, and Ca. To synthesise catalysts with high surface area, well dispersed and/or mixed acid and basic sites, and fine-tunability of comprising chemical elements, mixed-metal oxides synthesis via layered double hydroxides (LDHs) precursor has been selected as the choice of catalyst synthesis method in this thesis work.

The term LDH is used to designate synthetic or natural lamellar hydroxides with two kinds of metallic cations in the main layers and interlayer domains containing anionic species [41]. This broad family of compounds is also referred to as anionic clays whose interlamellar domains contain cationic species. LDHs are also reported as hydrotalcite-like compounds by reference to one of the polytypes of the corresponding Mg-Al based mineral.

1.3.1 LDH structure

The LDH structure is based on $M(OH)_6$ octahedral units sharing edges in order to build $M(OH)_2$ brucite-like layers. These octahedral units contain both bivalent and trivalent metallic cations; the main layers are therefore positively charged, and the charge density is proportional to the trivalent metal ratio $x = M^{III}/(M^{II}+M^{III})$. The whole structure is constituted by the stacking of such layers, intercalating charge-balancing anionic species and water molecules as shown in Figure 1.2 with the general formula $[M^{II}_{1-x}M^{III}_x(OH)_2]^{x+} [A_{x/n}]^{n-} \cdot mH_2O$. After

calcination the LDH structure is destroyed with formation of solid solution of mixed oxides.

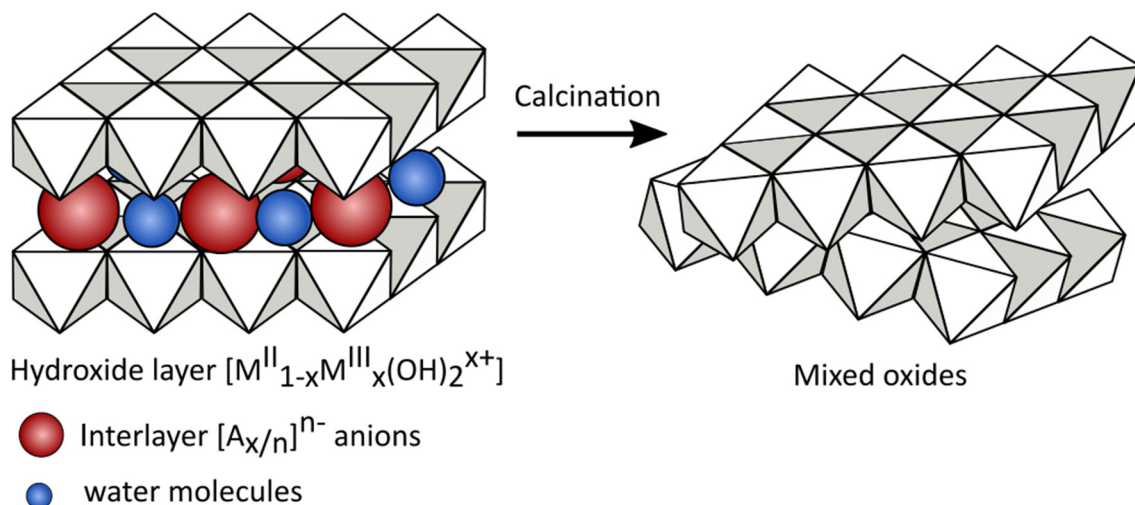


Figure 1.2. Structure of layered double hydroxide (LDH) before and after calcination.

1.3.2 Metal cations in the layers

Large variety of hydrotalcite-like compounds can be obtained by varying the identity and relative proportions of bivalent and trivalent cations (having ionic radius not so different to that of Mg^{2+}) in the layer as well as the nature of the interlayer anion. Moreover, many ternary LDHs involving mixtures of different M^{II} and/or M^{III} cations can also be prepared and even quaternary LDHs have been reported [42]. The bivalent and trivalent cations found in LDHs belong mainly to the third and fourth period of the periodic classification of the elements:

- bivalent cations: Mg, Mn, Fe, Co, Ni, Cu, Zn
- trivalent cations: Al, Mn, Fe, Co, Ni, Cr, Ga

In fact the range of materials synthesized as LDH is even larger than suggested. The evidence of materials containing monovalent lithium and having similar structure has been reported [43]. Although possible incorporation of tetravalent ions into the LDH layer is controversial, a number of papers have reported the possibility of synthesizing LDHs containing M^{IV} ions [44].

The combination of metal cations which can be introduced in LDH layers is displayed in Figure 1.3.

		bivalent cations								
		M ^{III} /M ^{II}	Mg	Fe	Co	Ni	Cu	Zn	Ca	Li
trivalent cations	Al									
	Cr									
	Fe									
	Co									
	Ni									
	Ga									
	V									
	Ti									

Figure 1.3. Combination of bivalent and trivalent metallic cations in LDHs [45].

1.3.3 Interlamellar anions

In LDHs, the interlamellar domains contain anions, water molecules and sometimes other neutral or charged moieties. Only weak bonding occurs between these interlamellar ions or molecules and the host structure. A great variety of anionic species can therefore be located between the layers during the formation of the lamellar structure, or by further anionic exchange.

These anions can be, for example:

- halides: fluoride, chloride
- oxo-anions: carbonate, nitrate, sulphate, bromate
- oxo and polyoxo-metallates: chromate, dichromate, $(\text{Mo}_7\text{O}_{24})^{6-}$, $(\text{V}_{10}\text{O}_{28})^{6-}$
- anionic complexes: ferro and ferricyanide, $(\text{PdCl}_4)^{2-}$
- organic anions: carboxylates, phosphonates, alkyl sulfates

Therefore, LDHs (or hydrotalcites) can be used as precursors to synthesize a variety of mixed oxides materials by subsequent controlled thermal decomposition. The thermal decomposition of LDH materials leads to a well dispersed mixture of oxides which have typically higher specific surface areas ($100\text{--}300\text{ m}^2\cdot\text{g}^{-1}$) than those observed in the parent LDH material. Acid-base properties of obtained mixed metal oxides can be tuned by changing the calcination temperature, the nature and amount of structural cations and also of the anions which are compensating the positive charge, as well as the preparative method [46]. Furthermore, these mixed metal oxides can have synergistic effects between the elements and the possibility of structural reconstruction under mild conditions, all of which are very important possible attributes for catalysts.

1.4 Rational and statistical approaches in enhancing EC synthesis

According to the knowledge available in the literature as discussed above, selective production of EC with high yield via transesterification of urea with EG requires proper selection of catalytic material and optimal reaction conditions. The complexity of the reaction and the lack in solid understanding of the roles of acid-base sites in EC synthesis make improvement of the catalytic performance highly empirical using classical approaches to study catalytic reactions.

This thesis work employs two approaches largely unexplored to date for such a complex reaction – rational and statistical ones – which have great potential in enhancing EC synthesis. By rational approach it is meant that, insights into reaction network and kinetics are gained and correlated to catalytic properties and reaction conditions to effectively optimize critical parameters influencing the reaction performance. Using statistical approach mathematical models of the reaction are created taking reaction conditions as parameters and

optimum reaction conditions are mathematically predicted. The exact approaches taken are briefly described below.

1.4.1 *In situ* reaction monitoring by attenuated total reflection (ATR)-IR dip-in probe

To study a reaction taking place in solution using heterogeneous catalyst, the fundamentally important steps are to identify all reaction products, determine reaction pathways and know kinetics of the comprising reaction process. The common method for this is off-line sample analysis. The major difficulty with this method is that the reaction solution contains catalyst solids, and samples must be accordingly treated before the off-line analysis. The treatment increases risks of potential transformation or degradation of the sample if reaction components are unstable or sensitive. Additionally, off-line monitoring is often time-consuming and cost-demanding. Also, it may not be always safe since samples can be toxic or not easy to handle.

In situ reaction monitoring is nondestructive analysis performed at reaction conditions, which prevents risks of above-mentioned problems with sample treatment and increases efficiency of the analysis. It can also provide highly valuable data with respect to process optimization [47]. This statement is especially true for time-resolved spectroscopic *in situ* techniques, which allow gaining insights into evolution of chemical species, shedding light on mechanistic aspects.

The attenuated total reflection (ATR) infra-red (IR) spectroscopy using a dip-in probe is used in a wide range of applications and recently it has been proven to be a useful tool for real-time monitoring and *in situ* studies of liquid phase reactions under working conditions [48].

Such *in situ* monitoring is performed by immersing the ATR-IR probe directly into the reaction mixture (Figure 1.4) As mentioned before such analysis

eliminates steps of workup of samples prior to analysis [49]. Obtained time-resolved spectra (Figure 1.4) carry information of temporal evolution of individual chemical components.

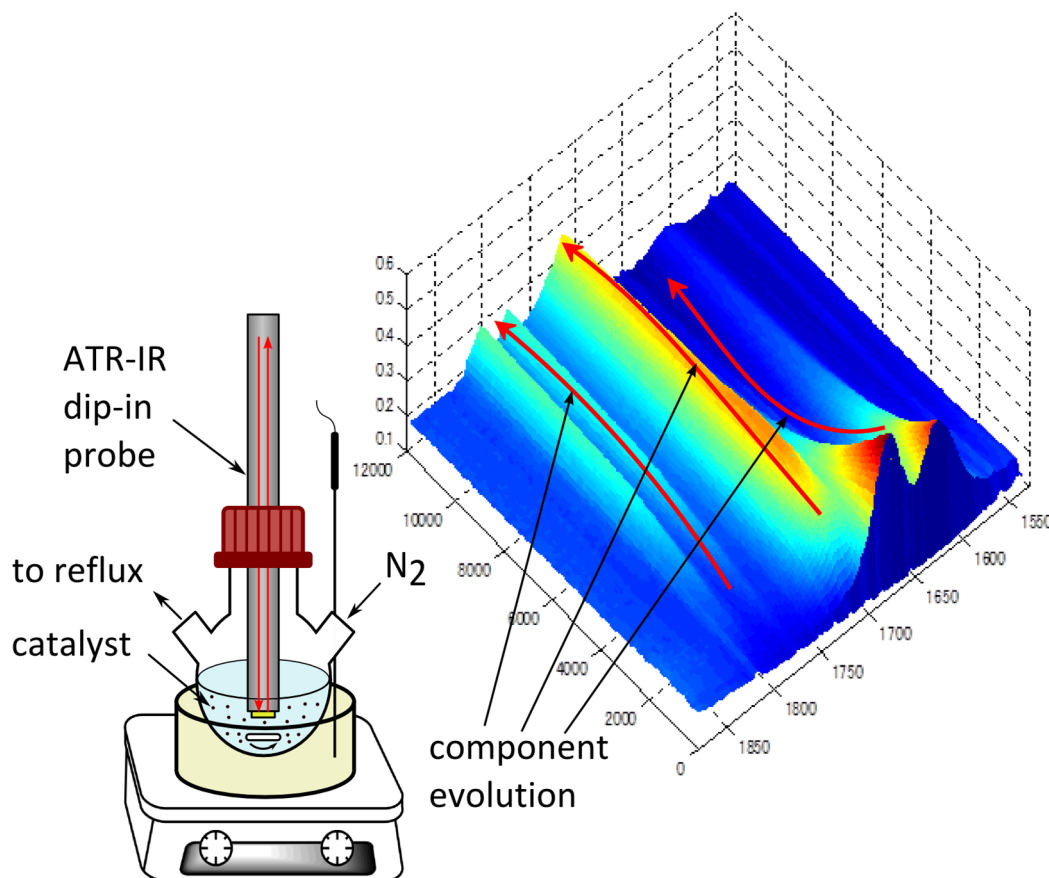


Figure 1.4. ATR-IR *in situ* monitoring with an example of urea transesterification with EG.

After identification of chemical components one can possibly gain information about how reactants are converted to intermediates and products, get clear picture of reaction pathways, and obtain kinetic data. The method is highly beneficial for this work since urea transesterification with EG is a complex reaction and understanding the reaction network and kinetics is the prerequisite to establish the relationship between catalyst properties (e.g. acid-base property) and catalytic performance at every reaction step.

The analysis of individual components in the complex reaction mixtures can be performed by either evaluating isolated bands or by applying modern

chemometric methods, which can facilitate processing the entire spectral information to obtain information about individual chemical species and their temporal evolution. The advantages of chemometric analysis will be discussed later in this Chapter.

Despite the obvious advantages of *in situ* spectroscopic reaction monitoring this method does not provide information about reactive species formed on the catalyst surface. To monitor behaviour of reaction components on the catalyst surface, a method suited for studying solid-liquid interfaces is required as described in the next section.

1.4.2 *In situ* ATR-IR study of catalytic solid-liquid interfaces

To understand acid-base catalysis it is very important to know which active species and intermediates are formed at catalytic active sites and which products will be formed as the results. To gain most precise information about active sites and species, studies should be performed under operating condition. In the case of urea transesterification with EG, the detection method should be capable of studying catalytic solid-liquid interface sensitively. One of the few techniques allowing to study such complex interfaces is *in situ* ATR-IR spectroscopy. The method and principle is the same as above dip-in probe for online monitoring, but the detection configuration is markedly different. In case of interface studies, catalysts are coated over the ATR crystal as described in Chapter 2. By doing so, the method becomes very surface-sensitive minimizing the signals from typically overwhelming reaction solution as demonstrated by Ferri and Bürgi [50].

ATR-IR spectroscopic study of solid-liquid interfaces can provide chemical information about surface species and possibly their evolution, which may allow gaining insights into the kinetics of observed species and reactions. Establishing correlations between catalytic performance and spectroscopic features may lead to understanding the nature of active sites and reaction mechanisms.

Although *in situ* ATR-IR spectroscopy may become sensitive to the signals originating from the catalytic interfaces, some challenges remain. Such as:

- surface of acid-base catalyst may contain a number of different chemical species and spectra may be “crowded”, ranging from reactants, intermediates, products, solvent and adsorbed spectators.
- signals of interest (active species) from the interface may be lower compared to unwanted signals of spectators and from the species in the liquid phase
- selectivity; is the observed signal due to adsorbate active species or just a spectator?
- detection sensitivity; enhancing time-resolution decreases signal-to-noise ratio

To tackle these challenges, transient techniques can be applied to selectively study behaviour of active surface species [51]. In such experiments, an external perturbation (e.g. reactant concentration change) is given so that only the concentration of the species of interests is affected. The principle of transient experiments is shown in Figure 1.5, where “stars” represent species of interest (active species) and other symbols are spectators or the species of non-interests. Picture on the left illustrates the situation of original “crowded” spectra of a complex system and on the right spectra obtained after transient experiments, with selectively highlighting surface species of interests.

Transient experiments can be performed using a pulse, step, or sinusoidal change of an external parameter influencing reaction kinetics. To be compatible with modulation excitation spectroscopy (MES) [51] a periodic variation of step-wide concentration changes was employed.

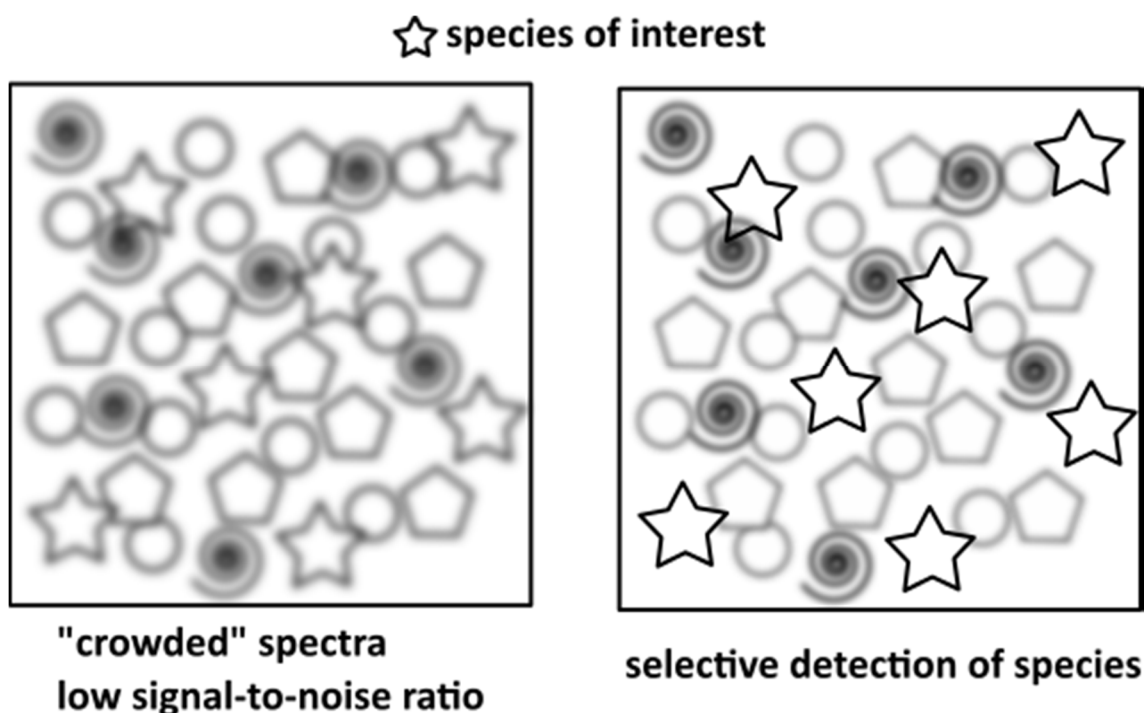


Figure 1.5. Adding detection selectivity by transient experiments.

Using the mathematical engine of MES, phase sensitive detection (PSD), one can improve signal-to-noise ratio drastically. However, in this work we employed chemometric (multivariate analysis) method to deconvolute the complex spectra into a set of comprising “pure component” spectra. The used multivariate analysis method for spectral analysis of reaction mixture as well as surface species is described in the following section.

1.4.3 Multivariate Curve Resolution (MCR)

As discussed previously, one of the major challenges in spectral analysis is to extract pure component spectra and their kinetic profiles. This holds for the spectral chemical analysis of both liquid phase and also surface species. One can select a sub-set of most interesting features for analysis by eye, but it fails in extracting the details when one is dealing with dynamics of complex systems, where spectral features and bands often overlap. In this case, application of multivariate spectral analysis can be very helpful.

Multivariate analysis involves simultaneous statistical analysis of all the variables. They are fast and efficient, use simultaneously all measured analytical signals and improve signal-to-noise ratio due to kinetic resolution. One of the basic and most employed multivariate techniques is Principal Components Analysis (PCA). Applying PCA to a set of chemical spectra normally result in positive and negative peaks and results are often not physically meaningful unless reference spectra are available. In this case, one possible solution can be Multivariate Curve Resolution (MCR). MCR is designed for recovery of chemical spectra and contribution from a multi-component mixture, when little or no prior information (such as reaction composition and spectra references) is available. Advantages of MCR over manual and PCA analysis are summarized in Table 1.3.

Table 1.3 Comparison of manual and multivariate data analyses.

Attributes	Manual analysis	PCA	MCR
Ease of interpretation	Difficult Peak overlap	Medium/Difficult Abstract, orthogonal factors	Easy Non-negative scores (component spectra) and loadings (component concentrations)
Identification	Difficult Characteristic peaks only	Medium Important peaks and correlation	Easy Full spectra obtained
Detection of minor components	Difficult Only if substance is known	Easy Higher factors capture small variance	Depends on the studied system
Most suitable for	Simple dataset with good prior knowledge	Discrimination of similar chemical phases	Identification for unknown mixtures

MCR is a very powerful blind source and spectral separation method and allows disentangling overlapping spectral features based on the kinetic resolution of comprising underlying spectral bands [53]. Such technique addresses one of

the most difficult problems in analytical spectroscopy, the qualitative and quantitative characterization of mixtures containing unknown amounts of an unknown number of unknown components. In principle, MCR does not need any spectra libraries or any a priori information on the number of components or concentration profiles. Results of MCR analysis are the kinetically pure component spectra and their concentration profiles [54]. This way of spectral analysis is significantly more precise to evaluate concentration profiles and kinetics than taking such information from the absorption band maxima because the latter method suffers from the overlaps of bands, which is common in IR spectroscopy and often leads to inaccurate extraction of kinetic parameters and incorrect data interpretations.

1.4.4 Design of Experiments (DoE)

Above described rational (i.e. towards/based on understanding) approach of studying urea transesterification provides detailed views over a reaction network and possibly reveals roles of catalytic active sites at each reaction step. Besides, it should be emphasized that a large number of experimental parameters such as temperature and reaction time may influence the catalytic performance as discussed above. To date, the studies that have been devoted to finding optimum reaction conditions for EC synthesis rely on one-factor-at-the-time approach [30-31, 35]. Although this common approach can reveal how certain factors affect product yields, it explores the space of experimental parameters very poorly and also reveals little about the interaction (correlation) between these parameters for better optimization of the targeted quantity (here, EC yield and selectivity).

Statistical methods can be applied to efficiently study and improve processes. Particularly Design of Experiment (DoE) [55] is a helpful tool to identify

experimental parameters affecting EC synthesis and to optimize them with as few experiments as possible.

The idea of DoE is to perform the least number of experiments to cover the design space in an efficient way. The comparison between DoE principles and one-factor-at-the-time approach is illustrated in Figure 1.6, where design space can be covered randomly by performing three sequential studies, each exploring one variable (Figure 1.3a); or exploring three variables in a structured manner (Figure 1.3b).

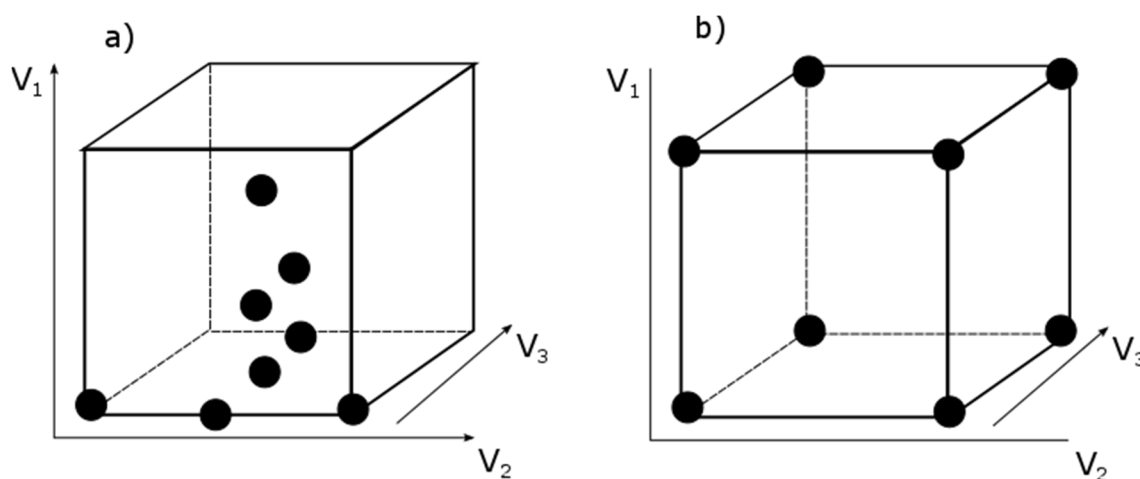


Figure 1.6. a) one-factor-at-the-time study; b) full-factor study. V – variables of the reaction, • – experiments.

Statistical DoE approach is based on sequent application of screening analysis of important parameters influencing reaction performance and optimization of most significant ones, i.e. most impacting EC yield and selectivity. The outcome of this analysis generates a mathematical model, predicting optimum values for selected parameters. Additionally, application of DoE allows reducing number of experiments by efficiently exploring the variable (design) space; therefore minimizing experimental costs and time.

1.5 Aim and overview of the thesis: enhance of EC synthesis

The present work aims at investigating the catalytic process of transesterification of urea with EG, targeting at selective and high-yield synthesis of EC based on the rational and statistical approaches. The global aim and sub-goals of present research work are summarized in Figure 1.7.

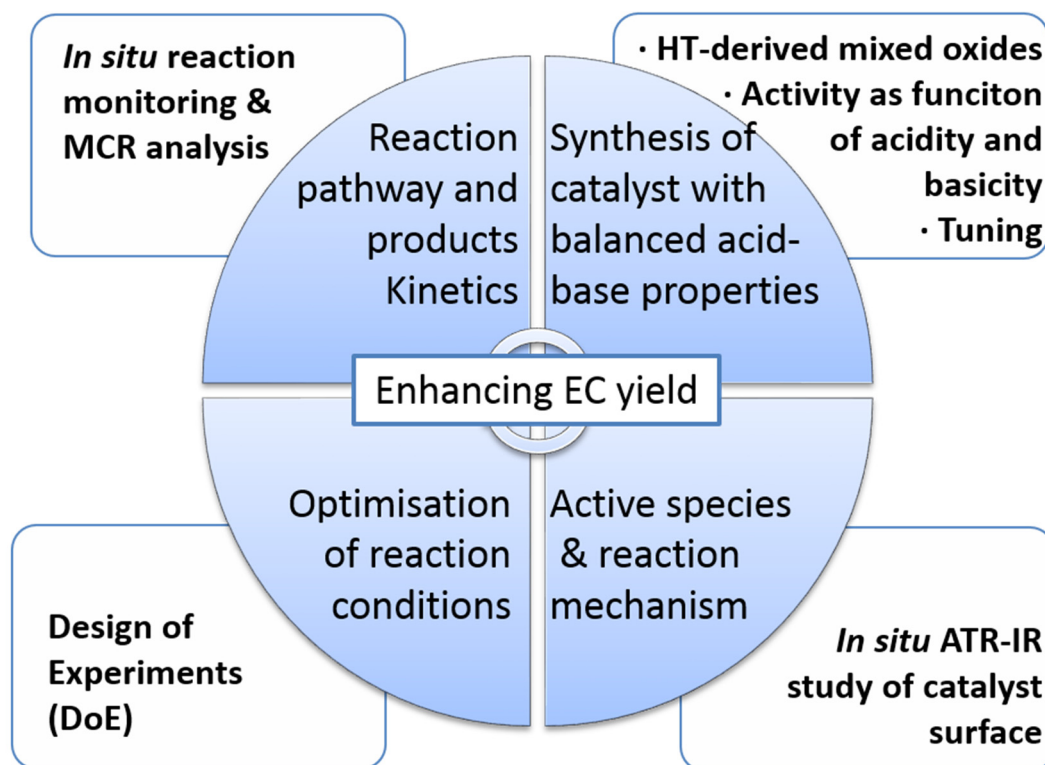


Figure 1.7. Aim and sub-goals with the employed methodologies of this work.

The main motivation to choose the above multi-faceted experimental methodologies was to understand the role of acidic and basic sites in urea transesterification with EG to rationally select catalyst with suitable acid-base properties for EC synthesis. To fully characterize catalytic activity we suggested to study reaction performance in separate reaction steps. The separate reaction study would clarify the contribution of each reaction step to overall reaction pathway, reaction kinetics, and also the influence of acidic or basic sites on the

reaction steps. For this purpose, reaction monitoring by *in situ* ATR-IR dip-in probe and post treatment of spectroscopic data by modern chemometric analysis (MCR) were performed.

According to the previous studies, metal oxides possessing balanced Lewis acidic and basic sites exhibited the best catalytic performance towards EC formation. Therefore, synthesis of mixed metal oxides derived from hydrotalcites possessing distinct acid-base properties was prepared and tested. The use of hydrotalcites as precursors afforded the synthesis of materials with high surface area and good distribution of acidic and basic sites.

After establishing the role of acidic and basic sites we intended to optimize the best performing catalyst by tuning its acid-base properties and additionally explore catalytic performance of new class of materials (zeolites).

To gain understanding about active sites and reaction mechanism a mechanistic study of catalyst surface under reaction conditions was performed. This challenging study of the catalytic solid-liquid interfaces under operating conditions was made possible by transient experiments using ATR-IR spectroscopy. This approach provides identification of active species formed on the catalyst during the reaction and their temporal evolution, giving insights into possible reaction mechanism.

Aiming to further enhance EC selectivity and yield, reaction conditions were optimized by applying statistical method (DoE). In spite of classical one-factor-at-the-time approach, our idea was to use more reliable statistical method and predict optimal conditions for selective and high-yield EC synthesis based on mathematical models.

References

1. Swarup, S. Process for forming a waterborne composite polyurethane/acrylic polymer dispersion. US Patent 8153708, 2012.
2. Laurence G.; Coffey-Dawe, L.-A. Nail varnish comprising a phenylated silicone resin. US Patent 20100074854, 2010.
3. (a) Bernini, R.; Mincione, E.; Barontini, M.; Crisante, F.; Fabrizi, G.; Gambacorta, A., *Tetrahedron* 2007, 63 (29), 6895-6900; (b) Schäffner, B.; Holz, J.; Verevkin, S. P.; Boerner, A., *Chemsuschem* 2008, 1 (3), 249-253; (c) Schäffner, B.; Holz, J.; Verevkin, S. P.; Boerner, A., *Tetrahedron Lett.* 2008, 49 (5), 768-771; (d) Quaranta, E.; Carafa, M.; Trani, F., *Appl Catal B* 2009, 91 (1-2), 380-388.
4. Pensado, A. S.; Padua, A. A. H.; Comunas, M. J. P.; Fernandez, J., *J. Phys. Chem. B* 2008, 112 (18), 5563-5574.
5. (a) Lombardo, L.; Brutti, S.; Navarra, M. A.; Panero, S.; Reale, P., *J. Power Sources* 2013, 227, 8-14; (b) Li, Z.; Shan, F.; Wei, J.; Yang, J.; Li, X.; Wang, X., *J. Solid State Electrochem.* 2008, 12 (12), 1629-1635.
6. Zhang, H.; Grinstaff, M. W., *J. Am. Chem. Soc.* 2013, 135 (18), 6806-6809.
7. Park, J. H.; Jeon, J. Y.; Lee, J. J.; Jang, Y.; Varghese, J. K.; Lee, B. Y., *Macromolecules* 2013, 46 (9), 3301-3308.
8. Toshiyasu Sakakura, K. K., *Chem Commun (Camb)* 2009, 1312-1330.
9. (a) Li, X. L.; Chen, H. Y.; Zhu, Z. Y.; Zhen, H., *Energy Convers. Manage.* 2006, 47 (11-12), 1438-1448; (b) Dan Li, W. F., Yan Xing, Yongsheng Guo, Ruisen Lin *J. Hazard. Mater.* 2009, 161 (2), 1193-1201; (c) Rudnick, L. R., *Synthetics, mineral oils, and bio-based lubricants chemistry and technology.* Boca Raton : CRC Press, 2013: 2013; 245.
10. (a) Xiaowei Miao, C. F., Christian Bruneau. Pierre H. Dixneuf, *Chemsuschem* 2008, 1 (10), 813-816; (b) Mutlu, H.; Ruiz, J.; Solleder, S. C.; Meier, M. A. R., *Green Chem.* 2012, 14 (6), 1728-1735.
11. <http://www.ccr.com.cn/new/>.

12. (a) Delledonne, D.; Rivetti, F.; Romano, U., *Appl. Catal. A-Gen.* 2001, 221 (1-2), 241-251; (b) Uchiumi, S.; Ataka, K.; Matsuzaki, T., *J. Organomet. Chem.* 1999, 576 (1-2), 279-289.
13. (a) Mei, F. M.; Pei, Z.; Li, G. X., *Org. Process Res. Dev.* 2004, 8 (3), 372-375; (b) Du Zhiping, K. W., Chen Tong, *J. Mol. Catal. A: Chem.* 2006, 246 (1/2), 200-205; (c) Tong, D.-S.; Yao, J.; Wang, Y.; Niu, H.-Y.; Wang, G.-Y., *J. Mol. Catal. A-Chem.* 2007, 268 (1-2), 120-126; (d) Chen, T.; Han, H.; Yao, J.; Wang, G., *Catal. Commun.* 2007, 8 (9), 1361-1365.
14. (a) Cooper J. F.; Lichtenwalter, M. Catalytic process for producing alkylene carbonates. US Patent 2773070, 1956; (b) McClellan, P. P. Catalytic process for producing alkylene carbonates. US Patent 2873282, 1959.
15. Fukuoka, S.; Tojo, M.; Hachiya, H.; Aminaka, M.; Hasegawa, K., *Polym. J* 2007, 39 (2), 91-114.
16. (a) Etacheri, V.; Marom, R.; Elazari, R.; Salitra, G.; Aurbach, D., *Energy Environ Sci* 2011, 4 (9), 3243-3262; (b) Beattie, C.; North, M.; Villuendas, P., *Molecules* 2011, 16 (4), 3420; (c) Schäffner, B.; Schäffner, F.; Verevkin, S. P.; Börner, A., *Chem. Rev.* 2010, 110 (8), 4554-4581.
17. North, M., *Chem. Today* 2012, 30 (3), 3-5.
18. (a) Aresta M.; Quaranta, E., *Chem. Tech.* 1997, 27 (3), 32-40; (b) Strega P.E.; Renga, J. M. Process for making alkylene carbonates. US Patent 4344881, 1982.
19. Darensbourg, D. J.; Holtcamp, M. W., *Coord. Chem. Rev.* 1996, 153, 155-174.
20. (a) Backvall, J. E.; Karlsson, O.; Ljunggren, S. O., *Tetrahedron Lett.* 1980, 21 (51), 4985-4988; (b) Calo, V.; Nacci, A.; Monopoli, A.; Fanizzi, A., *Org. Lett.* 2002, 4 (15), 2561-2563; (c) Kihara, N.; Hara, N.; Endo, T., *J. Org. Chem.* 1993, 58 (23), 6198-6202; (d) Kruper, W. J.; Dellar, D. V., *J. Org. Chem.* 1995, 60 (3), 725-727; (e) Nomura, R.; Ninagawa, A.; Matsuda, H., *J. Org. Chem.* 1980, 45 (19), 3735-3738; (f) Peppel, W. J., *Ind. Eng. Chem.* 1958, 50 (5), 767-770; (g) Yamaguchi, K.; Ebitani, K.; Yoshida, T.; Yoshida, H.; Kaneda, K., *J. Am. Chem. Soc.* 1999, 121 (18), 4526-4527.

21. (a) Jacobson, S. E. Process for the production of alkylene carbonates and oxides. EP 118248, 1984; (b) Aresta, M.; Dibenedetto, A., *J. Mol. Catal. A: Chem.* 2002, 182–183, 399-409.
22. Aresta, M.; Dibenedetto, A.; Tommasi, I., *Appl. Organomet. Chem.* 2000, 14 (12), 799-802.
23. Tomishige, K.; Yasuda, H.; Yoshida, Y.; Nurunnabi, M.; Li, B. T.; Kunimori, K., *Catal. Lett.* 2004, 95 (1-2), 45-49.
24. Tomishige, K.; Yasuda, H.; Yoshida, Y.; Nurunnabi, M.; Li, B.; Kunimori, K., *Green Chem.* 2004, 6 (4), 206-214.
25. Tomishige, K.; Yasuda, H.; Yoshida, Y.; Nurunnabi, M.; Li, B.; Kunimori, K., *Catal. Lett.* 2004, 95 (1-2), 45-49.
26. Huang, S.-Z.; Liu, S.-G.; Li, J.-P.; Zhao, N.; Wei, W.; Sun, Y.-h., *J. Fuel Chem. Technol.* 2007, 35 (6), 701-705.
27. Mennen, J. H. Urea stripping process for the production of urea. US Patent 20120302789, 2012.
28. <http://mcgroup.co.uk/news/20140418/propylene-glycol-market-reach-supplydemand-balance-2015.html>.
29. <http://www.grandviewresearch.com/press-release/global-ethylene-glycols-market>.
30. Zhao, X.; An, H.; Wang, S.; Li, F.; Wang, Y., *J. Chem. Technol. Biotechnol.* 2008, 83 (5), 750-755.
31. Bhanage, B. M.; Fujita, S.; Ikushima, Y.; Arai, M., *Green Chem.* 2003, 5 (4), 429-432.
32. Li, Q.; Zhang, W.; Zhao, N.; Wei, W.; Sun, Y., *Catal. Today* 2006, 115 (1-4), 111-116.
33. Kawabe K.; Murata K. ; Furuya, T. Ethylene glycol process. US Patent 5763691 1998.
34. Bhadauria, S.; Saxena, S.; Prasad, R.; Sharma, P.; Prasad, R.; R., D., *Eur. J. Chem.* 2012, 3 (2), 235-240.
35. Wang, P.; Liu, S.; Zhou, F.; Yang, B.; Alshammari, A. S.; Lu, L.; Deng, Y., *Fuel Process. Technol.* 2014, 126 (0), 359-365.
36. Su W.-Y.; Speranza, G. P. From Alkylene Glycols and Urea. US Patent 5003084, 1991.

37. Doya M.; Ohkawa T.; Kanbara Z.; Okamoto A.; Kimizuka, K. Process for producing alkylene carbonates. US Patent 5349077, 1994.
38. Ball, P.; Fullmann, H.; Heitz, W., *Angew. Chem. Int. Ed. (English)* 1980, 19 (9), 718-720.
39. Li, Q.; Zhao, N.; Wei, W.; Sun, Y., *J. Mol. Catal. A: Chem.* 2007, 270 (1-2), 44-49.
40. Climent, M. J.; Corma, A.; De Frutos, P.; Iborra, S.; Noy, M.; Velty, A.; Concepción, P., *J. Catal.* 2010, 269 (1), 140-149.
41. Rives, V., *Layered Double Hydroxides: Present and Future*. Nova Science Publishers: 2001.
42. Allada, R. K.; Navrotsky, A.; Berbeco, H. T.; Casey, W. H., *Science* 2002, 296 (5568), 721-723.
43. Thiel, J. P.; Chiang, C. K.; Poeppelmeier, K. R., *Chem. Mater.* 1993, 5 (3), 297-304.
44. (a) Saber, O.; Tagaya, H., *J Incl Phenom Macrocycl Chem* 2003, 45 (1-2), 107-115; (b) Curtius, H.; Ufer, K.; Dardenne, K., *Radiochim Acta* 2009, 97 (8), 423-428; (c) Bergaya, F.; Lagaly, G., *Handbook of Clay Science*. Elsevier Science: 2013.
45. De Roy A.; Forano C.; Malki K. E.; Besse, J. P., *Expanded Clays and Other Microporous Solids*. Van Nostrand Reinold, New York, 1992; II, 108-169.
46. (a) Zhao, J.; Yang, L.; Chen, T.; Li, F., *J. Phys. Chem. Solids* 2012, 73 (12), 1500-1504; (b) Xiang, X.; Hima, H. I.; Wang, H.; Li, F., *Chem. Mater.* 2008, 20 (3), 1173-1182.
47. (a) Bakeev, K. A., Ed., *Process Analytical Technology: Spectroscopic Tools and Implementation Strategies for the Chemical and Pharmaceutical Industries*, (John Wiley & Sons, Ltd, 2010); (b) Rubin, A. E.; Tummala, S.; Both, D. A.; Wang, C.; Delaney, E. J., *Chem. Rev.* 2006, 106 (7), 2794-2810.
48. (a) Mul, G.; Hamminga, G. M.; Moulijn, J. A., *Vib. Spectrosc* 2004, 34 (1), 109-121; (b) Hamminga, G.; Mul, G.; Moulijn, J., *Catal. Lett.* 2006, 109 (3-4), 199-206.

49. (a) Grabow, K.; Bentrup, U., *ACS Catal.* 2014, 4 (7), 2153-2164; (b) Lumpi, D.; Braunschier, C.; Hametner, C.; Horkel, E.; Zachhuber, B.; Lendl, B.; Fröhlich, J., *Tetrahedron Lett.* 2009, 50 (47), 6469-6471; (c) Lumpi, D.; Wagner, C.; Schöpf, M.; Horkel, E.; Ramer, G.; Lendl, B.; Fröhlich, J., *Chem. Commun.* 2012, 48 (18), 2451-2453.
50. Ferri, D.; Bürgi, T., *J. Am. Chem. Soc.* 2001, 123 (48), 12074-12084.
51. Urakawa, A.; Bürgi, T.; Baiker, A., *Chem. Eng. Sci.* 2008, 63 (20), 4902-4909.
52. Urakawa, A.; Wirz, R.; Bürgi, T.; Baiker, A., *J. Phys. Chem. B* 2003, 107 (47), 13061-13068.
53. (a) Massart D. L. ; Vandeginste B. G. M.; Buydens L. M. C.; De Jong S.; Lewi P. J.; Smeyers-Verbeke, J., *Handbook of Chemometrics and Qualimetrics: Part A.* Elsevier: Amsterdam, 1997; 20A, 643-738; (b) Brereton, R. G., *Chemometrics: Data Analysis for the Laboratory and Chemical Plant.* John Wiley & Sons, Ltd: 2003; (c) Tauler, R., *Chemometr. Intell. Lab.* 1995, 30 (1), 133-146.
54. (a) Meyers, R. A., Ed., *Encyclopedia of Analytical Chemistry: Applications, Theory and Instrumentation*, (John Wiley & Sons, Ltd, 2000); (b) de Juan, A.; Maeder, M.; Martinez, M.; Tauler, R., *Chemometr. Intell. Lab.* 2000, 54 (2), 123-141.
55. Esbensen, K. H.; Guyot, D.; Westad, F.; Houmoller, L. P., *Multivariate Data Analysis In Practice: an Introduction to Multivariate Data Analysis and Experimental Design.* Camo Process AS: 2002.

Chapter 2

Methods

2.1 Catalyst preparation

Sodium hydroxide (Alfa Aesar, 97%), zinc nitrate hexahydrate (Sigma-Aldrich, 98%), magnesium nitrate hexahydrate (Sigma-Aldrich, 98.0-102.0%), aluminum nitrate nonahydrate (Sigma-Aldrich, 98%), iron (III) nitrate nonahydrate (Alfa Aesar, 98.0-101.0%), sodium carbonate (Sigma-Aldrich, 99%), ethylene glycol (Alfa Aesar, 99%), urea (Alfa Aesar, 99-100.5%), 2-hydroxyethyl carbamate (Angene, 95%), ethylene carbonate (Sigma-Aldrich, 98%), and 2-oxazolidinone (Sigma-Aldrich, 98%) were used as received.

Mixed metal oxides with general formula $M_b^{2+}-M_t^{3+}$ containing Mg^{2+} or Zn^{2+} as bivalent cation (M_b^{2+}) and Al^{3+} or Fe^{3+} as trivalent cation (M_t^{3+}) with constant molar ratio $M_b^{2+}/M_t^{3+} = 3$ were synthesized by a co-precipitation method (Figure 2.1). $Mg^{2+}-Al^{3+}$, $Mg^{2+}-Fe^{3+}$ and $Zn^{2+}-Al^{3+}$ mixed metal oxide materials were synthesized as follows. An aqueous nitrate solution (100 mL) with appropriate amount of the bivalent and trivalent cations was added drop-wise into a beaker containing 100 mL of deionized water under vigorous stirring at room temperature. The pH of the solution was kept constant at 10 by adding a second aqueous solution of NaOH (2 M). The resultant slurry was aged for 18 h at room temperature, filtered, thoroughly washed with deionized water and dried at 373 K overnight. The resultant dried materials with the hydrotalcite structure were calcined at 723 K for 12 h to obtain the corresponding mixed metal oxides. The synthesis of the single metal oxide materials (ZnO , Al_2O_3 , MgO , Fe_2O_3) followed the same protocol but using the aqueous solution of a respective nitrate precursor. Concerning the synthesis of the $Zn^{2+}-Fe^{3+}$ mixed metal oxide, an aqueous solution of Na_2CO_3 (2 M) was used as the second solution because the resulting material after drying did not form hydrotalcite structure when the NaOH solution was used. The precipitated solid was washed, dried, and calcined as described above. Hereafter, $Mg^{2+}-Al^{3+}$, $Mg^{2+}-Fe^{3+}$, $Zn^{2+}-Al^{3+}$ and $Zn^{2+}-Fe^{3+}$ mixed metal oxide materials after calcination of the corresponding materials with

hydrotalcite structures are denoted simply Mg-Al, Mg-Fe, Zn-Al, and Zn-Fe, respectively, or with “mixed oxide” after the simplified notation.

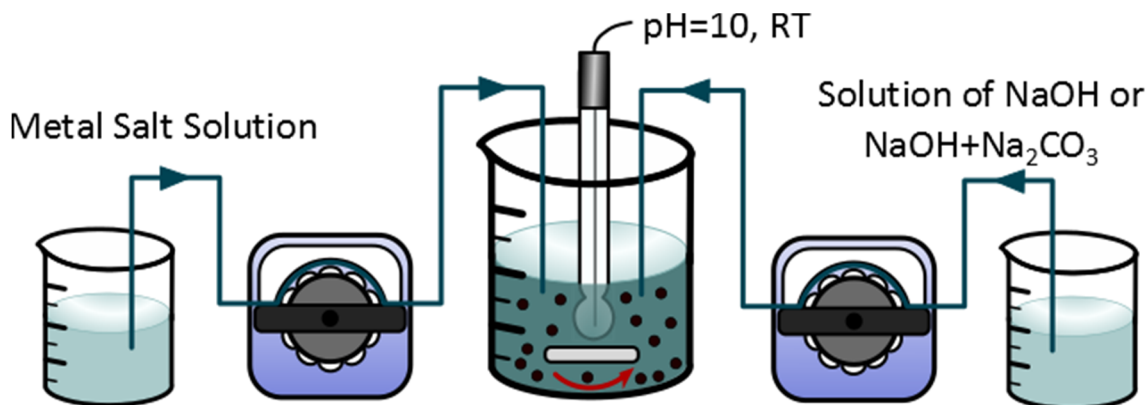


Figure 2.1. The schematic representation of the co-precipitation method.

2.2 *In situ* reaction monitoring by ATR-IR spectroscopy

ATR-IR spectroscopic detection in the form of dip-in probe has been proven to be a useful tool for real-time monitoring and *in situ* studies of liquid phase reactions under working conditions [1]. Details of the analysis and reaction setup are described below. For the sake of clarity the experimental method of ATR-IR spectroscopic study of catalytic solid-liquid interfaces is described in Chapter 7.

2.2.1 Reaction setup

Transesterification of urea with EG as well as intermediate reactions have been performed in a 25 mL three-necked-flask equipped with a magnetic stirrer and cycle reflux condenser (Figure 2.2). *In situ* IR data were collected using Mettler Toledo React-IR™ 4000 equipped with a diamond ATR crystal placed inside the probe. The probe was fitted into one of the 24/40 ground glass fittings at the top of the reactor using a Teflon adapter and inserted directly into the

reaction mixture. During all experiments the React-IR™ probe was under purge of N₂ gas.

Sampling systems include DiComp™ (diamond internal reflection element (IRE) for highest chemical resistance) ATR insertion probe. Figure 2.3 shows a more detailed schematic drawing of a Comp™ probe. The head of a Comp™ probe mainly consists of two elements. A ZnSe crystal focuses and orients the IR beam to the IRE that consists of a chemical and mechanical resistant material (diamond or silicon; here diamond). The IR light ray undergoes six total internal reflections at the interface with the substrate before it is seen by the detector. The probe immersed in the reaction medium measures the absorption in the mid-infrared region and hence the relative concentration changes of the components during the reaction. Comp™ probes permit the analysis of reactions and temperatures in the range of 193K up to 473 K. The spectral range was 4000–650 cm⁻¹ (due to the absorbance of the diamond crystal the cut-off region between 2250 and 1950 cm⁻¹ cannot be used for spectral analysis).



Figure 2.2. Reactor with dipped ATR-IR probe.

Prior to each experiment, background of the air was measured for 32 scans at 4 cm^{-1} resolution. Then reactor was charged with EG and heated up to desired temperature using oil bath. When the temperature was reached desired amount of urea and catalyst were loaded in the reactor and IR measurements were started. Spectra were recorded every 2 min for a period of 6 h at 4 cm^{-1} resolution. The reaction temperature was continuously monitored by a thermocouple during experiments. To remove ammonia forming in the course of the reaction, N_2 was continuously passed through the reactor.

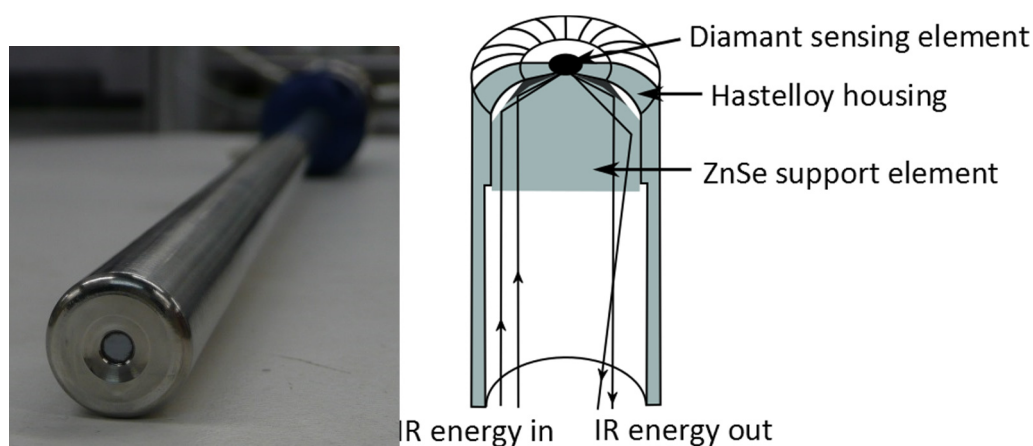


Figure 2.3. Schematic drawing of the Comp™ probe: infrared radiation is reflected into the chemically resistant IRE disk which is in contact with the reaction mixture.

Products in the solution after reaction were analyzed by GC (Agilent 6890N) equipped with an FID detector and a capillary column HP-35 and GC-MS (Agilent 6890N (GC) 5973(MSD)) equipped with a capillary column HP-5.

2.2.2 Time-resolved spectra

IR spectra obtained during 6 h of the reaction are shown in Figure 2.4a and 2.4b. 3D figure clearly shows the temporal evolution of the reactants and products. The absorbance is directly proportional to the concentration of chemical species and one can evaluate the concentration profiles, thus reaction kinetics,

from the band intensity. However, such analysis is not straightforward due to the band overlaps as shown in this 2D plot (Figure 2.4a) of the same data.

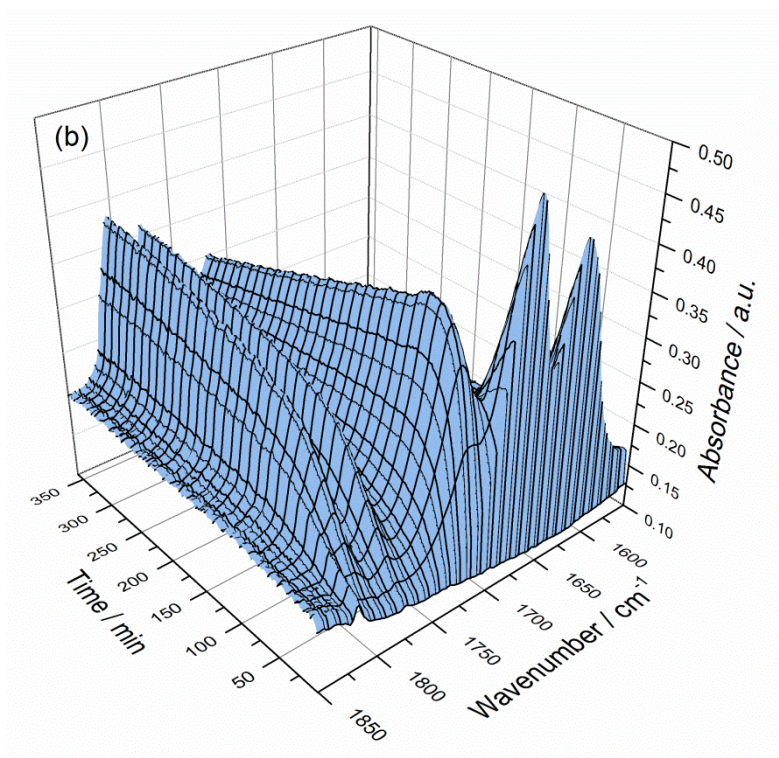
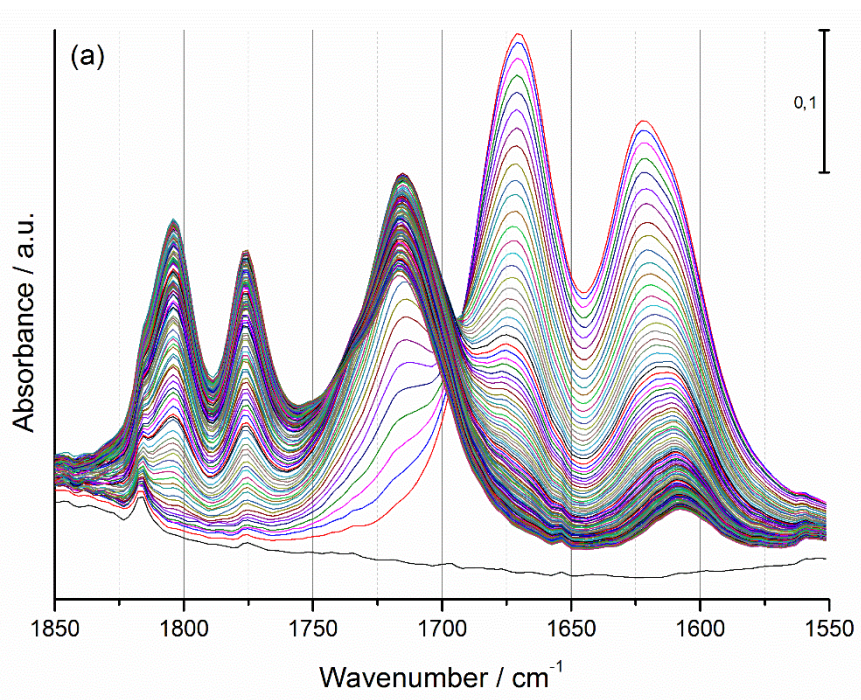


Figure 2.4. 2D (a) and 3D (b) representation of spectra obtained during *in situ* ATR-IR reaction monitoring.

Deconvolution of the spectra into pure component spectra is necessary and in order to facilitate this process, chemometric analysis was applied. In this work Multivariate Curve Resolution (MCR) analysis was used to process signals of individual compounds.

2.3 Multivariate Curve Resolution (MCR) analysis

MCR was applied to extract from sequences of spectra the number of independent (kinetically pure) chemical components, their spectra and the temporal profiles of concentration. This analysis allows studying evolution of reactants and products over the reaction time. Catalytic behavior of different materials was compared in this manner.

2.3.1 Basic theory of MCR

When the reaction is monitored by IR spectroscopy, a series of spectra are collected along the course of the reaction progress, containing the contributions from the n chemical components existing in the system. The resulting spectral dataset can be treated by Multivariate Curve Resolution – Alternating Least Squares (MCR-ALS) to extract the spectra of the individual chemical components and their concentration profiles.

Spectroscopic measurements data are ordered in a data matrix $\mathbf{D}_{(r \times c)}$, whose rows contain the spectra acquired at different times (r) and whose columns are the process signals (absorbance) at different wavelengths (c). The algorithm of MCR analysis seeks the optimal decomposition of the data matrix $\mathbf{D}_{(r \times c)}$ into the pure contributions of the components of the reaction according to the following equation.

$$\mathbf{D}_{(r \times c)} = \mathbf{C}_{(r \times n)} \mathbf{S}_{(n \times c)}^T + \mathbf{E}_{(r \times c)} \quad (2.1)$$

Matrix \mathbf{C} contains the concentration information of the n sample components of the system and \mathbf{S}^T represents the matrix of pure spectra, and \mathbf{E}

contains the residual (model error). MCR-ALS solves this equation in an iterative, alternating least squares manner by minimizing the residual matrix \mathbf{E} .

In MCR, the first step is the estimation of the number of components (n) involved, which can be initially obtained by application of the singular value decomposition [2]. MCR-ALS also needs a preliminary estimation of \mathbf{S}^T or \mathbf{C} , which is provided either by evolving factor analysis [3], by selection of the pure variables [4], or by any previous estimation of them. The spectra of standards of the components, when available, are also suitable to preliminary estimate \mathbf{S}^T .

Given the initial estimates of matrices \mathbf{C} or \mathbf{S}^T , the ALS algorithm executes a constrained optimization process [5]. It carries out the decomposition of matrix \mathbf{D} , as presented in Equation (2.1), iteratively to find a model able to minimize the residual sum of squares (rss), employed as an error criterion by Equation (2.2).

$$\text{rss} = \|\mathbf{E}\| = \|\mathbf{D} - \mathbf{C}\mathbf{S}^T\| \quad (2.2)$$

To that end, ALS iteratively solves two alternating least-squares problems, the minimization of rss over \mathbf{C} for a fixed \mathbf{S} and the minimization of rss over \mathbf{S} for a fixed \mathbf{C} (Equations (2.3) and (2.4)), calculating new estimations of \mathbf{S}^T and \mathbf{C} at the end of each cycle [6]. It does so until rss reaches a minimum value. Because of rotational ambiguities, constraints must be added with the aim to guide the iteration process toward a mathematically as well as chemically meaningful solution [7]:

$$\text{Min}(\mathbf{C}) \|\mathbf{D} - \mathbf{C}\mathbf{S}^T\| \rightarrow \mathbf{C} = \mathbf{D}\mathbf{S}(\mathbf{S}^T\mathbf{S}) \quad (2.3)$$

$$\text{Min}(\mathbf{S}^T) \|\mathbf{D} - \mathbf{C}\mathbf{S}^T\| \rightarrow \mathbf{C} = \mathbf{D}^T\mathbf{C}(\mathbf{C}^T\mathbf{C})^{-1} \quad (2.4)$$

The iteration procedure ends after completion of a preselected number of cycles or when the percentage of lack of fit (%LOF) does not change significantly between consecutive iterations and convergence is achieved. The explained variance (rss) is indicative of the quality of MCR-ALS modeling results [8].

2.3.2 Component spectra and component concentrations

Figure 2.5 displays pure component spectra obtained after MCR analysis and separated from the time-resolved spectra measured during the reaction (e.g. Figure 1.4). However, since the deconvolution into pure component spectra is based on the distinct kinetics of characteristic bands, chemical compounds having similar kinetic profiles of characteristic bands cannot be well distinguished and, thus, separated. This is the case of parallel reactions with simultaneous formation of multiple compounds with the same kinetic profile (e.g. EC and 2-Ox in Figure 2.5).

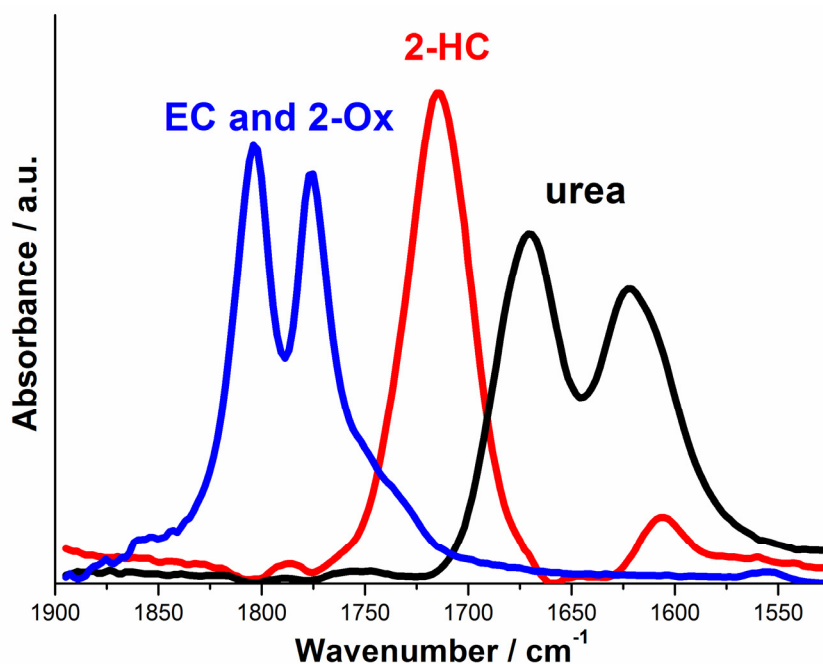


Figure 2.5. Component spectra obtained after MCR analysis.

Concentration profiles of corresponding components are shown in Figure 2.6. The important advantage of multivariate spectral analysis method like MCR is that the concentration profile is much more reliable than the peak intensity profile because of the absence of band overlaps. These concentration profiles are used to study reaction kinetics (see the next section) and in the rationalization

of catalytic performance which will be correlated with the amount and strength of acidic and basic sites.

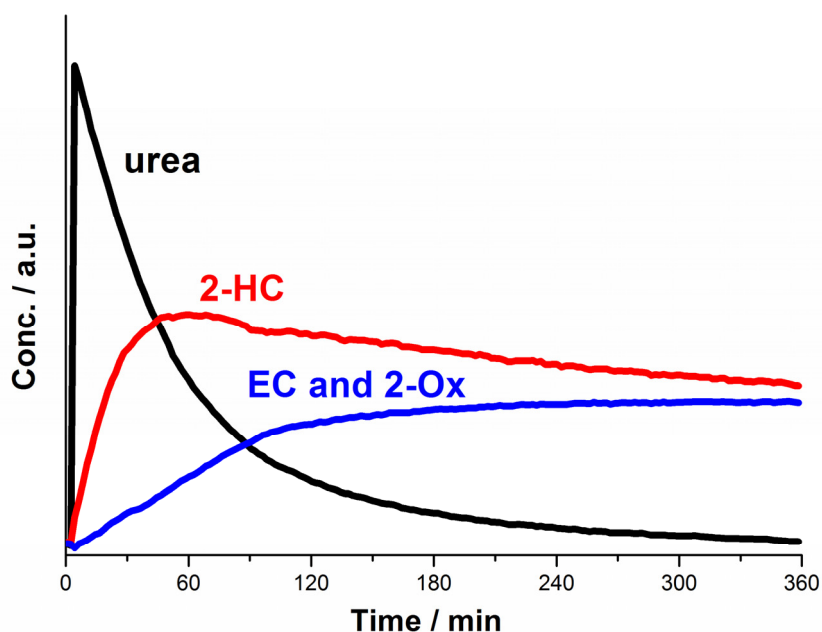


Figure 2.6. Component concentration profiles obtained after MCR analysis.

2.4 Kinetic study

The pure component decomposition can be used to extract information of the chemical system from the concentration profiles by obtaining kinetic information of the chemical reaction. The kinetic study of this work was performed using the information of the matrix \mathbf{C} , containing the profile concentrations (A_i) of kinetically differentiable species (i.e. the involved reactants and products) extracted by MCR. The concentrations of identified chemical species were normalized ($C_i = \frac{A_i}{A_{i,0}}$) to facilitate the kinetic modeling from the IR data obtained.

Kinetic study was performed with the followed assumptions and practical considerations.

1. Constant volume of the reaction solution
2. Isothermal

3. No mass transfer limitations

4. No explicit influence of catalyst surface

5. We considered investigated component (urea, 2-HC, EC, 2-Ox) isolated, due to excess of other reactant (EG).

6. Concentration profiles of first 120 min were considered to calculate reaction order and k values to extract kinetic parameters more characteristic for the reaction towards the product side with minimized influence of possible products-catalyst interactions.

References

1. (a) Mul, G.; Hamminga, G. M.; Moulijn, J. A., *Vib. Spectrosc* 2004, 34 (1), 109-121; (b) Hamminga, G.; Mul, G.; Moulijn, J., *Catal. Lett.* 2006, 109 (3-4), 199-206.
2. Golub, G. H.; Van Loan, C. F., *Matrix Computations*. Johns Hopkins University Press: 2013.
3. Tauler, R.; Durand, G.; Barcelo, D., *Chromatographia* 1992, 33 (5-6), 244-254.
4. Sánchez, F. C.; Toft, J.; van den Bogaert, B.; Massart, D. L., *Anal. Chem.* 1996, 68 (1), 79-85.
5. Bro, R.; De Jong, S., *J. Chemom.* 1997, 11 (5), 393-401.
6. Tauler, R., *Chemometr. Intell. Lab.* 1995, 30 (1), 133-146.
7. Malinowski, E. R., *Factor Analysis in Chemistry*. John Wiley & Sons, Ltd: 1991.
8. De Luca, M.; Mas, S.; Ioele, G.; Oliverio, F.; Ragno, G.; Tauler, R., *Int. J. Pharm.* 2010, 386 (1-2), 99-107.

Chapter 3

Catalyst Characterization

3.1 Introduction

Physical properties, such as surface area, structure and morphology were determined by N₂-physisorption and X-ray powder diffraction (XRD). Although the catalytic activity may be only indirectly related to the total available surface, evaluation of the surface area is generally considered as an important factor influencing catalytic performance. The Brunauer–Emmett–Teller (BET) method [1] is widely used and was chosen to evaluate the surface area of the catalysts. XRD is the main characterization tool when the solid materials are synthesized [2]. It is a standard method to provide information about the structure and crystallinity of materials. It is often used to determine if the desired product has been successfully synthesized. Thus, X-ray powder diffraction was used to verify all preparation steps in the synthesis of solid catalysts.

Regarding the chemical properties of the catalysts, acid-base properties were examined using temperature-programmed desorption (TPD) method and IR spectroscopy. TPD of probe molecules and reaction of simple bases or acids with catalyst materials (titration) are widely used to evaluate the total number and strength of acidic sites [3] or basic sites [4]. NH₃-TPD has been employed to characterize the acidity of the solid catalysts, while CO₂-TPD was used to evaluate the total number and strength of basic sites. TPD is widely used and accepted method to characterize acidity and basicity of solid materials but one cannot discriminate the type of acidic/basic sites, e.g. whether a base probe molecule is desorbing from Brønsted or Lewis acidic sites, or even from the both. Infrared spectroscopy (IR) has been proved to be one of the sensitive and adequate methods to gain deeper insights into such nature of acidic/basic sites and acid–base interactions on solid surfaces [5].

These characterization methods as well as the results for the catalyst materials used in this work are presented in the following sections.

3.2 Experimental section

The surface area of the catalysts was determined by N₂-physisorption (77 K) with the BET method using Autosorb 1-MP (Quantachrome) equipment.

Powder X-ray diffraction (XRD) experiments were performed on a Bruker AXS D8 Advance diffractometer equipped with a Cu tube, a Ge (1 1 1) incident beam monochromator ($\lambda=1.5406 \text{ \AA}$), and a Vantec-1 PSD operated in transmission mode. Identification of the crystal phases was made by comparing with the reference data available in the Joint Committee on Powder Diffraction Standards (JCPDS).

Acid-base properties of the materials were characterized by TPD of adsorbed CO₂ and NH₃ and the procedure was as follows. Sample (100 mg) was pretreated for 2 h at 723 K in He, cooled down to 353 K, saturated with a gas containing the probe molecule (4.5% CO₂ / 5% NH₃ in He) and afterwards flushed with He for 20 min. Subsequently, TPD measurements were performed at a heating rate of 20 K·min⁻¹ under He flow (20 mL·min⁻¹) and the quantity of desorbed gases were recorded by a TCD detector in TPDRO 1100 (Thermo Fisher Scientific). The amount of basic and acidic sites was calculated from the CO₂ and NH₃ peaks, respectively, after deconvolution of comprising desorption peaks using the PeakFit v4 software. It should be noted that single and mixed metal oxides are generally exposed to the reactive components of air after the synthesis and during the storage. For instance, Mg-containing materials readily interact and react with H₂O and CO₂ to form magnesium hydroxide and carbonate, affecting acid-base properties of the materials [6]. Therefore, it was important to treat the samples under a controlled atmosphere before the reaction and characterization (in our case high temperature treatment at 723 K for 2 h in He) to remove majority of the surface carbonates as discussed later.

Diffuse reflectance infrared Fourier transform (DRIFT) spectra were recorded on a Bruker Tensor 27, equipped with a high temperature DRIFT cell (HVC, Harrick) with CaF_2 windows. The catalyst (10 wt%) was ground with KBr and 100 mg of resulting powder was placed in the cell, heated up to 723 K under a flow of He ($30 \text{ mL}\cdot\text{min}^{-1}$) with a ramp of $10 \text{ K}\cdot\text{min}^{-1}$ and kept at this temperature for 2 h. After the sample was activated the sample was cooled down to adsorption temperature. The adsorption of pyridine was carried out at 348 K by passing a stream of saturated pyridine in He keeping the partial pressure of pyridine constant (48 mbar) until adsorption–desorption equilibrium was attained. After pyridine adsorption, the sample was purged in He at 348 K for 30 min, and DRIFT spectra were recorded. Same procedure was performed for CO_2 adsorption. The spectra of background (after the thermal treatment) and after/during sorption of the probe molecule were collected as an average of 200 scans at 4 cm^{-1} resolution.

3.3 Results and discussion

3.3.1 XRD

3.3.1.1 Hydrotalcite precursors of mixed metal oxides

The ordered layer structure characteristic of hydrotalcite was confirmed for all precursors of the mixed metal oxides (Mg-Al, Mg-Fe, Zn-Al, Zn-Fe) examined in this work. Figure 3.1 shows the X-ray diffraction patterns of the as-synthesized materials. As-synthesized Zn-Al, Mg-Al, and Mg-Fe materials showed d-spacing values and reflection peaks which are characteristic of hydrotalcite materials as indicated in JCPDS file No. 14-0191 (sharp intense reflections of (003), (006) planes in the angle region ($2\theta < 25^\circ$), broad reflections of (012), (015) and (018) planes in the middle angle region ($2\theta = 30\text{-}50^\circ$) and sharp reflections of (110), (113) and (116) planes in the high angle region ($2\theta = 55\text{-}65^\circ$)). The XRD pattern

of as-synthesized Zn-Fe is notably different from the other hydroxalate materials, but it is similar to SO_4 -LDH reported by Zhang et al. [7]. The difference stems from the anion in the structure caused by the use of Na_2CO_3 for Zn-Fe synthesis instead of NaOH for the other materials. We observed that hydroxalate structure cannot be formed with NaOH for Zn-Fe and the incorporation of CO_3^{2-} anion in Zn-Fe matrix was apparently necessary to form ordered layered material for this combination of cations.

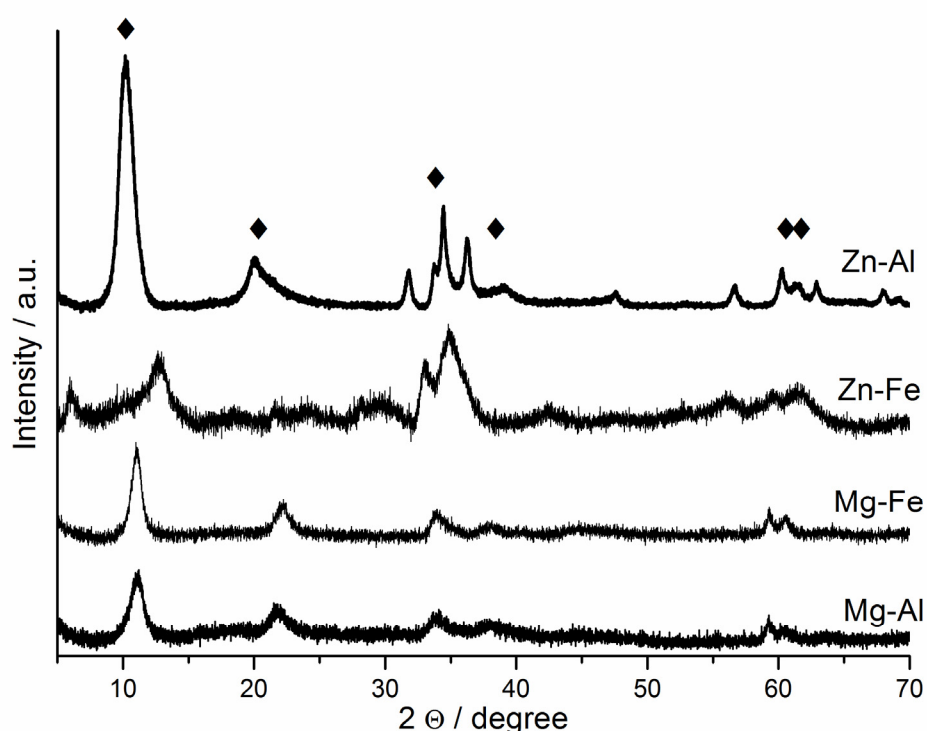


Figure 3.1. XRD patterns of hydroxalate precursors. Characteristic layered double hydroxide (LDH) phase is indicated with \blacklozenge symbol.

3.3.1.2 Single metal oxides and hydroxalate-derived mixed metal oxides

For the single metal oxides (Figure 3.2), the XRD pattern of ZnO was well characterized by the hexagonal wurtzite phase with characteristic peaks at 31.7,

34.2, and 36.1° (JCPDS: 36-1451). MgO showed clearly the cubic periclase phase ($2\theta = 36.7, 42.8, 62.1^\circ$, JCPDS: 45-0946) and Fe_2O_3 was crystallized in the hematite phase ($2\theta = 24.5, 33.2, 35.7, 40.9, 49.5, 54.1, 62.5, 64.1^\circ$, JCPDS: 33-0664). Al_2O_3 showed low crystallinity with characteristic peaks of γ phase ($2\theta = 37.0, 45.6$ and 67.1° , JCPDS: 29-0063).

After calcination at 725 K, the hydrotalcite structure is destroyed with formation of new phases as shown in Figure 3.2. The calcined materials showed the presence of oxides of bivalent cation (Zn^{2+} or Mg^{2+}) as the major crystalline phase (hexagonal wurtzite or cubic periclase structure, respectively, Table 3.1) due to the ratio of 3 for M_b^{2+}/M_t^{3+} in the hydrotalcite structure. Zn-Al and Zn-Fe mixed oxides revealed the presence of hexagonal ZnO phase. For Mg-Al and Mg-Fe mixed oxides, the cubic periclase phase of MgO was well recognized. In all Al- and Fe-containing materials, there was no aluminum oxide and iron oxide phases detected, implying the well incorporation and thus high dispersion of these metal ions in the oxide structures.

The XRD pattern of Zn-Fe reveals the reflections of zinc franklinite (ZnFe_2O_4), which is a single phase spinel-type structure consistent with the JCPDS card (22-1012), in addition to the hexagonal ZnO phase. The characteristic reflections of (111), (220), (311), (400), (422), (511), and (440) of the spinel structure were well recognized. Similar phase was reported by Zhao et al. [8]. They observed the phase for Zn-Fe mixed oxides prepared by the mechanical mixing of the corresponding metal precursors prior to a calcination treatment. This is in contrast to the results of Mg-Fe which showed mainly the reflections of cubic periclase phase of MgO and no such single mixed phase could be identified.

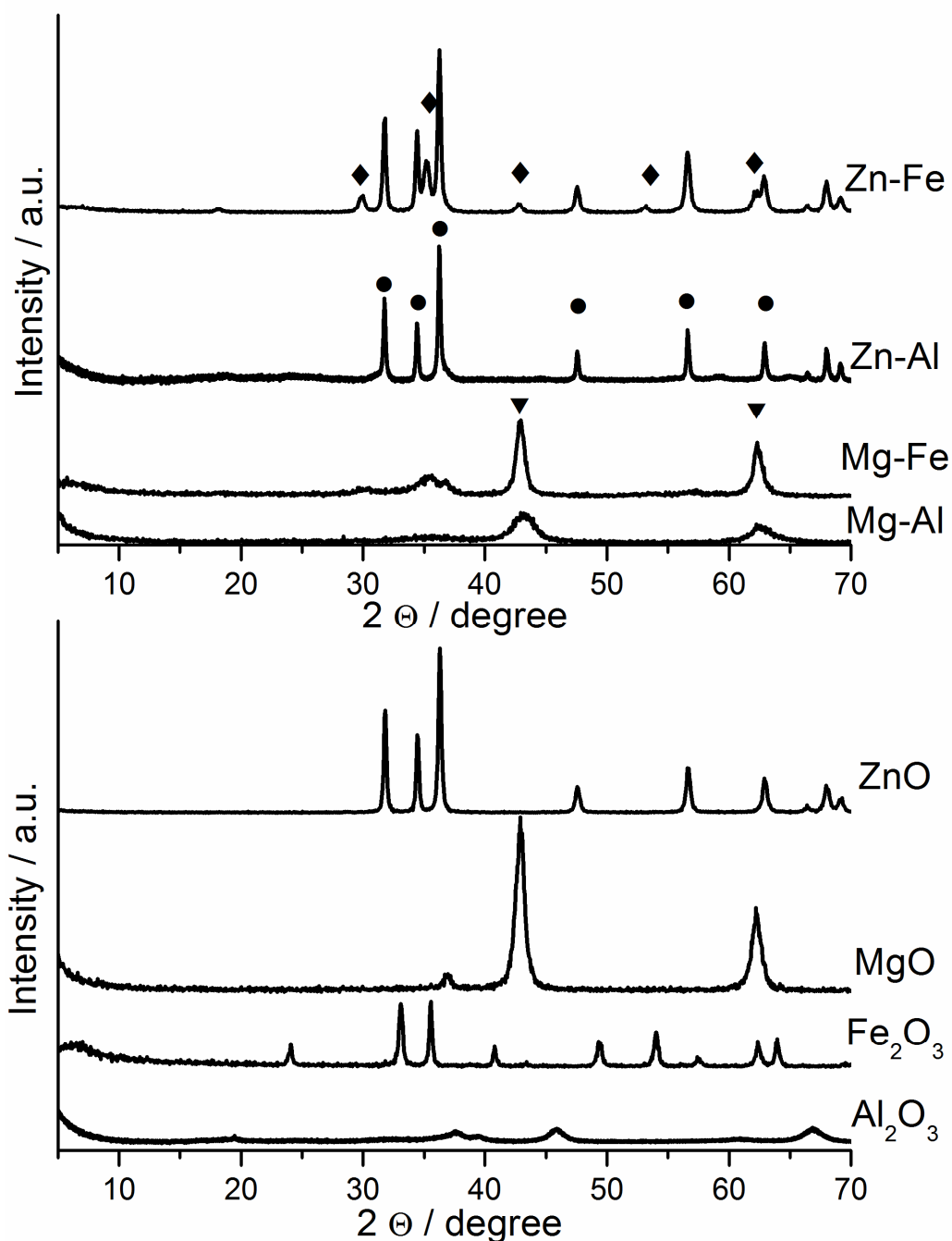


Figure 3.2. XRD patterns of calcined metal and mixed oxides. The symbols indicate the following crystal phases: ● hexagonal wurtzite phase of ZnO, ▼ cubic periclase phase of MgO and ◆ Franklinite ZnFe₂O₄.

3.3.2 Textural property

Specific surface areas of the metal oxides are presented in Table 3.1. The order of the values was Al₂O₃ > MgO > Fe₂O₃ > ZnO for the single metal oxides.

For the mixed metal oxides, the major contributions made by the bivalent ions (Zn^{2+} and Mg^{2+}) to the surface areas were obvious. The trends in lowering or enhancing surface area given by the trivalent ions (Al^{3+} and Fe^{3+}) were also clearly visible and consistent with those observed for the corresponding single metal oxides.

3.3.3 CO_2 - and NH_3 -TPD

The strength as well as the total amount of basic and acidic sites of the single and mixed metal oxides were characterized by TPD of CO_2 and NH_3 , respectively. The amount of desorbed gases, corresponding to the amount of basic and acidic sites, is reflected in the peak area, whereas desorption peak temperature indicates the strength of acidic and basic sites. Figure 3.3 presents the desorption profiles of CO_2 and NH_3 from the thermal treated catalysts (in He at 723 K). The quantified results are summarized in Table 3.1. TPD was performed up to 723 K which is the same temperature as that used in the pretreatment before catalytic testing in order to characterize relevant acidity and basicity of the catalysts in the reaction.

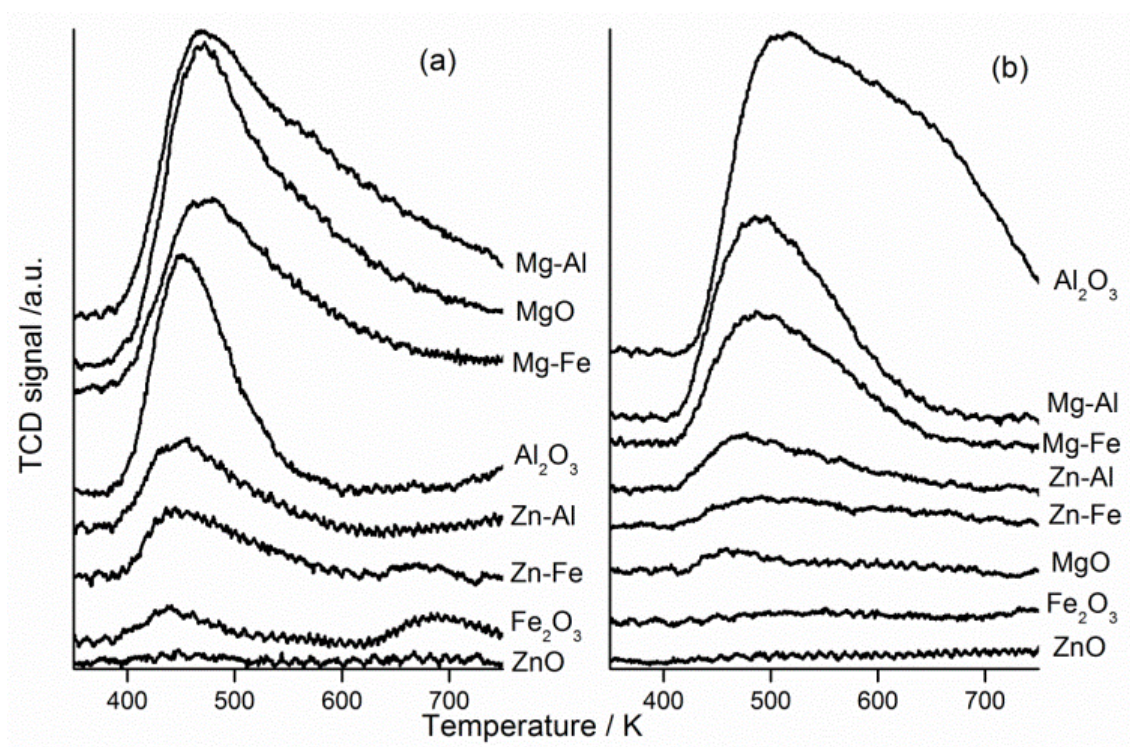


Figure 3.3. (a) CO₂- and (b) NH₃-TPD profiles of the metal oxides.

Table 3.1. BET surface area, the amount of acidic and basic sites, and identified crystalline phases of the single and mixed metal oxides.

Catalyst	BET surface area / m ² ·g ⁻¹	CO ₂ uptake / μmol·g ⁻¹	NH ₃ uptake / μmol·g ⁻¹	Crystalline phase
Al ₂ O ₃	294	2.88	0.61	γ-Al ₂ O ₃
ZnO	4	0.31	0.01	wurtzite
MgO	165	6.27	0.02	periclase
Fe ₂ O ₃	25	1.00	0.01	hematite
Zn-Al	36	1.40	0.07	ZnO (wurtzite)
Zn-Fe	21	0.44	0.06	ZnO (wurtzite), ZnFe ₂ O ₄
Mg-Al	173	6.22	0.22	MgO (periclase)
Mg-Fe	113	3.22	0.15	MgO (periclase)

All metal oxides showed CO₂ desorption peaks with the maxima at ca. 453 K. The Mg-containing materials, MgO, Mg-Al and Mg-Fe, exhibited a broad

CO₂ desorption peak over a wide temperature range of 373-673 K with a maximum at 473 K, indicating the presence of a large number of basic sites with different strengths (weak, moderate and strong sites) [9]. Zn-Al, ZnO, and Al₂O₃ showed narrower desorption peaks, compared to the Mg-containing materials, with the maxima at slightly lower temperatures of ca. 443 K. The differences indicate weaker and less types of available surface basic sites for Zn-Al, ZnO, and Al₂O₃. In contrast, CO₂ desorption profiles of Zn-Fe and more notably of Fe₂O₃ showed an additional peak at a higher temperature of ca 683 K, implying the presence of very strong surface basic sites besides the weaker ones for these two Fe-containing materials.

NH₃-TPD study of these materials clearly showed that Al₂O₃, with the largest and broadest peaks of all samples examined, has highly acidic character with different (weak and strong) types of acidic sites. On the contrary, other single metal oxides (MgO, ZnO, and Fe₂O₃) showed very small or negligible NH₃ desorption peaks, indicating poor availability of surface acidic sites. However, it is interesting to observe that when Al³⁺ or Fe³⁺ cations are introduced to ZnO (i.e. Zn-Al, Zn-Fe), the acidity and basicity became more prominent as confirmed by a larger peak of NH₃ and CO₂ desorption (Figure 3.3 and Table 3.1). Similar enhanced acidity and basicity by incorporation of foreign metal ions to metal oxide structure have been reported [10]. Also, total amount of acidic sites of MgO was improved by incorporation of Al³⁺ and Fe³⁺ cations (i.e. Mg-Al, Mg-Fe). These results show that introducing metal cation(s) in a single metal oxide can enhance surface acid-base properties.

3.3.4 DRIFTS characterization of surface acidity and basicity

3.3.4.1 Pyridine adsorption

According to the previous reports Lewis acidic sites are crucial in the transesterification of urea [10a], therefore discrimination between Brønsted and

Lewis sites is probably important in characterization of active sites. Pyridine is a popular IR probe molecule to distinguish Lewis and Brønsted acidic sites of metal oxide surfaces at room and higher temperature regimes, due to the following advantages.

- (i) more selective and stable than NH_3 ;
- (ii) much more strongly adsorbed than CO and CH_3CN ;
- (iii) more sensitive to the strength of Lewis acidic sites than NO [11].

The ring deformation vibrations in the region between 1400 and 1700 cm^{-1} are used to discriminate between pyridine molecules adsorbed on Brønsted acidic sites (BPy), Lewis acidic sites (LPy) and interacting via hydrogen-bonding with the surface (HPy). In this part of the spectrum, pyridine has strong IR absorption, i.e. ν_{8a} , ν_{8b} , ν_{19a} and ν_{19b} following Wilson's mode number for the assignment of the vibrations of benzene [12]. These ring vibrational modes 19a, 19b, 8a and 8b, especially modes 8a and 19b according to the assignment of Kline and Turkhevich, are the most sensitive vibrations with regard to the nature of intermolecular interactions via the nitrogen lone pair electrons [13]. The assignment of the vibrational modes of pyridine adsorbed on different sites is presented in Table 3.2.

Figure 3.4 shows FTIR spectra of adsorbed pyridine on mixed and metal oxides. After evacuation at 348 K all samples exhibit primarily Lewis acidity and the characteristic vibrations of LPy and HPy species were found. The bands attributed to the adsorption on Brønsted acidic sites were not observed for all samples.

Table 3.2. Vibrational frequencies of the infrared modes of pyridine used in the characterization of surfaces [14].

Mode	Lewis sites (LPy)	Brønsted sites (BPy)	Hydrogen-bonded (HPy)
	/ cm ⁻¹	/ cm ⁻¹	/ cm ⁻¹
8a	1600-1633	1640	1590-1600
8b	1580	1620	1580-1590
19a	1488-1503	1485-1500	1485-1490
19b	1447-1460	1540	1440-1447

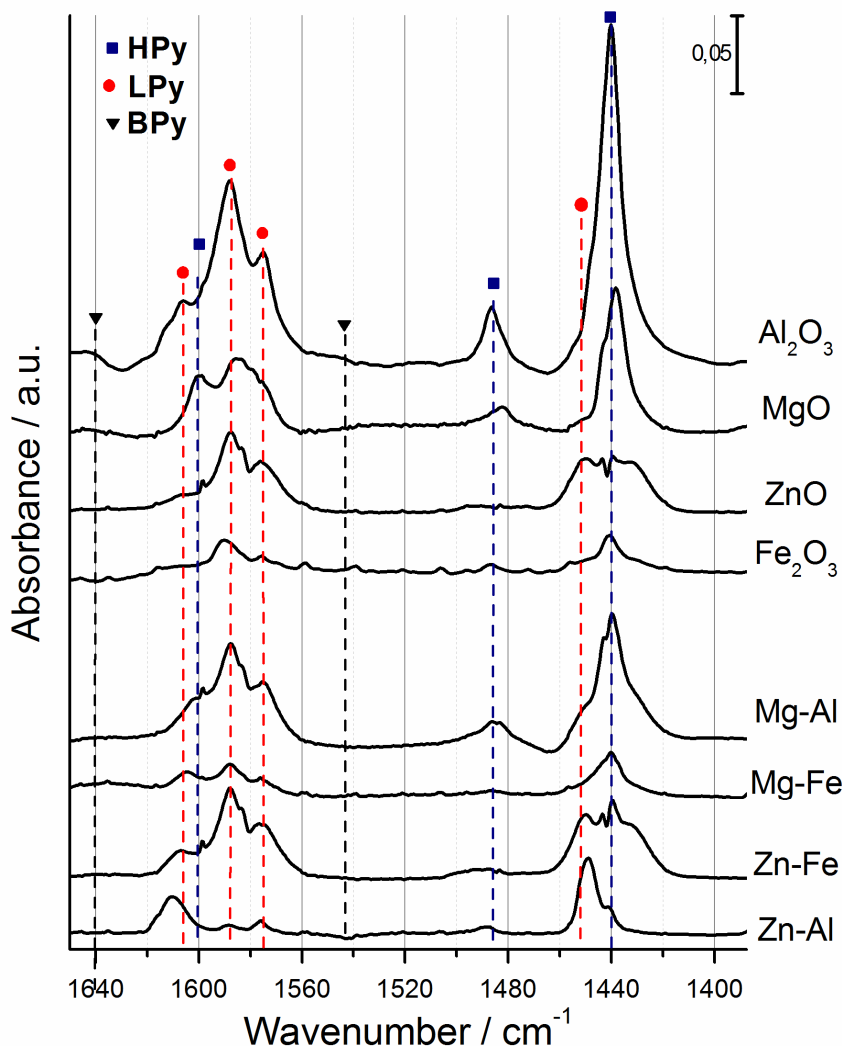


Figure 3.4. DRIFT spectra of adsorbed pyridine on metal oxides.

Two types of acidic sites can be discriminated: one resulting in weakly hydrogen-bonded Py species and the other resulting in strongly chemisorbed Py species on Lewis acidic sites. Characteristic bands displayed for all materials at around 1608, 1588, 1575 and 1450 cm^{-1} correspond to ν_{8a} and ν_{19b} vibrational modes of pyridine molecule and indicate the presence of strong acidic sites. On the other hand, the bands observed at 1443, 1483 and 1600 cm^{-1} are ascribed to hydrogen-bonded pyridine. The observed IR bands and their assignment are summarized in Table 3.3.

Table 3.3. Bands assignment of adsorbed pyridine over metal oxides.

IR bands	Adsorbed species	$\nu(\text{CCN})$ vibration mode	Reference
1610-1608	LPy	8a	[15]
1600	HPy	8b	[16]
1588	LPy	8a	[17]
1575	LPy	8a, 8b	[16, 18]
1485	HPy	19a	[16, 19]
1450	LPy	19b	[13, 15]
1443-1440	HPy	19b	[13, 15]

According to Busca [17] the position of the most sensitive 8a mode of pyridine (1600–1633 cm^{-1}) roughly correlates with the polarizing power of the adsorbant cation and consequently the strength of acidic site. Peak position of 8a mode shifted in the order Zn-Al>Zn-Fe>Al₂O₃>Mg-Fe indicating decrease in acidic strength in the same order. ZnO and Mg-Al displayed less pronounced band at lower frequencies, implying weak acidity of the materials. Metal oxides Fe₂O₃ and MgO have adsorption bands around 1600 cm^{-1} , attributed to weakly hydrogen-bonded pyridine.

3.3.4.2 CO₂ adsorption

The chemical state of surface oxygen bonded to adsorbed CO₂ species gives an indication of basic site structure and strength. Three species of adsorbed CO₂ were detected reflecting three different types of surface basic sites. Unidentate carbonate formation requires surface O²⁻ ions and exhibits a symmetric O–C–O stretching at 1360–1400 cm⁻¹ and an asymmetric O–C–O stretching at 1510–1560 cm⁻¹. Bidentate carbonate forms on a Mⁿ⁺-O²⁻ pair site where Mⁿ⁺ is a metal cation and shows a symmetric O–C–O stretching at 1320–1340 cm⁻¹ and an asymmetric O–C–O stretching at 1610–1630 cm⁻¹. Bicarbonate species formation involves surface hydroxyl groups. Bicarbonates show a C–OH bending mode at 1220 cm⁻¹ as well as symmetric and asymmetric O–C–O stretching at 1480 cm⁻¹ and 1650 cm⁻¹, respectively [20].

The IR spectra of adsorbed CO₂ on metal and mixed oxides are shown in Figure 3.5.

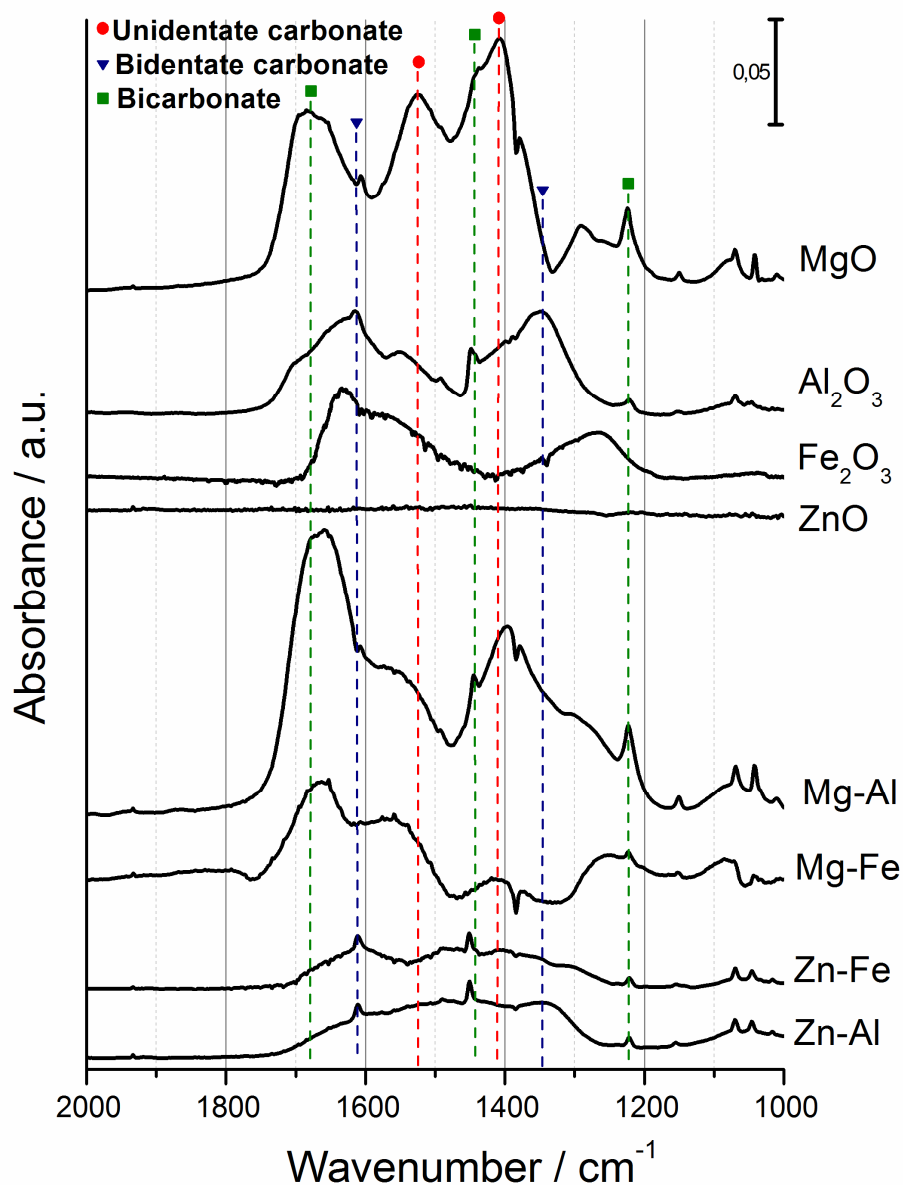


Figure 3.5. DRIFT spectra of adsorbed CO₂ on metal oxides.

Intense bands attributed to unidentate carbonate species of adsorbed CO₂ were observed on the surface of MgO, Mg-Al, Mg-Fe, and less intense bands were detected over Al₂O₃ and Fe₂O₃, indicating that these materials have strong basic sites. Signals of carbonate species adsorbed over moderate and weak basic sites were also found on these metal oxides. In contrast, Zn-Al and Zn-Fe showed characteristics of basic sites only of weak and moderate strength according to bands of bidentate carbonate and bicarbonate observed.

3.4 Conclusions

Prepared by the co-precipitation method, metal mixed oxides were synthesized, deriving from the calcination treatment of hydrotalcites precursors. The hydrotalcite structure was confirmed by the XRD study of as-synthesised materials. All calcined materials showed the presence of oxides of bivalent cation (Zn^{2+} or Mg^{2+}) as the major crystalline phase due to the ratio of 3 for $\text{M}_b^{2+}/\text{M}_t^{3+}$ in the hydrotalcite structure. Zn-Fe mixed oxide exhibited an additional phase of zinc franklinite (ZnFe_2O_4). The advantage of hydrotalcite precursors was demonstrated by the analysis of surface area.

The most important characteristic of the metal oxide catalysts for urea transesterification is expected to be their acid-base properties. The total amount of acidic and basic sites and their strength were evaluated by TPD of CO_2 and NH_3 . The materials presented diverse acid-base character, showing successfully that the introduction of a foreign metal cation in a single metal oxide can enhance the variety of surface acid-base properties, indicating advantage of mixed oxides over one-component metal oxides

The nature of acidic and basic sites was characterized by DRIFT spectroscopy of adsorbed probe molecules, pyridine and CO_2 , respectively. The presence of Lewis acidic sites was confirmed for all samples. Analysis of adsorbed CO_2 species indicated the presence of basic sites of weak, moderate and strong character in Mg-containing Al_2O_3 and Fe_2O_3 , whereas Zn-containing oxides exhibited only weak and moderate basic sites.

The obtained information about the acidity and basicity was further used in finding correlation with catalytic performance and in elucidating the function of acidic and basic sites in urea transesterification with EG as demonstrated in the following chapters.

References

1. Brunauer S.; Emmett P.H.; Teller, E., *J. Am. Chem. Soc.* 1938, 60 (2), 309-319.
2. (a) Azaroff L. V. ; Burger, L. E., *The Powder Method in X-ray Crystallography*. McGraw-Hill: New York, 1985; (b) Guinier, A., *X-ray Diffraction in Crystals, Imperfect Crystals and Amorphous Bodies*. Freeman: San Francisco, 1963; (c) Warren, B. F., *X-ray Diffraction*. Addison-Wesley, Reading: MA, 1969; (d) Roll, C., *Diffraction Physics*, 3rd Ed. North-Holland: Amsterdam, 1995; (e) Young, R. A., *The Rietveld Method*. International Union of Crystallography, Oxford University Press: Oxford, 1993.
3. (a) Sharma, S. B.; Meyers, B. L.; Chen, D. T.; Miller, J.; Dumesic, J. A., *Appl. Catal. A.-Gen* 1993, 102 (2), 253-265; (b) Farneth, W. E.; Gorte, R. J., *Chem. Rev.* 1995, 95 (3), 615-635; (c) Gorte, R. J., *Catal. Lett.* 1999, 62 (1), 1-13.
4. (a) Di Cosimo, J. I.; Torres, G.; Apesteguía, C. R., *J. Catal.* 2002, 208 (1), 114-123; (b) Li, J.; Davis, R. J., *Appl. Catal. A.-Gen* 2003, 239 (1-2), 59-70; (c) Li, J. H.; Davis, R. J., *J. Phys. Chem. B* 2005, 109 (15), 7141-7148.
5. (a) Paukshtis E. A. ; Yurchenko, E. N., *Russ. Chem. Rev.* 1983, 52, 42; (b) Kung, M. C.; Kung, H. H., *Catal. Rev.* 1985, 27 (3), 425-460; (c) Davydov, A. A., *Molecular Spectroscopy of Oxide Catalyst Surfaces*. Wiley: New York, 2003; (d) Paukshtis, E. A., *IR Spectroscopy in Heterogeneous Acid-Base Catalysis*. Nauka: Novosibirsk, 1992.
6. García-Sancho, C.; Moreno-Tost, R.; Mérida-Robles, J. M.; Santamaría-González, J.; Jiménez-López, A.; Maireles Torres, P., *Catal. Today* 2011, 167 (1), 84-90.
7. Zhang, H.; Wen, X.; Wang, Y. X., *J. Solid State Chem.* 2007, 180 (5), 1636-1647.
8. Zhao, X.; An, H.; Wang, S.; Li, F.; Wang, Y., *J. Chem. Technol. Biotechnol.* 2008, 83 (5), 750-755.

9. (a) Di Serio, M.; Ledda, M.; Cozzolino, M.; Minutillo, G.; Tesser, R.; Santacesaria, E., *Ind. Eng. Chem. Res.* 2006, 45 (9), 3009-3014; (b) Menezes, A. O.; Silva, P. S.; Hernandez, E. P.; Borges, L. E. P.; Fraga, M. A., *Langmuir* 2010, 26 (5), 3382-3387.
10. (a) Climent, M. J.; Corma, A.; De Frutos, P.; Iborra, S.; Noy, M.; Velty, A.; Concepción, P., *J. Catal.* 2010, 269 (1), 140-149; (b) Wang, H.; Yang, Y.; Xu, J.; Wang, H.; Ding, M.; Li, Y., *J. Mol. Catal. A: Chem.* 2010, 326 (1-2), 29-40.
11. Ferwerda, R.; Van der Maas, J. H.; Van Duijneveldt, F. B., *J. Mol. Catal. A-Chem.* 1996, 104 (3), 319-328.
12. Wilson, E. B., *Phys. Rev.* 1934, 45 (10), 0706-0714.
13. Kline, C. H.; Turkevich, J., *J. Chem. Phys.* 1944, 12 (7), 300-309.
14. Emeis, C. A., *J. Catal.* 1993, 141 (2), 347-354.
15. Akcay, M.; Yurdakoc, M.; Tonbul, Y.; Yurdakoc, K.; Honicke, D., *Spectrosc. Lett.* 1998, 31 (8), 1719-1732.
16. Urena, F. P.; Gomez, M. F.; Gonzalez, J. J. L.; Torres, E. M., *Spectrochim. Acta Mol. Biomol. Spectrosc.* 2003, 59 (12), 2815-2839.
17. Busca, G., *Catal. Today* 1998, 41 (1-3), 191-206.
18. Klots, T. D., *Spectrochim. Acta Mol. Biomol. Spectrosc.* 1998, 54 (10), 1481-1498.
19. Partal, F.; Fernandez-Gomez, M.; Lopez-Gonzalez, J. J.; Navarro, A.; Kearley, G. J., *Chem. Phys.* 2000, 261 (1-2), 239-247.
20. Di Cosimo, J. I.; Diez, V. K.; Apesteguia, C. R., *Appl. Clay Sci.* 1998, 13 (5-6), 433-449.

Chapter 4

Understanding the Role of Acidic and Basic sites

4.1 Introduction

In this chapter, catalytic performance of single and mixed metal oxides with distinct acid-base properties described in Chapter 3 is evaluated to gain detailed insights into the role of acidic and basic sites in every reaction step of urea transesterification with EG. Previously several attempts have been made to investigate comprising steps of urea transesterification with glycols [1], but the reaction pathway, more precise product distribution and role of acid-base sites driving each reaction step still remain unclear. In order to identify the reaction network, evolution of reactants and products was monitored by dip-in ATR-IR probe and combined with MCR. Based on the obtained chemical component spectra for identification and their concentration profiles, kinetics of the reactions were studied and correlated with the acidity and basicity of the materials investigated. The detailed procedure of MCR was described in Chapter 2.

4.2 Experimental section

Transesterification of urea with EG as well as reference reactions starting from the intermediates and products identified in the transesterification reaction were performed in a 25 mL three-necked-flask equipped with a magnetic stirrer and a reflux condenser. For the urea transesterification with EG, the reactor was initially charged with 89.51 mmol of EG and heated to the reaction temperature of 413 K. Subsequently, 8.33 mmol of urea and 0.16 g of catalyst (equivalent to 3 wt% of EG) was added to the solution and this point was considered as the starting point of the reaction. Catalyst material was pretreated at 723 K for 2 h under He flow prior to the catalytic testing and it was readily taken to the reactor to minimize the exposure to the air. All reactions were performed for 6 h under N₂ flow (0.5 L·min⁻¹) to remove formed gaseous ammonia which negatively affects the reaction performance. After 6 h of the reaction, the reactor was cooled to

room temperature, the solid catalyst was separated from the solution by filtration, and the chemical components of reaction mixture were identified by means of GC-MS and quantified by GC analysis. In case of the reactions starting from intermediates and products, 4.28 mmol of 2-HC, 5.11 mmol of EC, or 5.17 mmol of 2-Ox was charged into the reactor instead of urea, and the reactions were performed under identical condition.

Product selectivity was calculated without taking into account the amount of 2-HC because other products are derived from 2-HC and neglecting 2-HC selectivity helps understand the preferred paths of the reactions. For the reaction of urea transesterification with EG as well as the reaction of 2-HC in EG, product selectivity was determined by Formula 4.1.

$$S_{\text{product}} = \frac{[\text{product}]}{[\text{EC}] + [2\text{-Ox}] + [\text{DEG}] + [\text{TEA}] + [3 - (2\text{-EtOH}) - 2\text{-Ox}]} \quad (4.1)$$

In case of the reaction of 2-Ox with EG, Formula 4.2 was used to obtain product selectivity.

$$S_{\text{product}} = \frac{[\text{product}]}{[2\text{-Ox}] + [\text{TEA}] + [3 - (2\text{-EtOH}) - 2\text{-Ox}]} \quad (4.2)$$

Yield of EC was expressed by the molar amount of EC produced per gram of catalyst due to inaccurate quantification of EG and urea caused by the excess of EG used and possible decomposition of urea into NH_3 and CO_2 during the reaction.

In all the reactions examined in this work, the reaction mixture was also monitored *in situ* with the dip-in ATR-IR spectroscopic probe (Chapter 2) by immersing the probe into the reaction solution.

4.3 Results and discussion

4.3.1 Catalytic test of overall reaction

Table 4.1 lists the product selectivity in the absence of a catalyst (blank) and in the presence of the metal oxides.

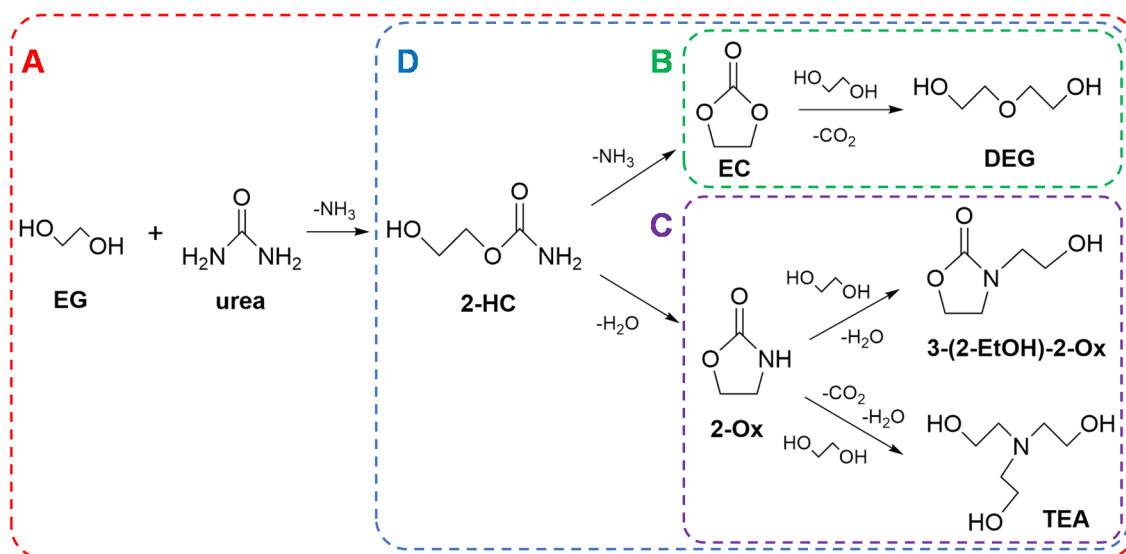
Table 4.1. Product selectivity in urea transesterification with EG. Only products formed after 2-HC in the reaction paths were considered (see Scheme 2, thus the amount of 2-HC was not taken into account in the selectivity calculation).

Catalyst	$Y_{EC} /$ $\text{mmol}\cdot\text{g}^{-1}_{\text{cat}}$	$S_{EC} /$ %	$S_{2\text{-Ox}} /$ %	$S_{\text{DEG}} /$ %	$S_{3\text{-(2-EtOH)-2-Ox}} /$ %	$S_{\text{TEA}} /$ %
blank	8.6	86.5	9.5	2.6	1.5	0
Al ₂ O ₃	8.6	96.4	2.9	0	0	0
ZnO	18.4	73.7	15.9	5.1	3.5	1.8
MgO	19.4	83.2	8.3	4.1	3.0	1.5
Fe ₂ O ₃	8.3	88.1	4.6	7.3	0	0
Zn-Al	20.1	82.0	9.7	4.0	2.8	1.6
Zn-Fe	25.9	91.5	5.1	3.5	0	0
Mg-Al	1.5	12.1	48.8	21.8	9.1	8.2
Mg-Fe	11.1	64.9	15.3	13.3	4.3	2.3

Reactions were performed at 413 K for 6 h starting with 89.51 mmol of EG, 8.33 mmol of urea, and 0.16 g of catalyst or without catalyst (blank) under N₂ flow (0.5 L·min⁻¹).

Besides the major reaction path and products generally reported [1a, 1b, 2] and described in Scheme 1.2, there were three other products identified. The first one is diethylene glycol (DEG) forming via the secondary ring-opening reaction of EC with EG accompanying a release of CO₂ (box B in Scheme 4.1). The other two products found in this work were 3-(2-hydroxyethyl)-2-oxazolidinone (3-(2-EtOH)-2-Ox)) and triethanolamine (TEA) via the reaction of 2-Ox with EG (box C in Scheme 4.1). Bhanage [1a] reported secondary product formation possibly from both EC and 2-Ox with EG, yielding 1-(2-hydroxyethyl)-2-imidazolidone and 3-(2-EtOH)-2-Ox. Besides, in a rare case a minor amount of ethylene urea (2-imidazolidone) was also found. In this work, 1-(2-hydroxyethyl)-2-imidazolidone and ethylene urea were not detected and, instead, DEG and TEA were newly identified. As shown later, the reaction paths towards DEG from EG

(box B) and 3-(2-EtOH)-2-Ox and TEA from 2-Ox (box C) shown in Scheme 4.1 were verified by testing the reactions starting from EC and 2-Ox with EG, respectively.



Scheme 4.1. Urea transesterification with EG: Identified reaction pathways.

It is important to note that the reaction could proceed without catalyst to a moderate extent with relatively high EC selectivity of 86.5% with $8.6 \text{ mmol} \cdot \text{g}_{\text{cat}}^{-1}$ EC yield and low but considerable (ca. 10%) selectivity to 2-Ox besides minor formation of DEG and 3-(2-EtOH)-2-Ox under the reaction condition of this work after 6 h (Table 4.1). In contrast, Li [2] reported that without catalyst no 2-Ox was found and EC yield was relatively low after 3 h of the reaction at 423 K under vacuum (11 kPa) starting from 0.75 mol of EG and 0.5 mol of urea with 0.9 g of catalyst.

The type of metals in the catalyst and how the metal ions are combined in the mixed metal oxides drastically affected both EC yield and product selectivity (Table 4.1). Regarding EC selectivity, most materials showed relatively high values except Mg-containing mixed metal oxides (Mg-Al and Mg-Fe). For these oxides, the selectivity to all undesired side products were very high, reaching even 48.8% 2-Ox for Mg-Al. On the contrary, MgO showed high EC selectivity (83.2%). This indicates that Mg is not the sole factor to lower the EC selectivity.

Al_2O_3 showed the highest EC selectivity (96.4%) of all materials tested with a clearer product distribution; only 2-Ox as a single side product.

The best catalytic performance in terms of EC yield was obtained for Zn-Fe showing $25.9 \text{ mmol}\cdot\text{g}_{\text{cat}}^{-1}$. The material effectively suppressed the formation of 2-Ox (5.1%) and the secondary reaction products, DEG, 3-(2-EtOH)-2-Ox, and TEA (the formation of the last two products was fully suppressed). The other Zn-containing mixed metal oxide, Zn-Al, showed also high EC yield, but there were noticeable increase in selectivity towards 2-Ox as well as secondary reaction products.

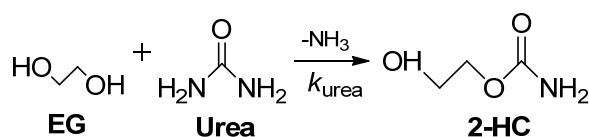
Furthermore, *in situ* IR monitoring of reaction solution together with GC and MCR spectral analyses (Chapter 2) was employed to investigate the reaction pathways and kinetics. The MCR analysis facilitated to extract comprehensive and quantitative concentration profiles of the major reactants, intermediates, and products during the course of the reaction for different catalyst materials. Performing the IR monitoring with the help of secondary reaction studies (testing the reaction from intermediate products) and product identification confirmed that urea transesterification with EG to EC is a consecutive two-step process and also EC as well as 2-Ox can react further with EG (box B and C in Scheme 4.1).

To rationalize the factors influencing the reactivity and product selectivity at each reaction step, we divided and looked into the overall reaction with wider and narrower scope of comprising reactions (Scheme 4.1): (A) overall reaction of urea transesterification, (B) EC decomposition with EG, (C) 2-Ox reaction with EG, and (D) 2-HC reaction in EG in the absence of urea. All reactions A-D were monitored by the dip-in IR probe and products were identified and quantified by GC. Thus obtained concentration profiles of urea and products were used in determination of reaction orders, reaction rate constants (k), and kinetic modeling of transesterification steps and overall process. Furthermore, the k values calculated for the single reaction steps were used for the rationalization of catalytic performance in relation to the amount of acidic and basic sites and also

for the comparison with the k values estimated from the overall reaction where the presence of other reactants and products may influence the kinetics of specific reaction paths.

4.3.2 Separate study of reaction paths

4.3.2.1 Reaction of urea with EG



Reaction was assumed irreversible and all urea was assumed to lead to 2-HC after the reaction with EG. Based on the concentration profiles, it was identified that the reaction is of a second order, whose rate is proportional to the square of the concentration of urea: $\frac{dC_{\text{urea}}}{dt} = -k_{\text{urea}}C_{\text{urea}}^2$

Integrated rate law describes the concentration of the reactant at a given time by Equation 4.3:

$$\frac{1}{C_{\text{urea}}} = \frac{1}{C_{\text{urea},0}} + k_{\text{urea}}t \quad (4.3)$$

According to the integrated rate law for a second-order reaction, a plot of $\frac{1}{C_{\text{urea}}/C_{\text{urea},0}}$ versus t is a straight line, as shown in part (b) in Figure 4.1.

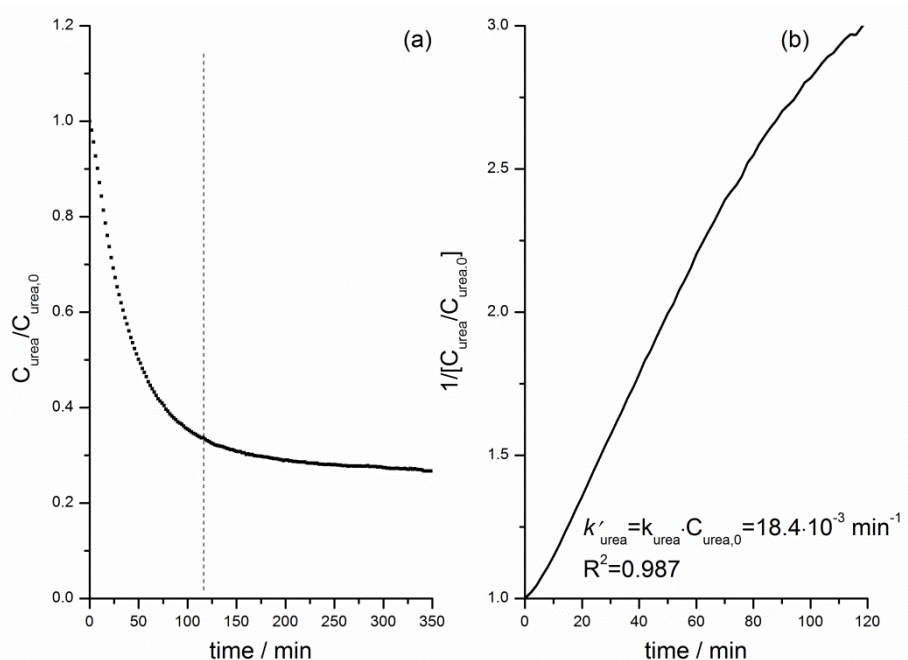


Figure 4.1. Determination of order and rate constant k for reaction of urea with EG in the presence of Zn-Fe catalyst. The straight line in (b) is expected for a second-order reaction.

The slope of straight line gives us reaction rate constant $k'_{\text{urea}} = k_{\text{urea}} \cdot C_{\text{urea},0}$, which was calculated for all catalysts and results are listed in Table 4.2.

Table 4.2. Rate constants k for reaction between urea and EG.

Catalyst	blank	Al ₂ O ₃	ZnO	MgO	Fe ₂ O ₃	Zn-Al	Zn-Fe	Mg-Al	Mg-Fe
$k'_{\text{urea}} \cdot 10^{-3}$ /min ⁻¹	7.5	8.9	14.6	15.4	10.8	16.9	18.4	14.4	19.4
R ²	0.979	0.994	0.987	0.982	0.988	0.991	0.987	0.961	0.990

We sought for the catalyst properties showing best correlated and compared with the reaction rate constant and identified that the total amount of acidic sites shows a trend with the rate constant (Figure 4.2).

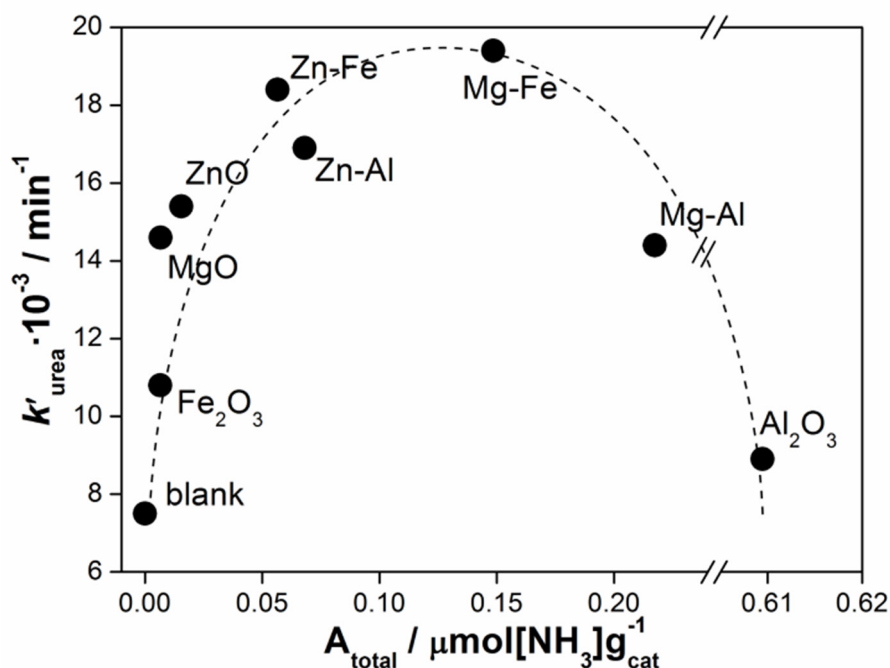


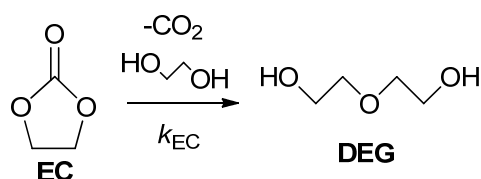
Figure 4.2. Urea reaction rate constant against the total amount of acidic sites in urea transesterification with EG. Dashed lines serve to guide the eyes only.

The reaction rate increases when surface of catalyst contains more acidic sites; however if catalyst surface possesses too many and/or too strong acidic sites, urea reaction rate decreases as observed for Mg-Al and Al_2O_3 . Al_2O_3 showed the lowest urea reaction rate due to the high concentration of acidic sites and their over-strong character. Li et al. [3] concluded that the reaction between diols and urea was inhibited over acidic oxides to some extent, due to the formation of steady ligand between O and N of urea and metal cation, which is in good agreement with our observation. Urea can be considered as an electron-pair donor and a weak basic molecule [4]. As will be reported in Chapter 7, urea interacts with and can adsorb strongly on the acidic sites of catalyst (surface metal atoms of metal oxides) via coordination of O atom of the carbonyl group. Through such strong interactions of surface acidic sites and urea, surface catalytic sites might be poisoned for further reactions. This well explains the

observed lower reaction rate of urea (Figure 4.2) when the catalyst contains more and stronger acidic sites.

4.3.2.2 Reaction of EC with EG

As described earlier, the desired target product, EC, reacts with EG, forming DEG accompanying a release of CO₂. This reaction takes place even in the absence of catalyst (Table 4.1) and should be avoided. Although the excess of EG present in the system as solvent makes prevention of this reaction path difficult, it is possible to fully suppress the formation of DEG as observed for Al₂O₃ (Table 4.1). In order to understand the nature of reaction in the light of the acidity and basicity of the catalysts, we investigated the reaction path (box B, Scheme 4.1, also shown below) by means of catalytic testing combined with *in situ* IR monitoring using all the catalysts.



The reaction was assumed irreversible and was best matching apparently as a first order on EC concentration (Equations 4.3-4.5)-

$$\frac{dC_{EC}}{dt} = -k_{EC}C_{EC} \quad (4.4)$$

$$\ln(C_{EC}) = \ln(C_{EC,0}) - k_{EC}t \quad (4.5)$$

The plot of the natural logarithm of EC versus time is linear as shown in Figure 4.3 (b) taking Zn-Fe as an example. The slope of the straight line gives the reaction rate constant k_{EC} , which was calculated for all catalysts and results are summarized in Table 4.3.

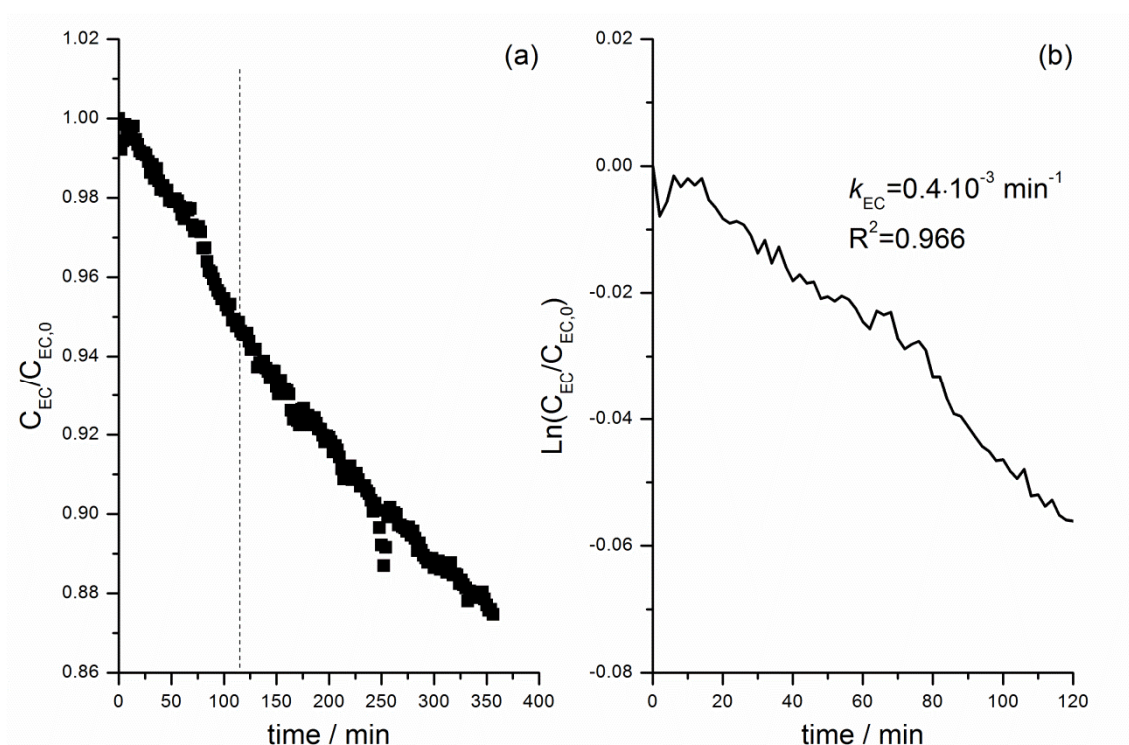


Figure 4.3. Determination of order and rate constant k for reaction of EC with EG in the presence of Zn-Fe catalyst. The straight line in (b) is expected for a first-order reaction.

Table 4.3. Rate constants k for reaction between EC and EG

Catalyst	blank	Al ₂ O ₃	ZnO	MgO	Fe ₂ O ₃	Zn-Al	Zn-Fe	Mg-Al	Mg-Fe
$k_{EC} \cdot 10^{-3}$ /min ⁻¹	0.3	0.5	0.5	1.6	2.4	0.4	0.4	2.3	1.7
R ²	0.924	0.905	0.966	0.991	0.994	0.939	0.966	0.939	0.931

Among different possibilities, good correlation between EC conversion/its rate constant k and the amount of basic sites was found. Figure 4.4 shows the plots of (a) EC conversion and (b) EC conversion rate constant against the total amount of basic sites determined by CO₂-TPD.

The EC conversion and its rate showed similar trends as expected. Clearly, the reactivity of EC with EG increases when more basic sites are available on catalyst surface. The materials with a small number of basic sites, e.g. Zn-containing materials, showed low activity in the reaction, whereas strongly basic Mg-containing materials exhibited high reactivity, even above 90% EC conversion to DEG using MgO. It is interesting to note that Fe_2O_3 showed high activity in the reaction, although it has a small amount of basic sites. The origin of the high activity might be attributed to the presence of strong basic sites as demonstrated by CO_2 -TPD analysis (Figure 3.3a). Also, Al_2O_3 showed a small but some activity in the reaction, although DEG was not observed for the reaction starting from EG and urea as mentioned above. This may be attributed the modification of acidity-basicity by the adsorption of urea and other products on the catalyst surface in urea transesterification with EG.

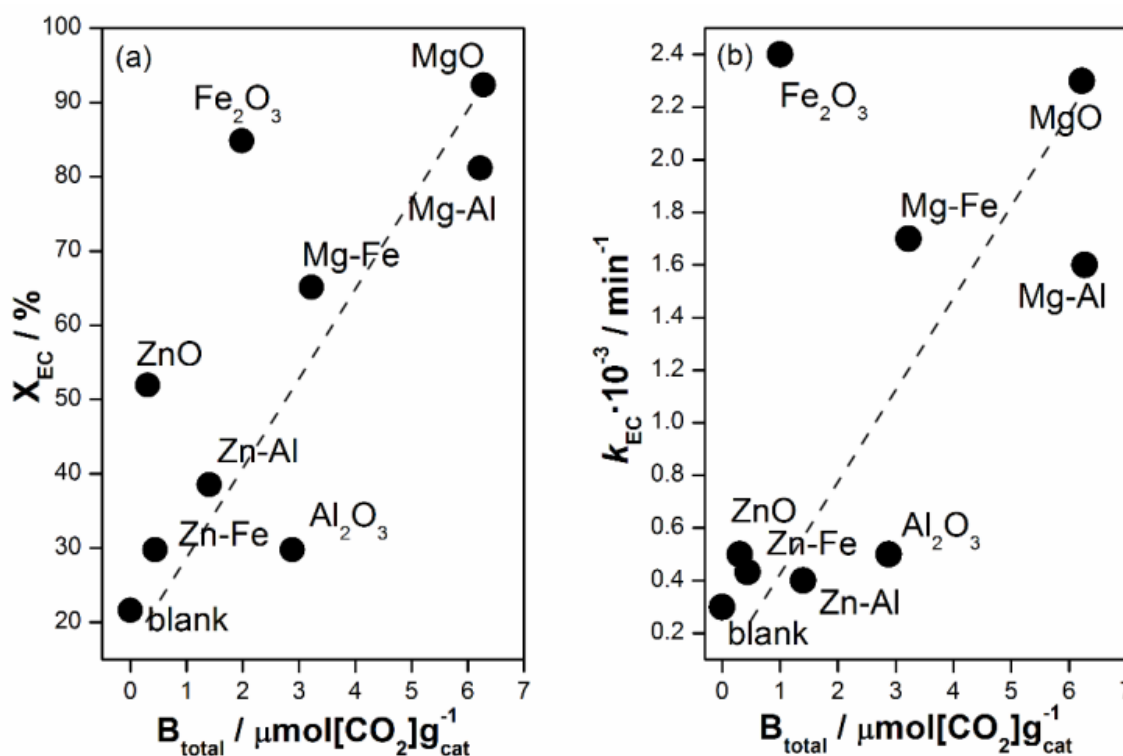


Figure 4.4. (a) EC conversion (X) and (b) EC reaction rate constant against the total amount of basic sites. Reactions were performed for 6 h at 413 K. Dashed lines serve to guide the eyes only.

In the course of careful investigation on factors influencing EC conversion and DEG yield, we observed that catalyst pretreatment conditions can drastically impact on the reactivity of the catalyst materials. Notably, DEG formation can be effectively suppressed by thermally treating catalysts under inert atmosphere (He flow). Figure 4.5 illustrates the DEG selectivity in the urea transesterification with EG over the metal oxides thermally treated at 723 K in He and also in air. Evidently, thermal treatment under inert atmosphere led to the suppression of DEG formation. Carlson reported that the reaction between EC and alcohols (particularly glycols) or thioalcohols can be promoted in the presence of basic materials such as alkali carbonates [5]. Therefore, it is probable that the thermal treatment in air permitted CO_2 in the atmosphere to react with the activated catalyst surface, forming surface carbonates with basic character which catalyzed the formation of DEG. Although the decomposition temperature of bulk inorganic carbonates is considerably higher (773-1173 K) than the pretreatment temperature used in this work (723 K), [6] the pretreatment is effective in keeping the surface less basic most likely due to the lower decomposition/desorption temperature of CO_2 from the catalyst surface as observed in CO_2 -TPD (Figure 3.3a). Figure 4.5 clearly shows the importance of catalyst pretreatment in inert atmosphere prior to catalytic testing. Therefore, we employed the inert thermal treatment for all catalytic testing in this work.

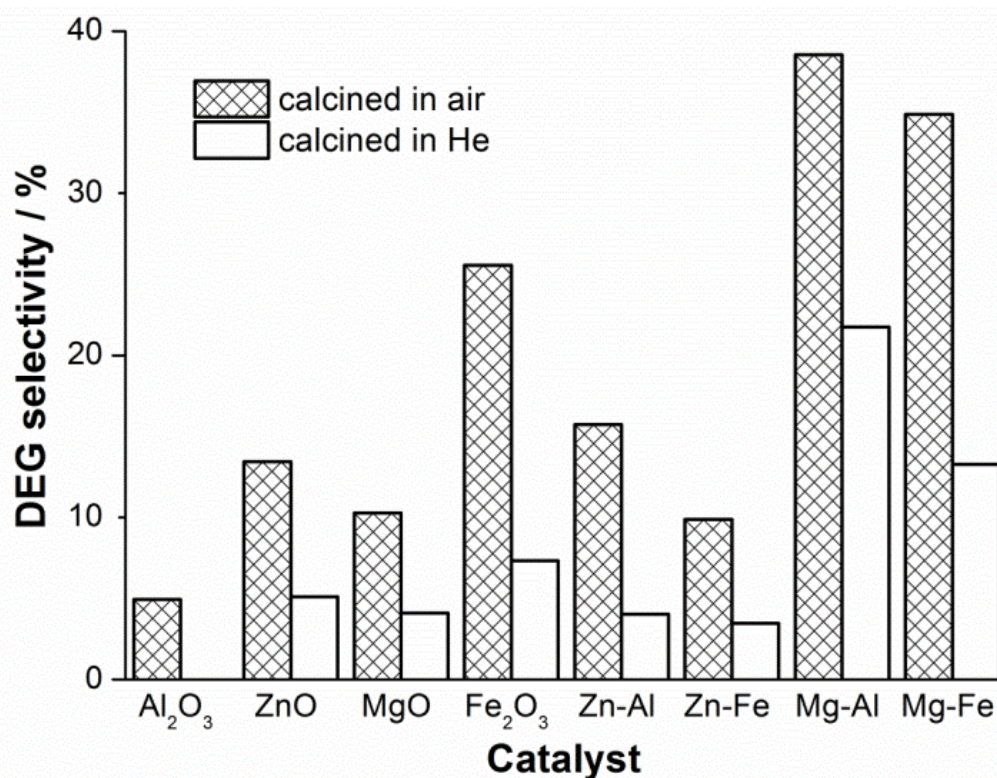


Figure 4.5. Selectivity to DEG in urea transesterification with EG for the catalysts calcined in the air and in He. Reactions were performed for 6 h at 413 K.

4.3.2.3 Reaction of 2-Ox with EG

In a similar fashion, we investigated one of the major undesired side reactions, i.e. reactions of 2-Ox with EG (Scheme 4.1, box C, shown below), producing TEA as the major product (ca. 90-95%) and also 3-(2-EtOH)-2-Ox as another by-product (Table 4.4).

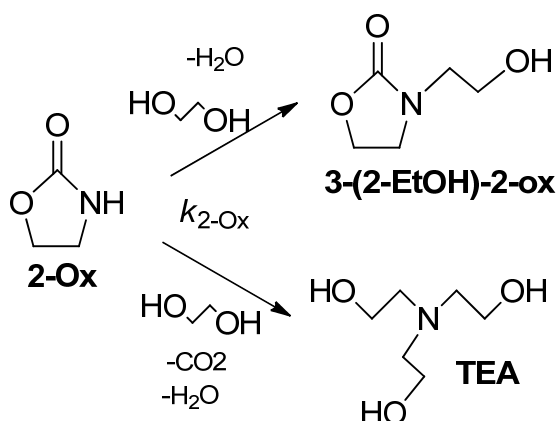


Table 4.4. Product selectivity and 2-Ox conversion in the reaction of 2-Ox with EG

Catalyst	X _{2-Ox} / %	S _{3-(2-EtOH)-2-Ox} / %	S _{TEA} / %
blank	17.6	8.4	91.6
Al ₂ O ₃	25.8	3.2	96.7
ZnO	23.0	1.8	98.2
MgO	33.7	2.5	97.4
Fe ₂ O ₃	57.0	36.2	63.7
Zn-Al	28.6	5.6	94.4
Zn-Fe	12.4	9.1	90.8
Mg-Al	31.3	3.8	96.2
Mg-Fe	35.3	5.9	94.1

In situ IR monitoring clarified that the reactions between 2-Ox with EG follow first order kinetics (Equations 4.6 and 4.7).

$$\frac{dC_{2-Ox}}{dt} = -k_{2-Ox}C_{2-Ox} \quad (4.6)$$

$$\ln(C_{2-Ox}) = \ln(C_{2-Ox,0}) - k_{2-Ox}t \quad (4.7)$$

The plot of the natural logarithm of reactant concentration versus time is linear as shown in Figure 4.6 (b) taking Zn-Fe as an example.

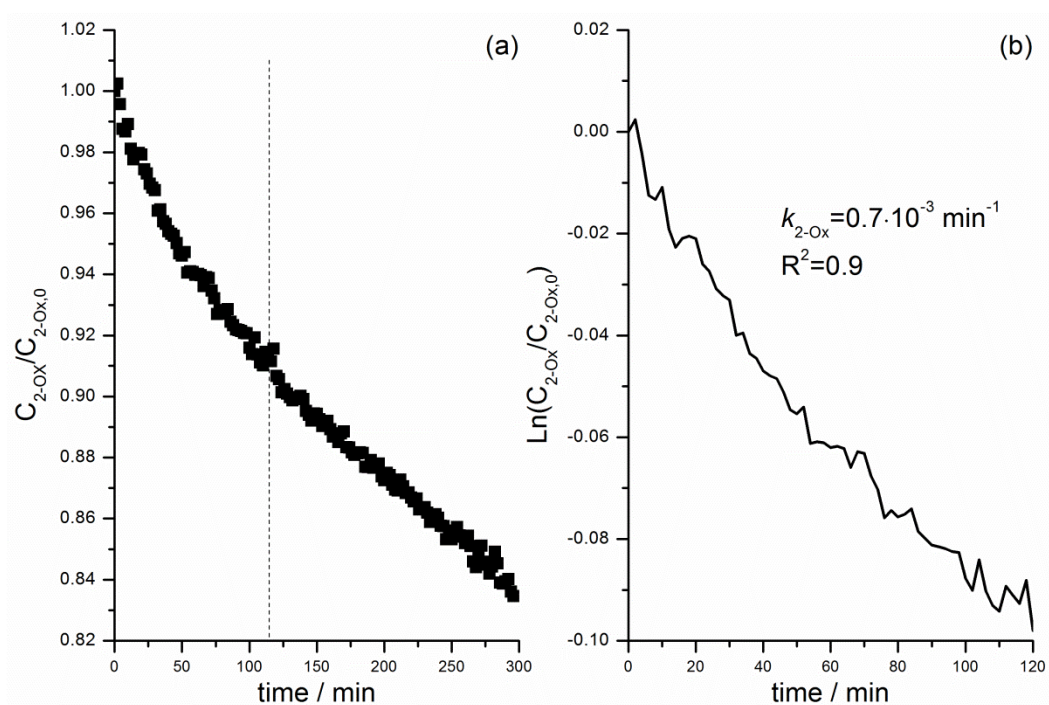


Figure 4.6. Determination of order and rate constant k for reaction 2-Ox with EG in the presence of Zn-Fe catalyst. The straight line in (b) is expected for a first-order reaction.

The slope of straight line gives the reaction rate constant k_{2-Ox} , which was calculated for all catalysts and results are listed in the Table 4.5.

Table 4.5. Rate constants k for reaction between 2-Ox and EG.

Catalyst	blank	Al ₂ O ₃	ZnO	MgO	Fe ₂ O ₃	Zn-Al	Zn-Fe	Mg-Al	Mg-Fe
$k_{2-Ox} \cdot 10^{-3}$ /min ⁻¹	0.4	0.5	0.7	0.8	1.5	0.7	0.7	0.8	0.6
R ²	0.850	0.979	0.959	0.956	0.997	0.926	0.904	0.956	0.930

Although correlation between 2-Ox conversion or reaction rate and a specific characteristic of catalysts was less obvious in comparison to the previous case of DEG formation from EC and EG, there was a general trend observed between the reactivity and the amount of basic sites (Figure 4.7).

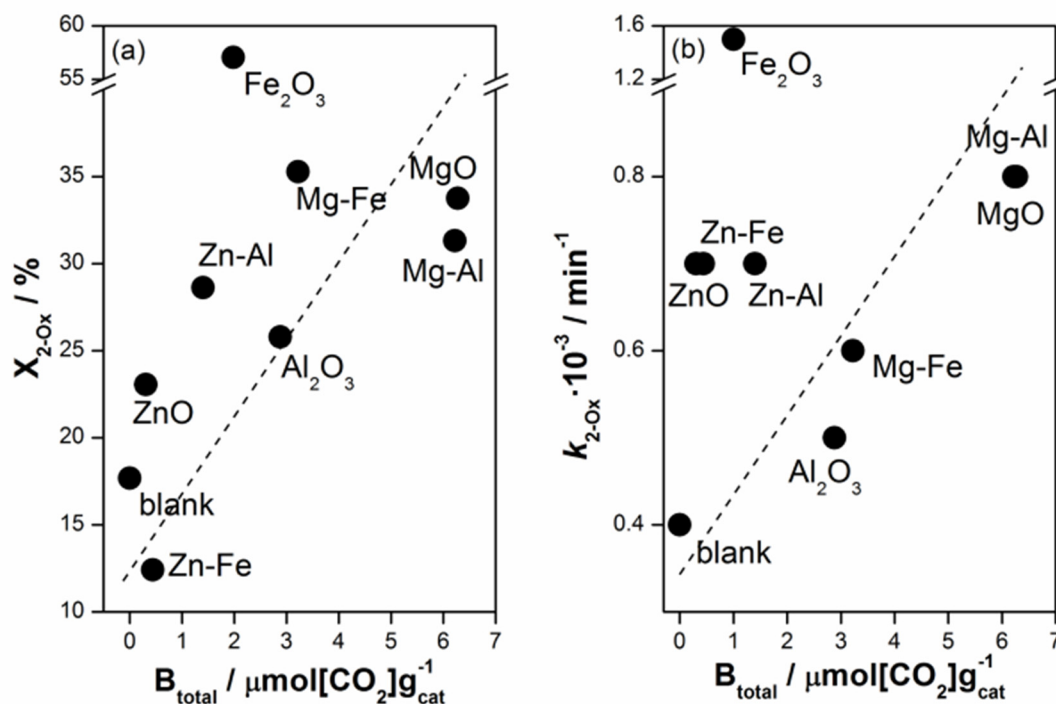


Figure 4.7. (a) 2-Ox conversion and (b) 2-Ox reaction rate constant against the total amount of basic sites. Dashed lines serve to guide the eyes only.

The relation of 2-Ox reactivity with the amount of basic sites was similar to that of EC reactivity (Figure 4.4), showing lower and higher 2-Ox reactivity for Zn- and Mg-containing materials, respectively. Also, Fe_2O_3 promoted the reaction significantly as in the reaction between EC and EG likely due to the presence of strong basic sites (Figure 3.3a). It is worth noting that Zn-Fe with one of the lowest amount of basic sites (Table 3.1) converts only 14% of 2-Ox whereas reaction without catalyst (blank) results in 18% of 2-Ox conversion. Based on the higher initial reaction rate of 2-Ox using Zn-Fe compared to a few other materials (Figure 4.7b), the lowest 2-Ox conversion (Figure 4.7a) implies that the active sites in Zn-Fe catalyzing the reaction was poisoned in the course of the reaction. These poisoning effects (more precisely selective site-blocking) seem very effective starting from urea and EG where no formation of TEA and 3-(2-EtOH)-2-Ox was observed using Zn-Fe (Table 4.1). Bhanage [1a] mentioned that catalysts with strong basic character as CaO and La_2O_3 are highly active in the formation

of 2-Ox and its further reaction products as 3-(2-EtOH)-2-Ox, which is in accordance with the findings of this work. Hence these undesired side reactions of 2-Ox are likely catalyzed by basic sites and possibly prevented by reducing the number and/or weakening the strength of basic sites.

4.3.2.4 Reaction of 2-HC with EG

Furthermore the reaction starting from the intermediate (2-HC) was investigated (Scheme 4.1, box D, shown below) to uncover the roles of acidic and basic sites towards the cyclization and the formation of EC or 2-Ox in the absence of urea in the reaction mixture. As observed in the overall reaction (Scheme 4.1, box A), EC and all other side products were detected with somewhat different product selectivity (Table 4.6).

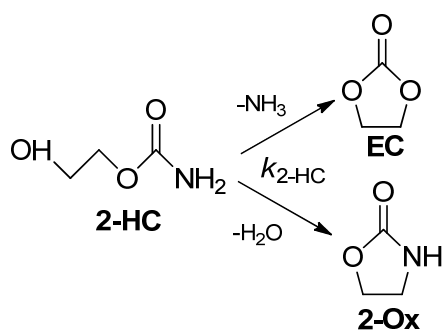


Table 4.6. Product selectivity and 2-HC conversion in reaction of 2-HC with ethylene glycol.

Catalyst	X _{2-HC} / %	S _{EC} / %	S _{2-Ox} / %	S _{DEG} / %	S _{3-(2-EtOH)-2-Ox} / %	S _{TEA} / %
blank	2.6	100	0	0	0	0
Al ₂ O ₃	16.4	100	0	0	0	0
ZnO	66.5	90.7	0	0	0	9.3
MgO	93.8	76.4	0	9.1	0	14.5
Fe ₂ O ₃	5.3	87.3	0	12.7	0	0
Zn-Al	48.6	100	0	0	0	0
Zn-Fe	24.7	100	0	0	0	0

Mg-Al	100	65.4	6.3	28.3	0	0
Mg-Fe	88.6	80.6	11.5	7.8	0	0

Non-reversibility of the reactions was assumed. The concentration profiles suggest an apparent first order reaction. In other words, the reaction rate is directly proportional to the concentration of 2-HC (Equation 4.8).

$$\frac{dC_{2-HC}}{dt} = -k_{2-HC}C_{2-HC} \quad (4.8)$$

The integrated rate law for the reaction can be written using logarithmic Equation 4.9.

$$\ln(C_{2-HC}) = \ln(C_{2-HC,0}) - k_{2-HC}t \quad (4.9)$$

As expected, the plot of the natural logarithm of 2-HC versus time is linear as shown in Figure 4.8 (b) taking Zn-Fe as an example. The slope of straight line gives the reaction rate constant k_{2-HC} , which was calculated for all catalysts and the results are listed in Table 4.7.

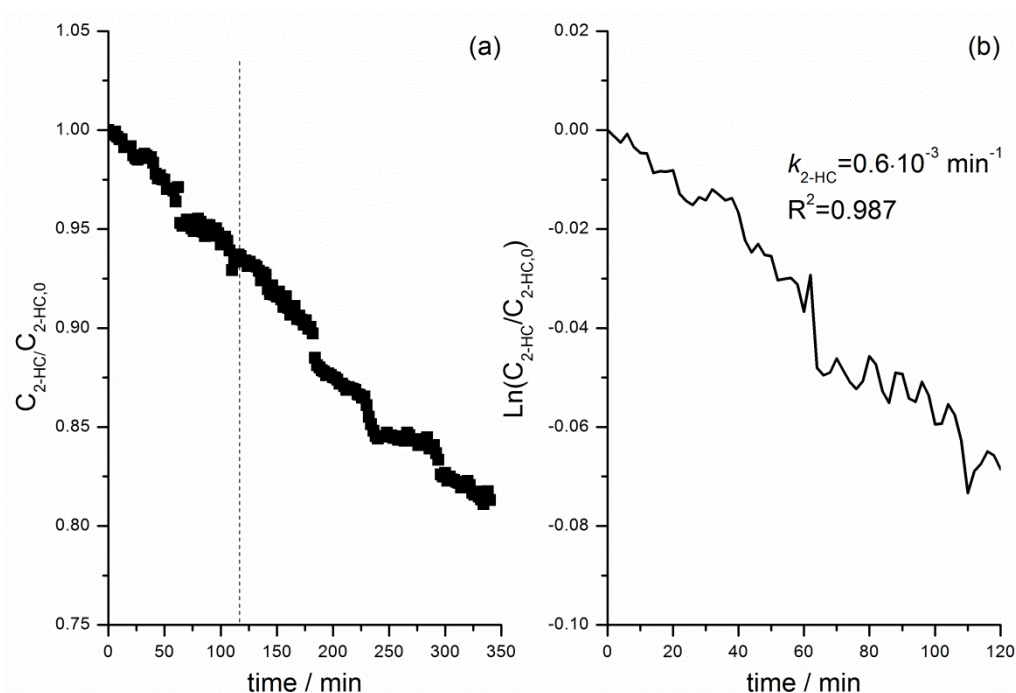


Figure 4.8. Determination of order and rate constant k for reaction of 2-HC with EG in the presence of Zn-Fe catalyst. The straight line in (b) is expected for a first-order reaction.

It is important to mention that there was no kinetic resolution between EC and 2-Ox; therefore, it was not possible to separate these two species by MCR. To obtain the respective concentration profile, experimentally obtained selectivity values towards EC (plus the secondary product) and toward 2-Ox (plus the secondary products) were used to scale the concentration values obtained for the mixture of EC and 2-Ox. In other words, C_{EC} and C_{2-Ox} were calculated by Formulas 4.10 and 4.11.

$$C_{EC} = C_{products} \cdot S_{EC} \quad (4.10)$$

$$C_{2-Ox} = C_{products} \cdot S_{2-Ox} \quad (4.11)$$

where $S_{EC} = \frac{[EC]}{[EC]+[2-Ox]+[DEG]+[TEA]+[3-(2-EtOH)-2-Ox]}$, and

$$S_{2-Ox} = \frac{[2-Ox]}{[EC]+[2-Ox]+[DEG]+[TEA]+[3-(2-EtOH)-2-Ox]}$$

Finally, the reaction rate constants of 2-HC to EC or 2-Ox were scaled using Formulas 4.12 and 4.13.

$$k_{2-HC \rightarrow EC} = S_{EC} \cdot k_{2-HC} \quad (4.12)$$

$$k_{2-HC \rightarrow 2-Ox} = S_{2-Ox} \cdot k_{2-HC} \quad (4.13)$$

These rate constants were used for kinetic modeling and in fitting as shown in the Table 4.7.

Table 4.7. Rate constants k for reaction between 2-HC and EG.

Catalyst	blank	Al ₂ O ₃	ZnO	MgO	Fe ₂ O ₃	Zn-Al	Zn-Fe	Mg-Al	Mg-Fe
$k_{2-HC} \cdot 10^{-3}$ /min ⁻¹	0.2	0.4	1.3	2.4	0.5	0.8	0.6	2.4	2.1
R ²	0.966	0.972	0.995	0.963	0.986	0.940	0.988	0.787	0.929

With the aim of maximizing EC selectivity, the factors such as the acidic and basic nature of catalysts influencing the cyclization selectivity to EC or 2-Ox were examined. After extensive search, no obvious relation was found between

2-HC conversion or reaction rate and the number of acidic or basic sites (the total number of sites or site density calculated by scaling the total site number by the surface area of the materials). Hence a more integral parameter representing integrated acid-base property of materials by taking the ratio between total amount of acidic and basic sites (A/B) was evaluated.

Figure 4.9 presents the plots of (a) 2-HC conversion and (b) EC selectivity (Table 4.5) against A/B . The same trend as 2-HC conversion was observed for 2-HC reaction rate and therefore it is not shown for the sake of brevity. The metal oxides with lower ratio of A/B , i.e. more basic material, exhibited very high conversion of 2-HC, reaching nearly full conversion as observed for Mg-containing materials (Figure 4.9a), with the exception of Fe_2O_3 showing low 2-HC conversion despite of the low A/B . On the contrary, metal oxides with higher A/B exhibit nearly full selectivity towards EC (Figure 7.9b). These materials such as Al_2O_3 and Zn-Fe have comparably higher amount of acidic sites and this property seems important to guide the reaction from 2-HC to the EC path (Scheme 4.1, box B) and not to 2-Ox path (Scheme 4.1, box C). Metal oxides with lower A/B , i.e. more basic materials, showed deteriorated EC selectivity, opening the 2-Ox path and also secondary reaction paths (Table 4.5). High A/B is important in guiding the reaction path towards EC as well as in suppressing the secondary reactions catalyzed by basic sites as previously clarified (4.3.2.2 & 4.3.2.3). When it comes to EC yield, the two factors 2-HC conversion as well as EC selectivity directly contribute and the presence of well-balanced acidic and basic sites (A/B) is expected to be crucial.

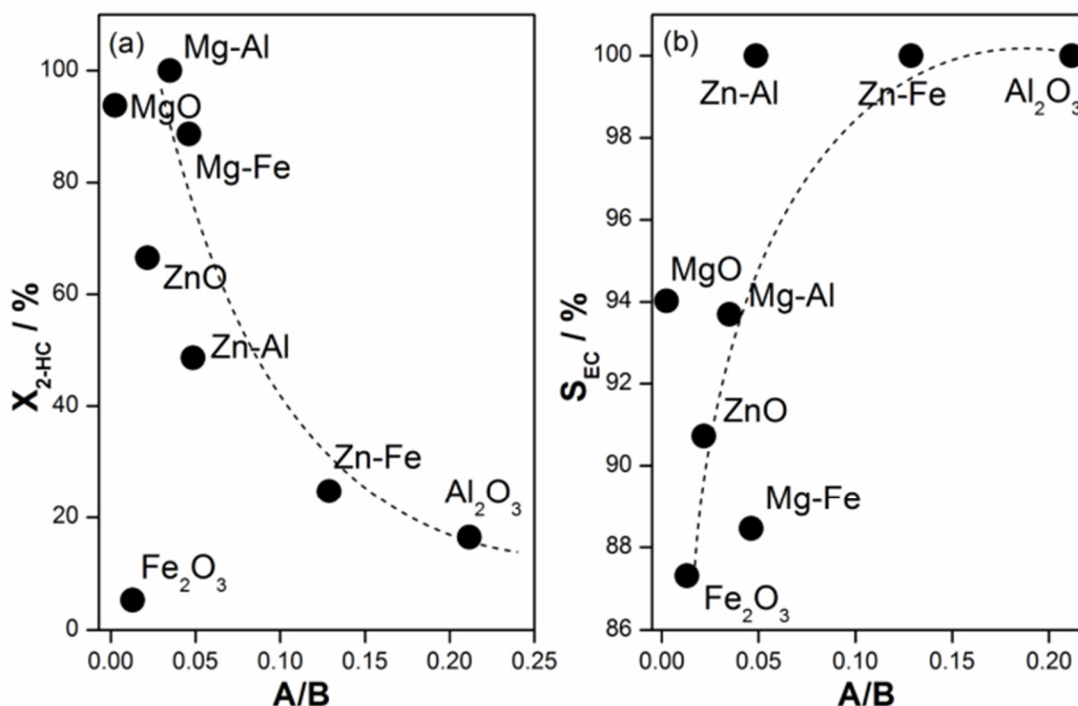


Figure 4.9. (a) 2-HC conversion and (b) EC selectivity against the ratio between the total amount of acidic and basic sites (A/B). Reactions were performed for 6 h at 413 K. Dashed lines serve to guide the eyes only.

4.3.3 Role of acidic and basic sites in urea transesterification with EG

From the studies above, the variation of constituting elements in single metal and mixed metal oxides was found to drastically alter the acid-base properties of the materials, thus reactivity, the reaction paths, and consequently EC yield. Fine tuning of acid-base properties and a balanced proportion of surface acidic and basic sites are suggested critical to high EC yield with high selectivity based on the reaction starting from 2-HC (Figure 4.9). The same conclusion is valid when reaction starts from urea and EG (Scheme 4.1, box A). Figure 4.10 shows the EC yield in urea transesterification with EG as a function of A/B. It shows the highest EC yield for a balanced A/B material (Zn-Fe) whereas lower EC yields were found for the more acidic or basic materials. The low basicity of

Zn-Fe is important in driving the reaction more selectively towards EC, while the presence of weak acidity is important for urea activation without being poisoned (Figure 4.2).

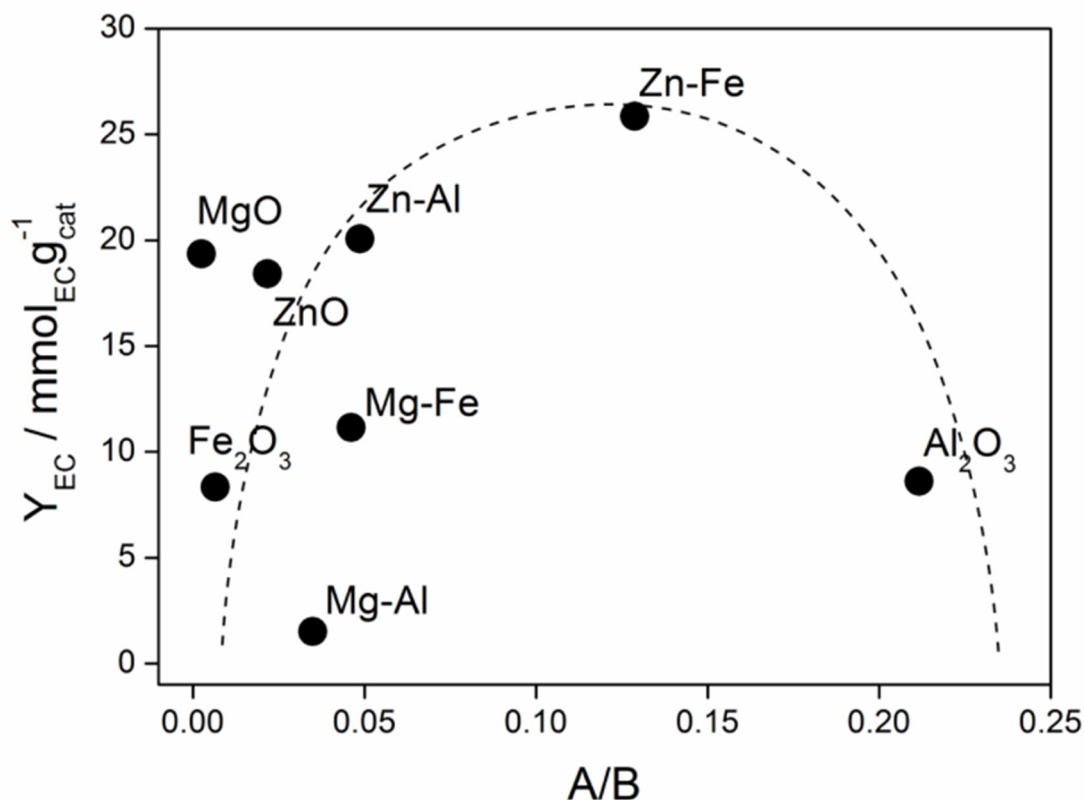


Figure 4.10. EC yield against A/B ratio. Reactions were performed for 6 h at 413 K. Dashed lines serve to guide the eyes only.

The importance of balanced acid-base properties of catalyst materials in this or similar reactions were concluded by other studies. Ball et al. reported that the reaction between primary and secondary alcohols with urea to form alkyl carbonates can be improved using an adequate combination of a weak Lewis acid and a Lewis base [7]. More recently, Climent et al. [8] concluded that high activity and selectivity of Zn-Al mixed oxide in urea transesterification with glycerol can be attributed to well-balanced acid-base properties of the catalyst. Therein, cooperative effects between active sites created by different metal

oxides were suggested; metallic weak Lewis acidic sites activate the carbonyl group of the urea and Lewis basic sites activate glycerol.

Wang et al. [9] investigated mixed Zn-Y oxides and demonstrated the importance of binary metal oxide phases which yielded higher catalytic activity than that of ZnO or Y₂O₃ due to the unique acid-base property given by the synergistic effects. Similar synergetic effects of Zn-Fe oxides were also reported by Zhao et al. [1b]. They concluded that the formation of ZnFe₂O₄ phase, as observed in our work, was responsible for the high catalytic performance. The presence of unique phase where Zn and Fe are well mixed on atomic scale in the oxide may be responsible for creating well-balanced acid-base sites in close vicinity and thus favorable for the reaction.

Furthermore, we observed substantial differences in product selectivity when we start the reaction from urea and EG (Scheme 4.1, box A) or from 2-HC and EG (Scheme 4.1, box D). The difference likely stems from the acid-base character of urea and also the modification of acidity and basicity upon its adsorption over the metal oxide surface. To gain detailed insights and highlight the influence of urea in the overall reaction paths, we compared the reaction rate constants of the two reactions (i.e. starting from urea and EG or from 2-HC and EG). The reaction rate constants for 2-HC conversion in the urea + EG case were obtained from a fitting of the concentration profiles determined by *in situ* IR monitoring. Rate constants giving minimum errors in fitting were used. The details of the fitting procedure are described in Appendix and the comparison of all rate constants is shown in Table A1. The major difference lies in the rate constant for 2-HC conversion, which is shown in Table 4.8.

Table 4.8. Reaction rate constants of 2-HC conversion starting from 2-HC in EG and from urea and EG in the presence and absence of the metal oxides.

Catalyst	$k_{2\text{-HC}} \cdot 10^{-3}/\text{min}^{-1}$ 2-HC and EG	$k_{2\text{-HC}} \cdot 10^{-3}/\text{min}^{-1}$ urea and EG
blank	0.2	1.0
Al ₂ O ₃	0.4	1.1
ZnO	1.3	13.9
MgO	2.4	7.1
Fe ₂ O ₃	0.5	1.1
Zn-Al	0.8	8.2
Zn-Fe	0.6	10.4
Mg-Al	2.4	6.2
Mg-Fe	2.4	18.2

Clearly, the rate constant starting from urea and EG are much higher than starting from 2-HC. For some catalysts like ZnO and Mg-Fe, the 2-HC reaction rate boosting was particularly prominent. According to the knowledge gained in this work (Figure 4.9), it is speculated that urea adsorbs on the acidic sites and renders the surface more basic, thus accelerating 2-HC conversion.

Higher 2-HC conversion rate is in principle advantageous to enhance EC yield, but this is only true when the path to EC is dominant compared to the path to 2-Ox (Scheme 4.1). To clarify the effects of urea on the selectivity from 2-HC towards EC or 2-Ox, we compared the selectivity to 2-Ox path calculated by Formula 4.14.

$$S(2\text{-Ox path}) = \frac{[2\text{-Ox}] + [\text{TEA}] + [2\text{-(1-EtOH)-2-Ox}]}{[\text{EC}] + [\text{DEG}] + [2\text{-Ox}] + [\text{TEA}] + [2\text{-(1-EtOH)-2-Ox}]} \times 100 \quad (4.14)$$

Figure 4.11 shows the effect of the starting reaction conditions on the 2-Ox path selectivity. Generally, we observed remarkably higher selectivity towards the 2-Ox path when reaction starts from urea and EG. In other words, selectivity to EC can drastically decrease in the presence of urea. These results suggest

that that urea poisons the acidic sites and enhances the basic character of the surface which drives the reaction towards the undesired 2-Ox path. The excellent catalyst, Zn-Fe, shows low 2-Ox path selectivity in the urea + EG reaction, with even lower value than that of blank reaction. This might be due to the fact that weakly acidic materials may not strongly adsorb urea and thus the enhancement of surface basicity is minimized, while in the liquid phase urea itself likely functions as a basic catalyst.

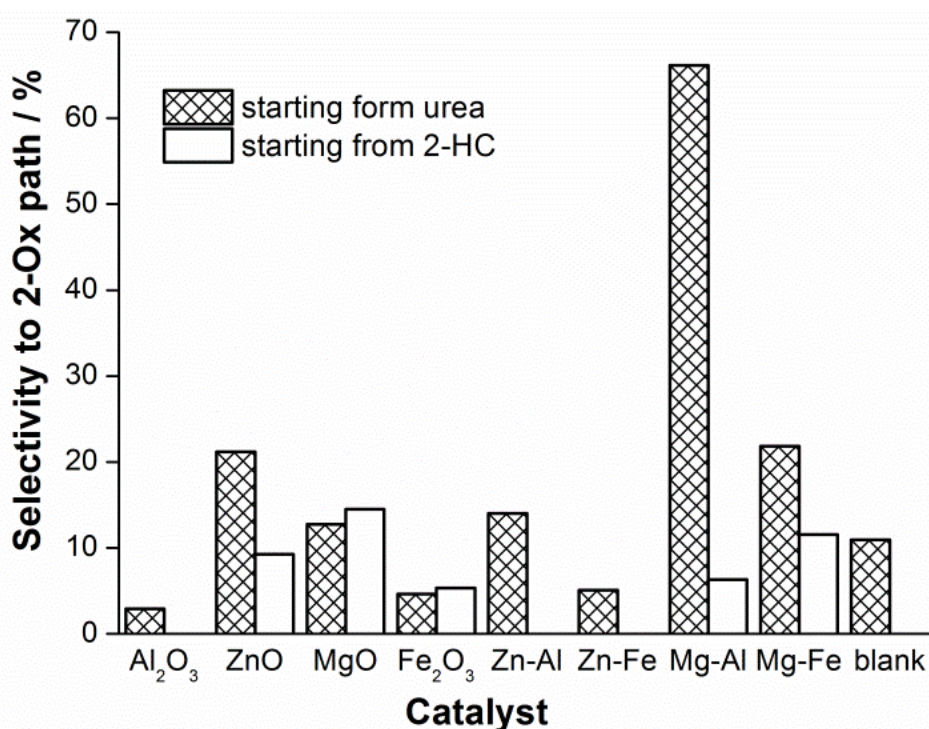


Figure 4.11. Selectivity to the 2-Ox path (Scheme 4.1, box C) against the EC path (Scheme 4.1, box B) starting from urea and EG (shadowed bar) or from 2-HC and EG (unfilled bar). Reactions were performed for 6 h at 413 K.

4.4 Conclusions

A series of single- and mixed-metal oxides, mostly derived from hydrotalcite precursors, consisting of four metal cations (Zn, Mg, Al, Fe) were synthesized with the aim of fine-tuning the acid–base properties. These materials

were tested in urea transesterification with EG and in every comprising reaction pathway identified in this work (Scheme 4.1). The concentration profiles of the reactants/products and kinetics parameters were obtained by means of IR monitoring using a dip-in ATR-IR probe with subsequent multivariate analysis (MCR). The roles of acidity and basicity at each reaction step were unambiguously clarified from the relations between acidity and basicity of the materials and the reaction performance or the kinetic information (reaction rate constants).

From the separate investigation of each reaction step, it can be concluded that the reaction of EC with EG is catalyzed by basic sites and carbonate species formed upon exposure to air (reaction with CO_2 in air) also promote EC conversion. Therefore, preliminary catalyst thermal treatment in an inert atmosphere is important to avoid carbonate formation and suppress this side reaction. The undesired side reaction between 2-Ox and EG is also enhanced with increasing the amount of basic sites according to rising 2-Ox conversion and reaction rate.

For the reaction between 2-HC and EG the presence of well-balanced acidic and basic sites (A/B) is crucial. Metal oxides with low A/B, (more basic material) improve and accelerate conversion of 2-HC but with higher selectivity to undesired products as described above. On the contrary more acidic metal oxides exhibit low 2-HC conversion and reaction rate but afford high EC selectivity.

Regarding urea conversion, it appeared to be catalyzed by acidic sites, although their excess and/or too strong acidic character drastically inhibit the reaction. This strong surface adsorption of urea alter the surface acidity/basicity and influence the overall reaction performance, especially product selectivity. The kinetic studies indicate that urea poisons the acidic sites and enhances the basic character of the surface via its strong adsorption over the metal oxide and drives reaction towards undesired products.

As it was shown, transesterification of urea with EG is a complex reaction, consisting of reaction steps, which are influenced by different active sites. Still, we could generalize that the reactions accompanying NH_3 release are acid-catalyzed and those accompanying CO_2 or H_2O release are base-catalyzed. Selective and high-yield synthesis of EC requires a catalyst with proper combination of acidic and basic sites, favorable to fully convert reactants and suppress side reactions. Hydrotalcite-derived mixed metal oxide Zn-Fe presents well dispersed and balanced acidic and basic sites featuring high urea conversion and reaction rates, selective intermediate (2-HC) conversion to EC and minimizing side reaction products, thus giving high EC yield.

References

1. (a) Bhanage, B. M.; Fujita, S.; Ikushima, Y.; Arai, M., *Green Chem.* 2003, 5 (4), 429-432; (b) Zhao, X.; An, H.; Wang, S.; Li, F.; Wang, Y., *J. Chem. Technol. Biotechnol.* 2008, 83 (5), 750-755; (c) Calvino-Casilda, V.; Mul, G.; Fernández, J. F.; Rubio-Marcos, F.; Bañares, M. A., *Appl. Catal. A-Gen* 2011, 409-410 (0), 106-112.
2. Li, Q.; Zhang, W.; Zhao, N.; Wei, W.; Sun, Y., *Catal. Today* 2006, 115 (1-4), 111-116.
3. Li, Q.; Zhao, N.; Wei, W.; Sun, Y., *J. Mol. Catal. A: Chem.* 2007, 270 (1-2), 44-49.
4. Newman, M. S.; Lala, L. K., *Tetrahedron Lett.* 1967, (34), 3267-3269.
5. Carlson, W. W. Process of hydroxyethylation. US Patent 2448767, 1948.
6. Rowland, R. A., *Clays Clay Miner.* 1952, 1 (1), 151-163.
7. Ball, P.; Fullmann, H.; Heitz, W., *Angew. Chem. Int. Ed. (English)* 1980, 19 (9), 718-720.
8. Climent, M. J.; Corma, A.; De Frutos, P.; Iborra, S.; Noy, M.; Velty, A.; Concepción, P., *J. Catal.* 2010, 269 (1), 140-149.
9. Wang, P.; Liu, S.; Zhou, F.; Yang, B.; Alshammari, A. S.; Lu, L.; Deng, Y., *Fuel Process. Technol.* 2014, 126 (0), 359-365.

Chapter 5

Catalyst Tuning and New Materials

5.1 Introduction

Material tuning by improving the balance of acidic and basic sites is an obvious approach to rationally enhance the catalytic performance further based on the results presented in Chapter 4. The best catalytic results were obtained in the presence of Zn-Fe mixed oxide at the molar ratio of 3:1. In this Chapter, we intend to fine-tune acid-base properties of best performing catalyst by varying the composition of constituting elements. We investigated the effect of Zn-Fe molar ratio on the acid-base properties as determined by TPD of CO₂ and NH₃ and on catalytic performance. Additionally influence of another metal element (Al, Mg) in Zn-Fe mixed oxides on surface and catalytic properties were investigated.

Based on the finding that acidic material gives, in principle, high selectivity towards EC (Chapter 4), another class of catalytic materials with fine-tunability of acidity – zeolites – was studied. Along with good textural properties (surface area, porosity), a large number of active sites, tenability of the structure and acidity/basicity by exchanging Si/Al ratio or cations, and good thermal stability are important features of zeolites, possibly modifying the material with ideal acid-base properties [1]. The thermal treatment of zeolites previously exchanged with a different metal cation is the method often used for the preparation of bi-functional acid-base catalysts. They are composed of both acidic sites and metal clusters. It is well known that strong Brønsted acids are conjugated to weak Brønsted bases, so that the existence of protons in zeolites has to be associated with basic sites [2]. Also, a complete ion-exchange with alkali metal ions neutralizes not only the Brønsted acid centres but also creates weak basic centres, so that alkali ion-exchanged zeolites can be used as bi-functional catalysts [3]. In addition to the Brønsted acidity in zeolites, in these materials the Lewis acidity and basicity is present as well, making them possibly good candidates as catalysts in EC synthesis by urea transesterification [4].

Furthermore, basicity of zeolites can be further enhanced by impregnating them with a solution of alkali or transition metal salt with further decomposition to form corresponding metal or metal oxides [5]. Moreover, it has been reported that high surface areas of zeolite as a support can positively affect the dispersion of metal and metal oxide particles and improve their stability.

In this work, Y-type zeolites were chosen to clarify the effect of the acid site nature (Lewis and/or Brønsted) and tune acid-base properties by ion-exchange with alkali metals. Other approach was to use Y-zeolite as a support for active metal oxides such as ZnO in order to improve catalytic activity by metal dispersion and basicity tuning. ZnO was chosen as the secondary active phase due to the high activity of Zn-containing materials studied earlier (Chapter 4).

5.2 Experimental section

5.2.1 Catalyst synthesis

Mixed oxides with general formula $M_b^{2+}-M_t^{3+}$ containing Zn^{2+} as bivalent cation (M_b^{2+}) and Fe^{3+} as trivalent cation (M_t^{3+}) with molar ratio $M_b^{2+}/M_t^{3+} = 0.5, 3, 6, 6$ were synthesized by the co-precipitation method using an aqueous solution of metal nitrate precursors. The procedure was as follows: an aqueous nitrate solution (100 mL) with appropriate amount of the bivalent and trivalent cations was added drop-wise into a beaker with 100 mL of deionized water under vigorous stirring at room temperature. The pH of the solution was kept constant at 10 by adding a second solution of NaOH (2 M). The resultant slurry was aged for 18 h at room temperature, filtered, thoroughly washed with deionized water and dried at 373 K overnight. Finally the resultant dried materials were calcined at 723 K for 12 h to obtain the corresponding mixed oxides.

Tri-metallic mixed oxides with general formula $M_b^{2+}-M_t^{3+}$ containing Zn^{2+} or mixture of Zn^{2+} and Mg^{2+} as bivalent cation (M_b^{2+}) and Fe^{3+} or mixture of Fe^{3+} and

Al^{3+} as trivalent cation (M_t^{3+}) with molar ratio $M_b^{2+}/M_t^{3+}=3$ were synthesized by the same procedure described above. Prior to the reaction all samples were calcined at 723 K.

The metal-ion exchanged Y-zeolites were prepared by mixing sodium Y-zeolite (Na-Y, Alpha Aesar SiO_2/Al_2O_3 ratio of 5.1) and 0.25 M aqueous solutions of KNO_3 or $CsNO_3$. The mixtures were agitated at 353 K for 2 h and then filtered. The ion-exchanged zeolites were washed with distilled water, dried at 373 K for 12 h and then calcined in air at 873 K for 5 h. Proton-containing H-Y zeolite was obtained after calcination of NH_4 -Y zeolite with the same SiO_2/Al_2O_3 ratio at 873 K for 5 h.

NaY-ZnO catalysts were prepared by the impregnation method using the same NaY as a support. The impregnation of NaY zeolite was performed with an aqueous solution of $Zn(NO_3)_2 \cdot 6H_2O$ to give zinc oxide loadings of 3, 5, 10 and 15 wt% for 12 h at 353 K. The samples were dried in an oven at 373 K overnight before calcination at 773 K for 5 h. The resultant samples are denoted as NaY-3ZnO, NaY-5ZnO, NaY-10ZnO and NaY-15ZnO.

5.2.2 Catalyst characterization

Powder X-ray diffraction (XRD), NH_3 - and CO_2 -TPD, and N_2 physisorption were performed with the method described in Chapter 3.

5.2.3 Catalytic test

Transesterification of urea with EG was performed using the catalyst materials and the products were analyzed by the method described in Chapters 2 and 4.

5.3 Results and discussion

5.3.1 Mixed metal oxides

5.3.1.1 Catalyst characterization

Figure 5.1 (a) shows XRD patterns of calcined Zn-Fe mixed oxides with different molar ratios of Zn/Fe. All samples display the presence of ZnO phase (JCPDS file no. 01-089-0510). Additionally XRD patterns of Zn-Fe mixed oxides reveal the reflections of zinc franklinite (ZnFe_2O_4) which is with a spinel-type structure consistent with JCPDS card (22-1012). Intensity of diffraction peaks of ZnFe_2O_4 rises with increasing content of Fe in mixed oxides. $\text{Zn}_9\text{-Fe}_1$ has lowest amount of Fe and therefore there was no detectable signal of the franklinite phase. It should be noted that with increasing Fe amount the crystallinity of the samples decreases.

Figure 5.1 (b) represents XRD patterns of calcined tri-metallic mixed oxides. $\text{Zn}_3\text{-Al}_{0.5}\text{-Fe}_{0.5}$ displays major diffraction peaks of ZnO phase since the amount of Zn compared to those of other metal atoms is in excess. Peaks at around 30° , 36° and 44° can be assigned to the franklinite phase. As compared to $\text{Zn}_3\text{-Al}_{0.5}\text{-Fe}_{0.5}$, crystallinity of $\text{Zn}_{1.5}\text{-Mg}_{1.5}\text{-Fe}_1$ is lowered apparently due to increased Fe content as in the binary oxide case. Two crystalline phases are found to be present in $\text{Zn}_{1.5}\text{-Mg}_{1.5}\text{-Fe}_1$: MgO cubic periclase (JCPDS file no. 45-0946) and ZnFe_2O_4 . The latter has the major diffraction peak at 36° .

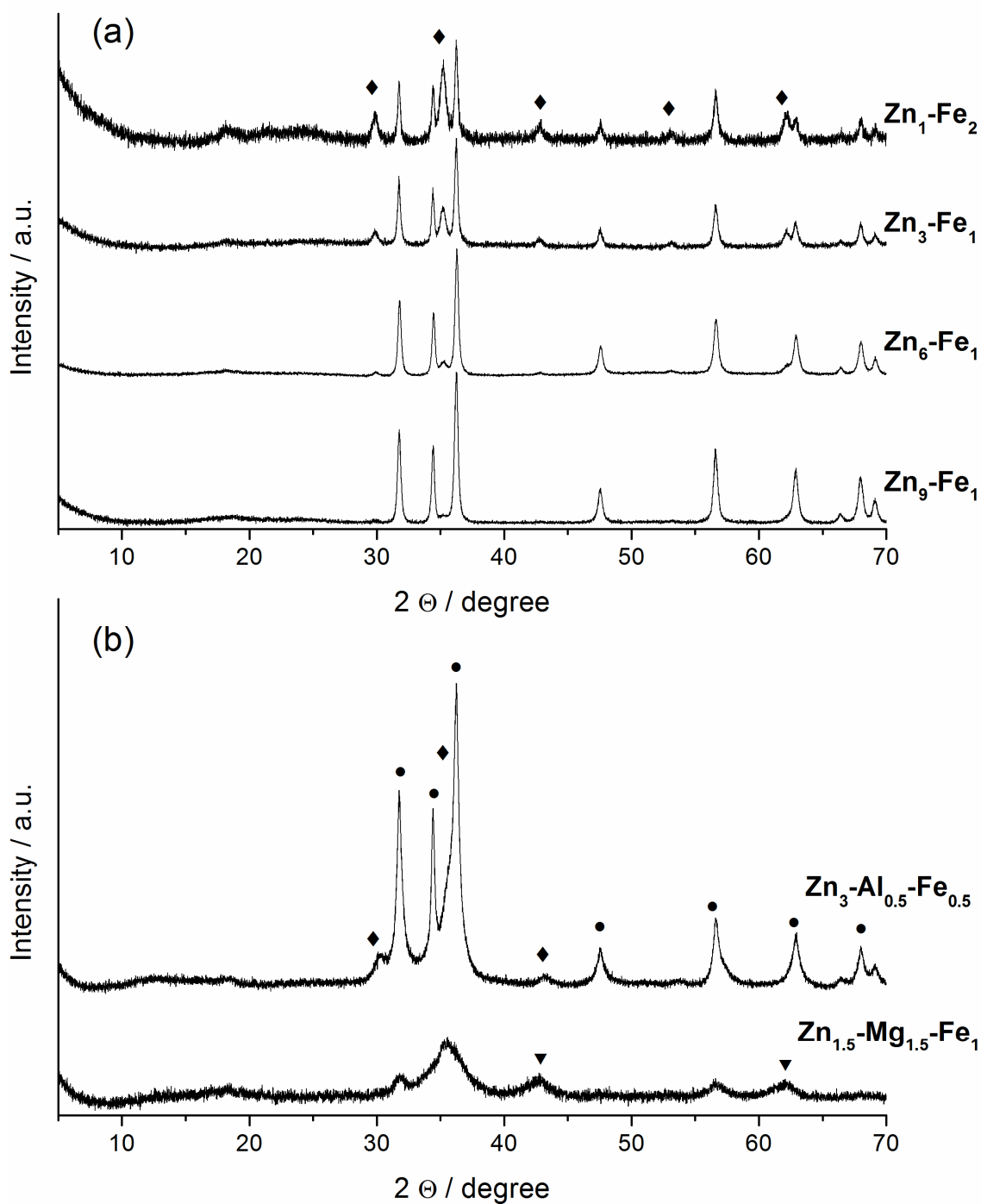


Figure 5.1. XRD patterns of (a) calcined Zn-Fe mixed oxides and (b) calcined tri-metallic mixed oxides. The symbols indicate the following crystal phases: ● hexagonal wurtzite phase of ZnO, ▼ cubic periclase phase of MgO and ◆ Franklinitite $ZnFe_2O_4$.

The results of CO₂- and NH₃-TPD over Zn-Fe mixed oxides are shown in Figure 5.2 (a) and (b), respectively. The amount of desorbed gases and therefore the amount of basic and acidic sites are reflected in the peak area. Peak position indicates strength of the sites.

TPD-CO₂ profiles of Zn₆-Fe₁ and Zn₉-Fe₁ indicate an extremely low amount of basic sites. The basic character of these mixed oxides is similar to that of pure ZnO discussed in Chapter 3. The broad peak observed at 473-773 K on Zn₁-Fe₂ is attributed to basic sites of moderate and strong character. The amount of strong basic sites in Zn₁-Fe₂ oxide is higher than in Zn₁-Fe₃, whereas weak sites are almost absent (desorption peak at 373-473 K)

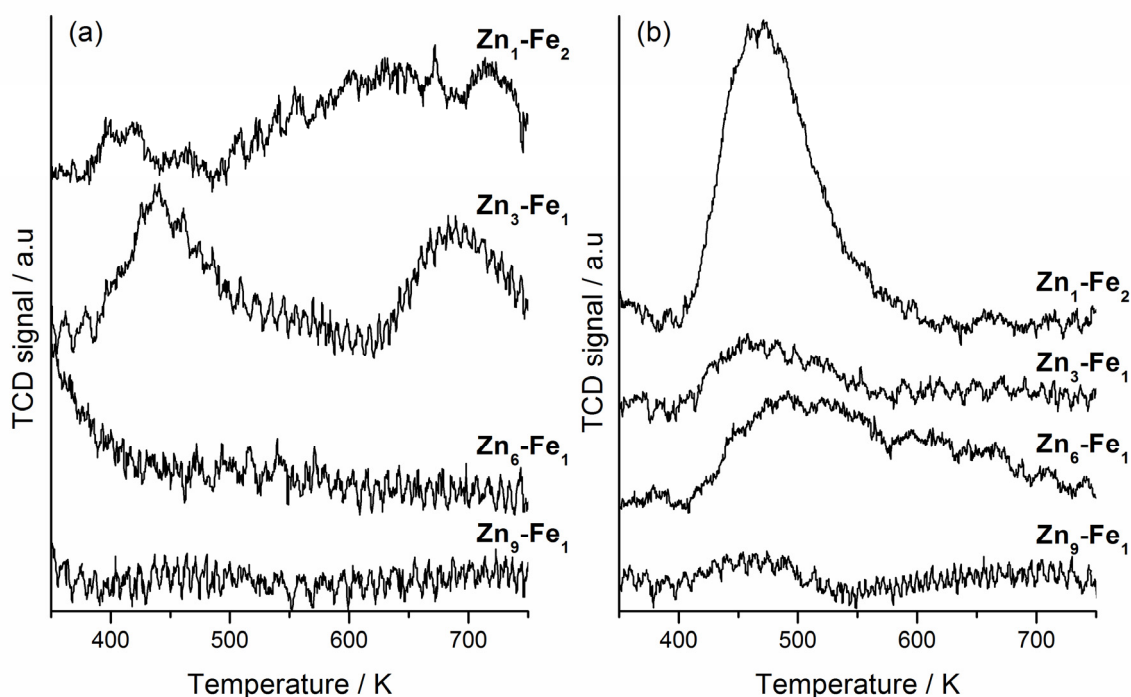


Figure 5.2. TPD profiles of adsorbed (a) CO₂ and (b) NH₃ on Zn-Fe mixed oxides.

NH₃-TPD over Zn-Fe mixed oxides shows the presence of weak acidic sites reflected by the peak at 373–573 K. Zn₁-Fe₂ shows the highest amount of acidic sites, whereas Zn₉-Fe₁ has very small number of acidic sites, similar to ZnO described earlier (Chapter 3).

Figure 5.3 presents TPD profiles of adsorbed (a) CO_2 and (b) NH_3 over tri-metallic mixed oxides. Based on the CO_2 -TPD profiles, it is clear that addition of Mg drastically enhances the basicity of the Zn-Fe mixed oxide. CO_2 desorption profile of $\text{Zn}_{1.5}\text{-Mg}_{1.5}\text{-Fe}_1$ has a broad and intense peak at 423–773 K, indicating the presence of moderate and strong basic sites in high amount. In contrast, Al containing tri-metallic oxide $\text{Zn}_3\text{-Al}_{0.5}\text{-Fe}_{0.5}$ gives only one peak of CO_2 -desorption in the range of 373-473 K attributed to weak basic sites. Profiles of NH_3 desorption of both tri-metallic mixed oxides have intense peaks around 373–673 K ($\text{Zn}_{1.5}\text{-Mg}_{1.5}\text{-Fe}_1$) and 373–773 K ($\text{Zn}_3\text{-Al}_{0.5}\text{-Fe}_{0.5}$) revealing weak and moderate acidic sites on the surface of catalysts.

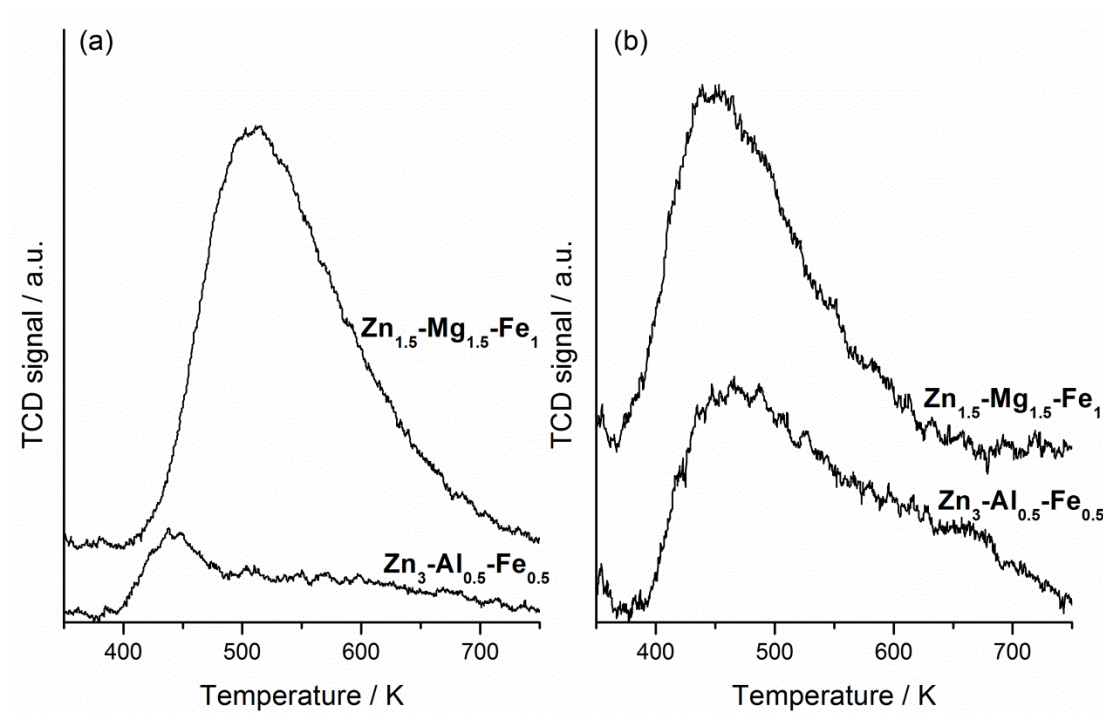


Figure 5.3. TPD profiles of adsorbed (a) CO_2 and (b) NH_3 on trimetallic calcined mixed oxides.

The total amount of acid and base sites from peak area of the TPD profiles, A/B ratio (total amount of acidic sites / total amount of basic sites) and BET surface area of the Zn, Fe-containing materials are summarized in Table 5.1.

Table 5.1. Amount of adsorbed NH_3 and CO_2 , A/B ratio and BET surface area of the mixed oxides.

Catalyst	NH_3 uptake / $\mu\text{mol}\cdot\text{g}^{-1}$	CO_2 uptake / $\mu\text{mol}\cdot\text{g}^{-1}$	A/B	BET surface area / $\text{m}^2\text{ g}^{-1}$
$\text{Zn}_1\text{-Fe}_2$	0.07	0.75	0.09	25
$\text{Zn}_3\text{-Fe}_1$	0.05	0.44	0.13	21
$\text{Zn}_6\text{-Fe}_1$	0.02	0.12	0.13	16
$\text{Zn}_9\text{-Fe}_1$	0.01	0.15	0.07	12
$\text{Zn}_{1.5}\text{-Mg}_{1.5}\text{-Fe}_1$	0.10	6.77	0.01	102
$\text{Zn}_3\text{-Al}_{0.5}\text{-Fe}_{0.5}$	0.08	1.50	0.06	52

According to Table 5.1, it is clear that addition of Fe to Zn-Fe mixed oxides enhances surface area, which is likely related to the decreased crystallinity at higher content of Fe in the materials and smaller crystallite and consequent particle sizes. Incorporation of Mg and Al results in increase of surface area and therefore increases the number of available active sites.

5.3.1.2 Catalytic test

Catalytic performance of the various Zn-Fe and tri-metallic mixed oxides in transesterification reaction of urea with EG is summarized in Table 5.2. Both EC yield and selectivity obtained in the presence of Zn-Fe mixed oxides with different Zn/Fe molar ratios were very similar. $\text{Zn}_3\text{-Fe}_1$ showed the best catalytic performance in terms of selectivity (reaction mixture contained 2-Ox as side product and DEG as the product of EC decomposition). The amount of latter was the lowest as compared with the other Zn-Fe catalysts, whereas the largest DEG amount was found for $\text{Zn}_1\text{-Fe}_2$. It might be attributed to the larger amount of Fe, resulting in enhancing basicity (Table 5.1), promoting EC decomposition to DEG as it was discussed earlier in Chapter 4.

With addition of Mg in Zn-Fe mixed oxide ($\text{Zn}_{1.5}\text{-Mg}_{1.5}\text{-Fe}_1$), EC selectivity and yield drastically decreased to 52.7% and 16.3 $\text{mmol}\cdot\text{g}_{\text{cat}}^{-1}$, respectively, whereas 2-Ox selectivity reached 42.6%. This is anticipated from the very strong basicity (Table 5.1). On the contrary, Al-containing tri-metallic mixed oxide $\text{Zn}_3\text{-Al}_{0.5}\text{-Fe}_{0.5}$ showed high EC selectivity, but the EC yield was not as high as observed for Zn-Fe mixed oxides.

Table 5.2. Catalytic performance of Zn- and Fe-containing mixed oxides.

Catalyst	$Y_{\text{EC}} / \text{mmol}\cdot\text{g}_{\text{cat}}^{-1}$	$S_{\text{EC}} / \%$	$S_{2\text{-Ox}} / \%$	$S_{\text{DEG}} / \%$	$S_{3\text{-(2-ETHO)}\text{-2-Ox}} / \%$	$S_{\text{TEA}} / \%$
$\text{Zn}_1\text{-Fe}_2$	26.8	88.5	2.5	8.5	0	0.5
$\text{Zn}_3\text{-Fe}_1$	25.9	91.5	5.1	3.5	0	0
$\text{Zn}_6\text{-Fe}_1$	25.6	88.2	2.8	7.1	0	1.8
$\text{Zn}_9\text{-Fe}_1$	25.8	91.2	3.2	5.4	0.1	0
$\text{Zn}_{1.5}\text{-Mg}_{1.5}\text{-Fe}_1$	16.3	52.7	4.1	42.6	0	0.5
$\text{Zn}_3\text{-Al}_{0.5}\text{-Fe}_{0.5}$	20.2	93.6	3.3	3.1	0	0

Reactions were performed at 413 K for 6 h starting with 89.51 mmol of EG, 8.33 mmol of urea, and 0.16 g of catalyst under N_2 flow ($0.5 \text{ L}\cdot\text{min}^{-1}$).

In Figure 5.4 the dependency of EC yield on the ratio of total amount of acid/basic sites (A/B) is presented. The markers on the graph representing Zn-Fe and tri-metallic mixed oxides follow the same trend observed earlier for pure metal and bi-metallic mixed oxides (Chapter 4, Figure 4.10). Addition of Mg enhances basicity of materials and suppresses EC selectivity and yield. Addition of Al increases EC selectivity but lowers EC yield, probably due to strong adsorption of urea on active sites of Al^{3+} cations as previously suggested for acidic materials (Chapter 4).

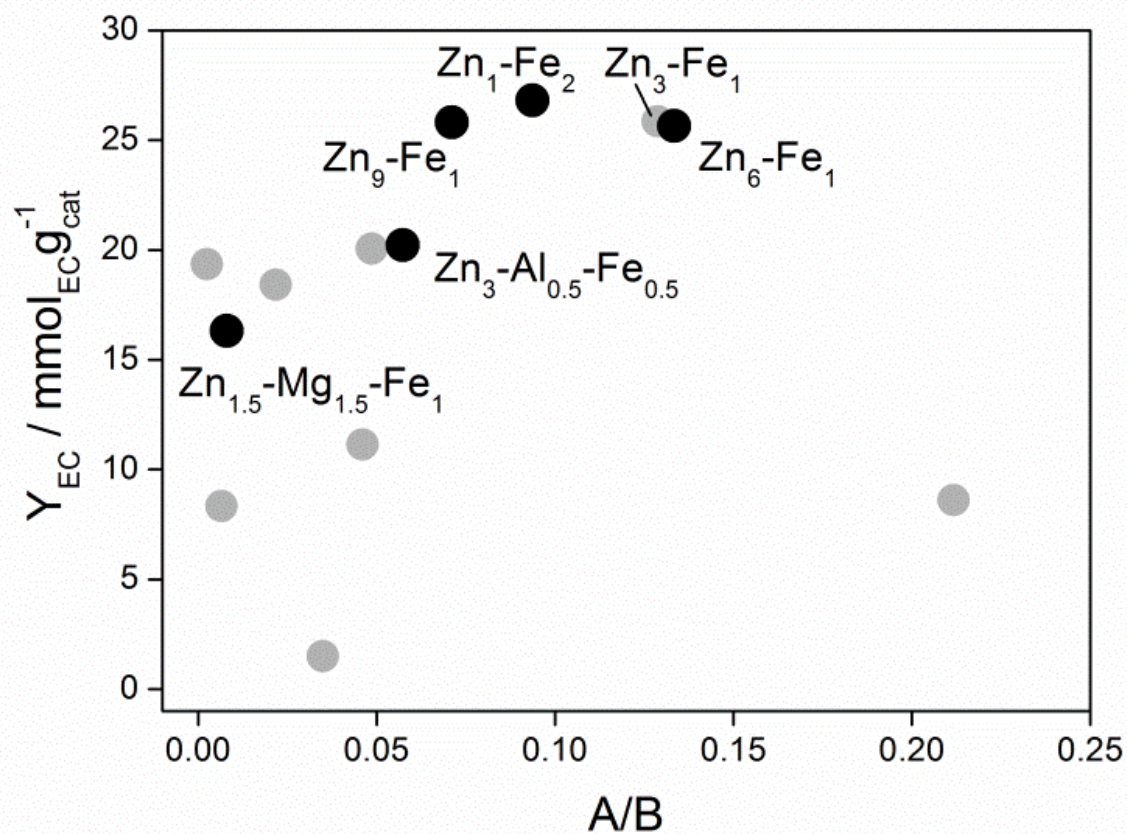


Figure 5.4. EC yield against A/B ratio of Zn-Fe based oxides with different Zn/Fe molar ratios and the oxides with an additional third metal (Al or Mg). Gray markers are the data points taken from Figure 4.10. Reactions were performed for 6 h at 413 K.

Tuning of Zn/Fe ratio and tri-metallic mixed oxide study confirm previously suggested importance of A/B balance. It is important to remark that the reaction performance in terms of product selectivity may not be satisfactory even when EC yields are high. According to Figure 5.4 and Table 5.2, all examined Zn-Fe mixed oxides exhibited similar EC yield. The best material in terms of EC yield (i.e., Zn₁-Fe₂) exhibited lower selectivity to EC and notably ca. 5% higher selectivity to DEG in comparison to Zn-Fe (i.e. 3:1), which makes Zn₃-Fe₁ the most attractive catalyst considering the slightly lower but comparable EC yield.

5.3.2 Y-Zeolites

5.3.2.1 Catalyst characterization

Zeolites acting as catalysts are known to be possibly used in ion-exchanged forms. Exchange of the most general sodium cation by less electronegative cations, e.g. potassium and cesium, leads to redistribution of the electron density and increases electron donor capacity of the oxygen atoms in the lattice which affects the weak Lewis base centers.

We evaluated basicity and acidity of Y zeolites with different cations (H-Y, Na-Y, K-Y and Cs-Y) by CO₂- and NH₃-TPD. The results are presented in Figure 5.5. The CO₂-TPD profiles (Figure 5.5a) indicate that all samples possess weak basic sites, as evidenced by the peak around 373-523 K. Cs-Y additionally shows a broad peak at 573-773 K assigned to strong basic sites. On the other hand all samples show a large amount of acid sites as evident from the NH₃-TPD study (Figure 5.5b). H-Y shows a broad and intense peak over all temperature range (373-773 K) pointing out the presence of acid sites of different strength (i.e. weak, moderate and strong). Na-Y and K-Y zeolites present acid sites of weak and moderate strength which are characterized by the desorption peak around 373-673 K. Only Cs-exchanged Y zeolite was of relative weak acidity, giving a peak on the TPD profile at 373-523 K.

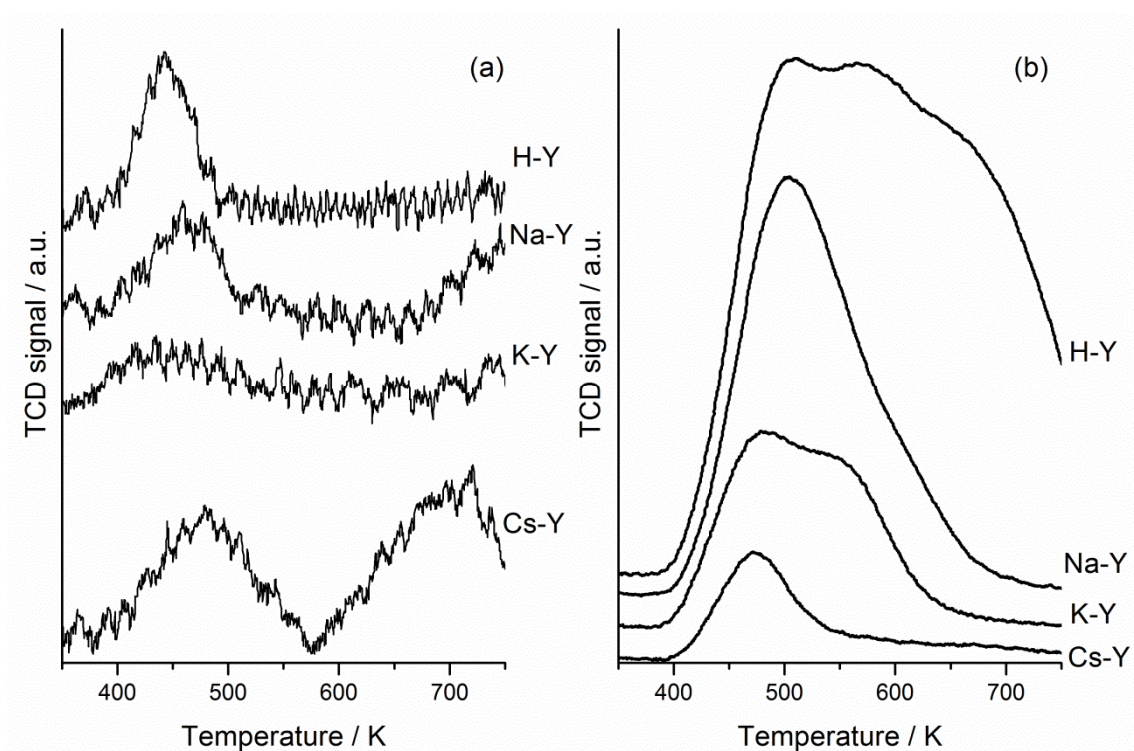


Figure 5.5. TPD profiles of adsorbed (a) CO_2 and (b) NH_3 on Y-zeolites.

The total amount of acid and basic sites, their ratio (A/B) as well as surface area are summarized in Table 5.3.

Table 5.3. Amount of adsorbed NH_3 and CO_2 , A/B ratio and BET surface area of Y-zeolites with different cations.

Catalyst	NH_3 uptake / $\mu\text{mol}\cdot\text{g}^{-1}$	CO_2 uptake / $\mu\text{mol}\cdot\text{g}^{-1}$	A/B	BET surface area / $\text{m}^2\cdot\text{g}^{-1}$
H-Y	2.06	0.61	3.39	660
Na-Y	1.34	0.99	1.36	622
K-Y	0.70	0.31	0.70	576
Cs-Y	0.29	1.29	0.29	558

From the obtained results it can be concluded that all zeolite samples are acidic, and the amount of acid sites and A/B ratio decreases in the following order H-Y>Na-Y>K-Y>Cs-Y.

5.3.2.2 Catalytic test

Catalytic performance of the Y zeolites was evaluated in transesterification of urea with EG, and the results are summarized in Table 5.4.

Table 5.4. Catalytic performance of H-Y, Na-Y, K-Y and Cs-Y.

Catalyst	$Y_{EC} / \text{mmol} \cdot \text{g}_{\text{cat}}^{-1}$	$S_{EC} / \%$	$S_{2-Ox} / \%$	$S_{DEG} / \%$	$S_{3-(2-EtOH)-2-Ox} / \%$	$S_{TEA} / \%$
H-Y	7.33	86.9	6.4	3.9	0	0
Na-Y	9.36	87.3	9.1	6.6	0	0
K-Y	7.27	86.8	3.2	6.7	0	0
Cs-Y	7.69	83.1	3.9	8.9	0	0

Reactions were performed at 413 K for 6 h starting with 89.51 mmol of EG, 8.33 mmol of urea, and 0.16 g of catalyst under N₂ flow (0.5 L·min⁻¹).

Clearly the zeolites show comparably low catalytic activity towards EC. Maximum yield (ca. 9.36 mmol·g_{cat}⁻¹) was obtained with Na-Y, which was very low as compared to that of Zn-Fe mixed oxides (ca. 26 mmol·g_{cat}⁻¹). However, results show high EC selectivity.

Taking into account the acidic character of Y-zeolites and the catalytic results, it can be concluded once again that strongly acidic character of materials restrains urea conversion. On the other hand EC selectivity was around 80-90% which means that the formation of side products was also suppressed. The observation confirms the effects of Lewis acid sites previously found, i.e. enhancing selectivity to EC but inhibiting urea conversion when the acidity is too strong. Acid sites of the zeolites are either of strong character or have majority of

Brønsted sites which are considered not catalytically active for this type of reaction. The introduction of alkali metal cations creates weak basic sites, but their amount as compared with acidic sites is negligible and the impacts of metal cations are minor. Among the zeolite materials, Na-Y showed the highest EC yield; hence the material was chosen as a support for further impregnation with ZnO due to its good catalytic performance to add mildly acidic and basic characters.

5.3.3 Na-Y zeolite supported ZnO

5.3.3.1 Catalyst characterizations

After Zn-precursor impregnation and calcination, obtained samples of different ZnO loading were analyzed by TPD of CO₂ and NH₃ (Figure 5.6). CO₂-TPD profiles of ZnO-loaded Na-Y zeolites show the presence of weak basic sites at around 373-523 K. Na-Y with 10 wt% of ZnO shows an additional strong peak above 573 K, indicating the formation of stronger basic sites. On the other hand, NH₃-TPD shows broad peaks for all samples, suggesting that the NaY-ZnO materials exhibit acid sites of different strengths.

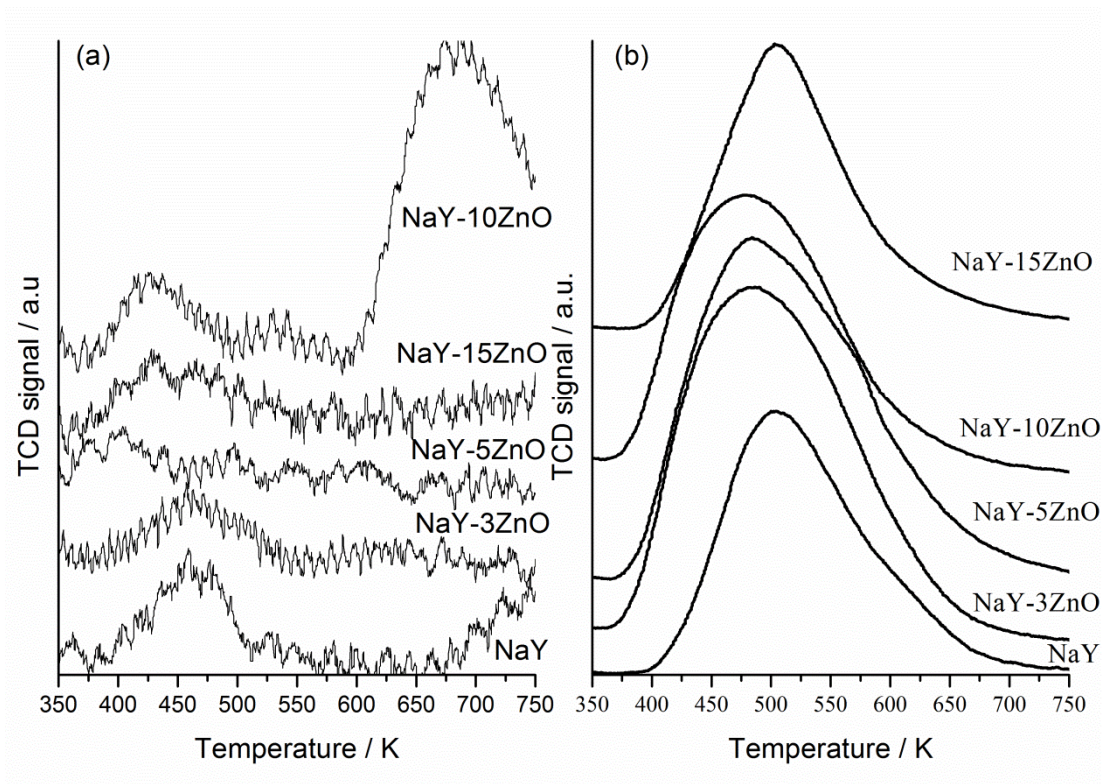


Figure 5.6. TPD profiles of adsorbed (a) CO₂ and (b) NH₃ over Na-Y supported ZnO.

Total amount of acidic and basic sites, A/B ratio and BET surface area are summarized in Table 5.5.

Table 5.5. Amount of adsorbed NH₃ and CO₂, A/B ratio and BET surface area of Na-Y-zeolites with different loadings of ZnO.

Catalyst	NH ₃ uptake / μmol·g ⁻¹	CO ₂ uptake / μmol·g ⁻¹	A/B	BET surface area / m ² ·g ⁻¹
Na-Y	1.34	0.99	1.36	622
NaY-3ZnO	2.14	0.18	11.89	549
NaY-5ZnO	1.58	0.18	8.93	448
NaY-10ZnO	1.36	1.35	1.01	468
NaY-15ZnO	1.35	1.53	0.88	500

The amount of acidic sites of Na-Y supported ZnO remained high as compared to pristine Na-Y. Slight decrease in surface area was also observed upon ZnO loading with possible pore blocking by ZnO.

5.3.3.2 Catalytic test

The catalytic performance of the Na-Y supported ZnO catalysts is summarized in Table 5.6.

Table 5.6. Catalytic performance of Na-Y supported ZnO.

Catalyst	$Y_{EC} / \text{mmol} \cdot \text{g}_{\text{cat}}^{-1}$	$S_{EC} / \%$	$S_{2-Ox} / \%$	$S_{DEG} / \%$	$S_{3-(2-EtOH)-2-Ox} / \%$	$S_{TEA} / \%$
Na-Y	9.36	87.3	9.15	6.61	0	0
NaY-3ZnO	15.5	92.2	4.75	4.67	0	0
NaY-5ZnO	16.08	91.6	5.54	4.73	0	0
NaY-10ZnO	17.8	95.4	0	4.62	0	0
NaY-15ZnO	17.7	88.0	4.87	8.83	0	0

Reactions were performed at 413 K for 6 h starting with 89.51 mmol of EG, 8.33 mmol of urea, and 0.16 g of catalyst under N_2 flow ($0.5 \text{ L} \cdot \text{min}^{-1}$).

The catalytic results show that the addition of ZnO to Na-Y zeolite doubles EC yield and reaches the value close to that of pure ZnO (ca. $18.4 \text{ mmol} \cdot \text{g}_{\text{cat}}^{-1}$, Chapter 4). It is interesting to observe that the ZnO loading had almost negligible effects, which is consistent with the similar TPD profiles of all samples (Figure 5.6). Although the EC yield of Na-Y supported ZnO was similar to that of pure ZnO, EC selectivity was significantly improved; the highest value of 95.4% was observed for NaY-10ZnO, whereas ZnO showed 73.4% (Chapter 4). This high selectivity is consistent with the high acidity of the materials. Based on the acidity and basicity (Table 5.5) a clear conclusion cannot be made, but ZnO addition induces the material to be more reactive (higher urea conversion) while retaining the high selectivity provided by the acidity.

5.4 Conclusions

Further investigation of A/B fine-tuning by evaluating Zn-Fe mixed oxides with varying Zn/Fe molar ratio and with introduction of another metal cation confirmed the hypothesis of the importance of acidity-basicity balance to maximize EC yield. Among tested Zn- and Fe-containing materials the highest yield was obtained in the presence of Zn₁-Fe₂. However, the EC selectivity over Zn₁-Fe₂ was lower than over Zn₃-Fe₁ (Chapter 4) due to the increase of basicity which promotes EC decomposition and formation of the side product DEG. Introduction of Al and Mg also influenced catalytic performance. Al addition increased the acidity of the material and therefore selectivity towards EC at the expense of considerably lower EC yield. Addition of Mg over-enhanced basicity, and both EC yield and EC selectivity were deteriorated.

Aiming to improve acid-base balance of catalysts we explored another class of materials – zeolites. We studied catalytic performance and acid-base balance of ion-exchanged forms (H⁺, Na⁺, K⁺, Cs⁺) of Y-zeolite. It was observed that the A/B ratio could be varied by this approach and was decreasing in the order of H-Y>Na-Y>K-Y>Cs-Y, but the EC yield was low in all cases. Taking advantage of high selectivity of the zeolite materials we attempted to introduce active Lewis acid/base sites in the form of ZnO to the best performing Na-Y zeolite. The catalytic results showed that EC yield was improved and almost reached the values of pure ZnO whereas EC selectivity of the ZnO-containing zeolites was much higher. Thus, the selective nature of zeolites towards EC formation can be beneficially used to achieve higher EC yield when they are combined with other active sites added, e.g. by incorporation of ZnO, thereby only slightly enhancing the basicity of the materials.

References

1. Weitkamp, J.; Puppe, L., *Catalysis and Zeolites: Fundamentals and Applications*. Springer: 1999.
2. Barthomeuf, D., Acidity and Basicity in Zeolites. In *Stud. Surf. Sci. Catal.*, Elsevier: 1991; 65, 157-169.
3. (a) Hölderich, W. F.; van Bekkum, H., Zeolites in Organic Syntheses. In *Stud. Surf. Sci. Catal.*, Elsevier: 1991; 58, 631-726; (b) Weitkamp, J., New Directions in Zeolite Catalysis. In *Stud. Surf. Sci. Catal.*, Elsevier: 1991; 65, 21-46.
4. Marakatti, V. S.; Halgeri, A. B., *Rsc Advances* 2015, 5 (19), 14286-14293.
5. Doskocil, E. J.; Bordawekar, S.; Davis, R. J., Catalysis by solid bases. In *Catalysis: Volume 15*, The Royal Society of Chemistry: 2000; 15, 40-72.

Chapter 6

Design of Experiments

6.1 Introduction

Apart from the tuning of catalytic active sites, which was the major focus of the previous two chapters, other experimental variables can influence EC yield. Herein we applied a statistical method (Design of Experiment, DoE) [1] to optimize the process with as few experiments as possible. Some studies have been devoted to finding suitable reaction conditions for EC synthesis [2], where a common one-factor-at-a-time approach was used. Although this intuitive approach can directly reveal how certain factors affect yield, it covers the experimental parameter space very poorly and also reveals nothing about the interaction of these factors. In contrast, using the DoE approach, the space can be explored more efficiently with the aid of the mathematical algorithm and at the same time interactions and correlations of the parameters can be revealed.

6.2 Methods

Our general strategy in DoE was based on a preliminary evaluation of all factors and possible interactions between factors using Fractional Factorial Experimental Design, [3] followed by an optimization of the significant factors using Central Composite Design [3b, 4]. All reactions were run in the batch reactor under the same conditions using the same chemicals as in the previous chapters. As a catalyst Zn-Fe mixed oxide was chosen due to its excellent catalytic performance. A complete set of experiments was performed in a random order to avoid systematic error. The experimental design procedures implemented in The Unscrambler® version 10.2 from Camo software were used.

6.2.1 Screening experimental design

For Fractional Factorial Design, appropriate variables and their levels have to be selected. We have selected representative experimental parameters,

namely EG/urea molar ratio, temperature, time and catalyst loading. For screening design, we evaluated a wide range of variables to obtain a clear picture of how these factors affect EC yield and selectivity. Two levels (upper and lower limits) were chosen for each variable, named as “high” and “low”. Temperature range was 393-443 K, initial EG/urea molar ratio was in the range of 4-10, amount of catalyst was varied from 1-3 wt% of EG and time was restricted in 2-12 h. With these four design variables at high and low values for each variable 2^{4-1} experiments are required to resolve all effects by factors and two-factor interactions with highest for this design resolution IV. Resolution III is too low since two-factor interactions might be confounded with effects. Four response variables were evaluated: EC yield and selectivity, selectivities to the major side product (2-Ox) and second major side product (DEG). The obtained values are displayed in Table 6.1.

Table 6.1. Levels of design and response variables obtained with screening experimental design.

Design variables		Levels of design variables	
EG/urea ratio	4		10
Temperature	393 K		443 K
Time	2 h		12 h
Amount of catalyst	1 wt% of EG		3 wt% of EG
Response variables		Range of obtained results	
Y_{EC}	$0.1 \text{ mmol} \cdot \text{g}_{\text{cat}}^{-1} \cdot \text{mmol}_{\text{urea}}^{-1}$		$10.9 \text{ mmol} \cdot \text{g}_{\text{cat}}^{-1} \cdot \text{mmol}_{\text{urea}}^{-1}$
S_{EC}	26.8%		100%
S_{2-Ox}	0%		19.9%
S_{DEG}	0%		47.1%

To obtain a clear picture of the precision and the accuracy of the model and also to estimate experimental error, three center points (points for which the value of every design variable is set at its middle level) were evaluated. These considerations led to a set of eleven reactions which were performed in the batch reactor under the specified reaction conditions.

6.2.2 Optimization experimental design

Central Composite Design was performed to examine important factors and finally generate response surfaces for the EC yield and selectivity as a function of two selected parameters (reaction time and temperature). Since we set the defined limits for the two variables, Inscribed Central Composite Design was applied to explore the design space over the central point which requires five levels (possible values) of each variable. Two variables at five levels and two center samples were used, giving in total ten experiments. The values of the variables are listed in Table 6.2.

Table 6.2. Levels of design and response variables obtained with optimization experimental design.

Design variables		Levels of design variables	
Temperature	393 K		443 K
Time	2 h		12 h
Response variables		Range of obtained results	
Y_{EC}	$0.9 \text{ mmol} \cdot \text{g}_{\text{cat}}^{-1} \cdot \text{mmol}_{\text{urea}}^{-1}$		$2.9 \text{ mmol} \cdot \text{g}_{\text{cat}}^{-1} \cdot \text{mmol}_{\text{urea}}^{-1}$
S_{EC}	67%		100%

The other experimental variables were fixed at the optimum values previously defined: EG/urea ratio 10 and the catalyst amount of 3 wt% of EG.

6.3 Results and discussion

6.3.1 Screening experimental designs

The results of the catalytic runs are summarized in Table 6.3.

Table 6.3. Catalytic results of a set of experiments suggested by screening experimental design.

Name	EG/ urea	Temp. / K	Time / h	Amount of catalyst / wt%	$Y_{EC} /$ $\text{mmol} \cdot \text{g}_{\text{cat}}^{-1} \cdot$ $\text{mmol}_{\text{urea}}^{-1}$	$S_{EC} /$ %	$S_{2\text{-Ox}} /$ %	$S_{DEG} /$ %
1	4	393	2	1	0.2	100	0	0
ad	10	393	2	3	0.1	100	0	0
bd	4	443	2	3	3.6	80.1	0	18.3
ab	10	443	2	1	10.9	92.4	3.1	4.5
cd	4	393	12	3	7.0	95.7	2.4	1.5
ac	10	393	12	1	7.4	100	0	0
bc	4	443	12	1	4.7	26.8	19.9	47.1
abcd	10	443	12	3	3.0	55.7	6.1	36.8
cp01	7	418	7	2	6.5	93.7	3.4	2.9
cp02	7	418	7	2	5.4	86.5	5.9	6.5
cp03	7	418	7	2	4.9	79.5	7.5	10.6

The detailed analysis of variance (ANOVA) is presented in Table 6.4. P-values and F-ratio show how well model fits responses – the lower the p-values, the higher the probability, meaning that model would be more adequate. For instance, p-values of Y_{EC} 0.03 mean, that the model is valid with the significance level of 97%. According to p-values, all models seem adequate, although the significance level of the model for S_{DEG} is less than 95%.

From the analysis of effects, it is also clear that the most significant factors influencing selectivity of products are temperature and time. Neither EG/urea ratio nor catalyst loading had considerable effects on the response variables.

Interaction of two variables – time and temperature was found to be the most significant to influence Y_{EC} . Interaction of temperature and time is also significant factor for selectivity of EC, 2-Ox and DEG.

Interaction between variables can also be represented graphically by plotting parameters against one of the variables overlaid with a second one. If the lines run in parallel, there is an independence of these variables, but if the lines are diverted this indicates the presence of interaction between them. Figure 6.1 displays interaction of variables “time” and “temperature” for parameters Y_{EC} , S_{EC} , S_{2-Ox} and S_{DEG} . A positive interaction between two variables means that when one variable increases the effect exerted by the second variable increases. From the plots it is clear that these variables have strong negative interaction in case of EC yield. For product selectivity, positive interaction between “time” and “temperature” was observed. The presence of such interaction implies that different optimum reaction times would exist at different temperatures, which is completely ignored in the one-factor-at-a-time method, where the interdependence of factors would have been missed.

After identifying the important variables, we initiated optimization study applying Central Composite Design in order to obtain response surface and optimum values for temperature and time.

Table 6.4. ANOVA Summary for response variables for screening design

ANOVA	Y _{EC}			S _{2-Ox}			S _{DEG}		
	F-ratio	p-value	F-ratio	p-value	F-ratio	p-value	F-ratio	p-value	
Model	12.06	0.032	13.36	0.03	9.44	0.05	7.94	0.06	
Variables									
EG/urea (A=BCD)	3.76	0.15	4.82	0.11	4.41	0.12	1.84	0.26	
Temperature (B=ACD)	6.23	0.09	46.26	0.01	18.07	0.02	31.17	0.01	
Time (C=ABD)	5.74	0.09	20.75	0.02	16.24	0.03	11.04	0.04	
Amount of catalyst (D=ABC)	9.69	0.05	0.35	0.59	5.38	0.10	0.07	0.80	
EG/urea·Temp (AB=CD)	3.14	0.17	3.18	0.17	1.78	0.27	1.44	0.31	
EG/urea·Time (AC=BD)	7.97	0.06	1.01	0.38	9.52	0.05	0.01	0.92	
Temp·Time (BC=AD)	47.85	0.01	17.17	0.02	10.66	0.05	10.01	0.05	

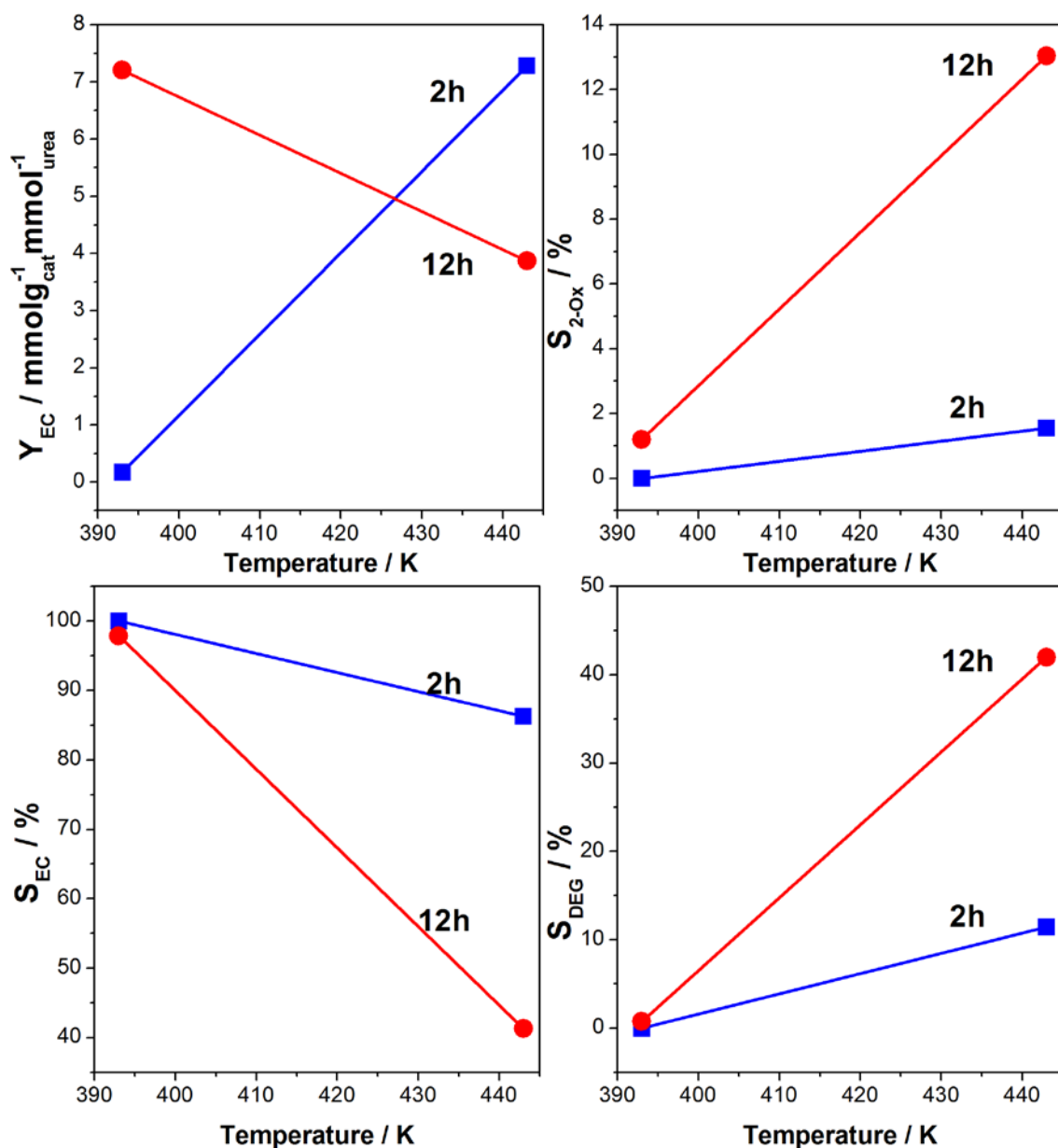


Figure 6.1. Time-temperature interaction graphs of the screening study.

6.3.2 Optimization experimental design

As it was shown previously, screening design is linear, which means it has only two levels. They connect all points with straight lines and a mathematical optimum cannot be modeled. The model of the reaction can be refined with a more detailed second non-linear study, such as response surface study (RSM) which is used in this work. The points in the RSM model were chosen according

to Central Composite Design. In this case, results of the experiments performed in optimization design were analyzed independently from results of screening design, i.e. previous values were not used. The factors investigated in this study were the only important ones identified earlier, i.e. reaction time and temperature.

The summary of performed experiments in optimization design is shown in Table 6.5.

Table 6.5. Catalytic results in optimization design.

Name	Temp. / K	Time / h	$Y_{EC} /$ $\text{mmol}\cdot\text{g}^{-1}_{\text{cat}}\cdot\text{mmol}^{-1}_{\text{urea}}$	$S_{EC} /$ %	$S_{2-Ox} /$ %	$S_{DEG} /$ %
Cube1	400	3.5	1.01	96.7	3.3	0
Cube2	436	3.5	4.07	82.1	7.2	8.9
Cube3	400	10.5	2.75	98.7	0	1.3
Cube4	436	10.5	3.36	59.8	27.6	10.0
Axial A(low)	393	7.0	1.35	100.0	0	0
Axial A(high)	443	7.0	2.75	67.1	21.7	9.3
Axial B(low)	418	2.0	3.54	86.1	8.3	5.2
Axial B(high)	418	12.0	1.91	98.4	0	1.6
cp01	418	7.0	2.76	92.8	3.7	3.3
cp02	418	7.0	2.82	93.5	2.7	3.8

The model generated by optimization design for EC selectivity is an approximation of the reality which is demonstrated in ANOVA table (Table 6.6). Significance level of the model (p-value) is 0.05 indicating that the model is useful. On the other hand, probability for the model of EC yield to be significant is quite low, 87% according to the p-value of 0.13. This implies the lower level of confidence for estimating the optimum experimental condition for EC yield using the model.

Table 6.6. ANOVA Summary for response variables of optimization design.

ANOVA Summary	Y_{EC}		S_{EC}	
	F-ratio	p-value	F-ratio	p-value
Model	6.71	0.13	19.28	0.05
Temperature (A)	25.54	0.03	91.45	0.01
Time (B)	5.64	0.14	13.07	0.06
Temp·Time (AB)	8.89	0.09	11.57	0.07
Temp·Temp (AA)	1.92	0.30	11.48	0.07
Time·Time (BB)	0.13	0.75	0.63	0.51
Temp·Temp·Temp (AAA)	23.42	0.04	97.04	0.01
Time·Time·Time (BBB)	8.22	0.12	13.81	0.06

The results of the optimization study are depicted at the response surfaces where the optima are clearly visualized. Figures 6.2 and 6.3 show the response surfaces of the two variables: EC yield and selectivity, respectively. Analyzing these 3D plots following general conclusions can be drawn:

- The higher the temperature and the shorter the reaction time, the better EC yield.
- The lower the temperature, the higher EC selectivity.

The optima in EC yield and selectivity are clearly defined on the response surfaces: $5.2 \text{ mmol}_{\text{cat}}^{-1} \cdot \text{mmol}_{\text{urea}}^{-1}$ when at 439 K in 2 h, and 118% EC selectivity at 395 K after 12 h. Although the analysis of variance indicated that predicted model for Y_{EC} has a relatively low significance level, the model of S_{EC} appears to be adequate (p-values around 0.05) as mentioned above.

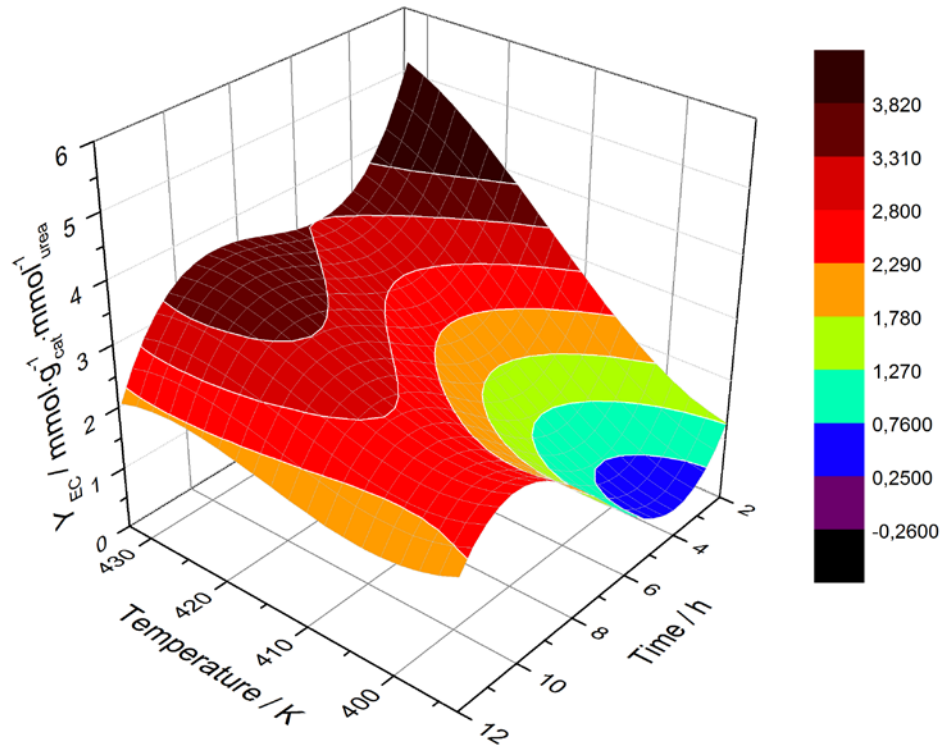


Figure 6.2. Response surface for Y_{EC} .

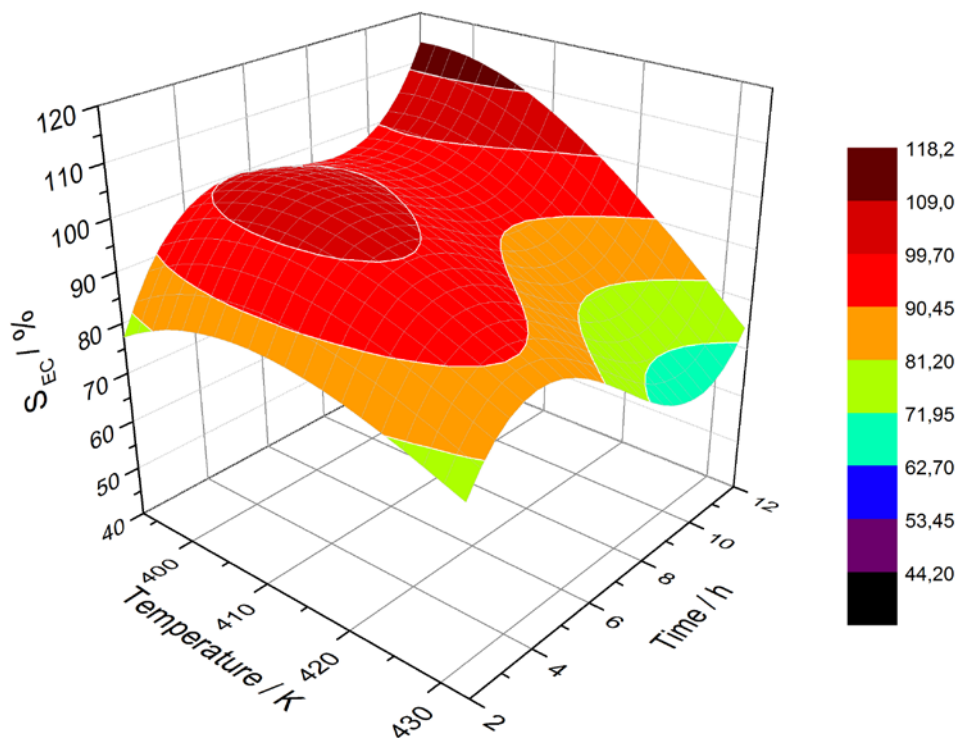


Figure 6.3. Response surface for S_{EC} .

To substantiate both generated models, verification experiments were performed under the two conditions (predicted by S_{EC} model and Y_{EC} model) using the Zn-Fe mixed oxide. Both reaction conditions were highly favorable for the EC synthesis. The first condition resulted in an excellent EC selectivity (99.6%) and a good EC yield ($16.1 \text{ mmol}\cdot\text{g}_{\text{cat}}^{-1}$), while the second case led to the highest obtained EC yield ($28.6 \text{ mmol}\cdot\text{g}_{\text{cat}}^{-1}$) and a good EC selectivity (93.3%). These are considerable improvements compared to the EC yield and selectivity obtained in our standard conditions (423 K and 6 h) which yielded $25.9 \text{ mmol}\cdot\text{g}_{\text{cat}}^{-1}$ with 91.5% EC selectivity.

The obtained EC yield for the latter case was lower than predicted by the model ($44.1 \text{ mmol}\cdot\text{g}_{\text{cat}}^{-1}$). The deviation from the model is likely due to the high complexity of underlying parameters influencing EC yield. Since the investigated reaction of urea transesterification with EG is consecutive and parallel with additional side reactions, it is not an easy task to predict precisely the yield of the target product. Nevertheless, the generated models are found to be useful approximation of the EC yield and selectivity, well predicting a set of parameters that yield excellent catalytic results.

6.4 Conclusions

In a sequential experimental design as a screening study we applied Fractional Factorial Design in order to estimate significance of the main effects and the variable interactions. Important variables were further optimized by Central Composite Design. The evaluation of the global linear model, global quadratic model, quadratic effects and shape of the response surface was done by analysis of variance (ANOVA).

Optimization of reaction conditions was performed for the selected catalyst (Zn-Fe) in a batch reactor. According to the response surfaces, two optimum sets of reaction time and temperature were suggested advantageous to yield high S_{EC}

and Y_{EC} : (1) 12 h at 395 K and (2) 2 h at 439 K. The reaction was performed under the two conditions and the standard conditions for the rest of the experimental parameters of this work using the Zn-Fe mixed oxide.

Both, very distinct, reaction conditions were highly beneficial for EC selectivity and yield. The first condition led to an excellent EC selectivity (99.6%) with a good EC yield ($16.1 \text{ mmol}\cdot\text{g}_{\text{cat}}^{-1}$), while in the second case, a very high EC yield ($28.6 \text{ mmol}\cdot\text{g}_{\text{cat}}^{-1}$) was obtained with a high EC selectivity (93.3%). Compared to the previously achieved values for EC yield ($25.9 \text{ mmol}\cdot\text{g}_{\text{cat}}^{-1}$) and selectivity (91.5%) at 423 K and 6 h, there is a clear advantage of DoE to improve the reaction parameters with a small number of tests, identifying important reaction conditions that would not be tested otherwise. EC selectivity was maximized using the specific reaction conditions at lower temperature and EC yield was maximized with the high reaction temperature but with the much shorter reaction time. This DoE study clearly shows the usefulness and effectiveness of statistical approaches to maximize the target product selectivity and yield in the complex, consecutive and acid-base catalyzed reactions.

References

1. Esbensen, K. H.; Guyot, D.; Westad, F.; Houmoller, L. P., *Multivariate Data Analysis In Practice: an Introduction to Multivariate Data Analysis and Experimental Design*. Camo Process AS: 2002.
2. (a) Zhao, X.; An, H.; Wang, S.; Li, F.; Wang, Y., *J. Chem. Technol. Biotechnol.* 2008, 83 (5), 750-755; (b) Bhanage, B. M.; Fujita, S.; Ikushima, Y.; Arai, M., *Green Chem.* 2003, 5 (4), 429-432; (c) Wang, P.; Liu, S.; Zhou, F.; Yang, B.; Alshammari, A. S.; Lu, L.; Deng, Y., *Fuel Process. Technol.* 2014, 126 (0), 359-365.
3. (a) Araujo, P. W.; Brereton, R. G., *TrAC, Trends Anal. Chem.* 1996, 15 (1), 26-31; (b) Massart D. L. ; Vandeginste B. G. M.; Buydens L. M. C.; De Jong S.; Lewi P. J.; Smeyers-Verbeke, J., *Handbook of Chemometrics and Qualimetrics: Part A*. Elsevier: Amsterdam, 1997; 20A, 643-738.
4. Araujo, P. W.; Brereton, R. G., *TrAC, Trends Anal. Chem.* 1996, 15 (2), 63-70.

Chapter 7

Static and Transient *In situ* ATR-IR Study of Activation Mechanism

7.1 Introduction

In the previous chapters, the roles of acidic and basic sites were discussed and correlated with the observed catalytic performance. It was shown that acidic sites can efficiently catalyze urea conversion and are also responsible for the selective formation of EC, whereas basic sites promote the undesired side reactions. It is, however, not yet understood how chemical components of the reaction mixture interact with the surface active sites and what kind of species are formed.

Previously some researchers reported a reaction mechanism by analyzing the species formed on the surface of the catalyst upon exposing it to urea [1]. Observed species were identified as isocyanates, as the product of urea decomposition [2]. However these studies were not performed under reaction conditions and dynamic chemical insights (reaction path) have not been studied. One of the few effective ways to elucidate active species and intermediates on the catalyst surface is *in situ* ATR-IR spectroscopy by coating the catalyst over IRE so that the obtained signals contain rich information about surface species.

In situ ATR-IR spectroscopy affords the detection of species adsorbed on a catalyst under reaction conditions [3]. However, the often-dominating signals due to solvents, spectator species and/or the catalyst itself make it very difficult to identify and track the truly active species. To selectively detect species directly involved in a reaction at solid-liquid interface and monitor their dynamic behavior, transient experiments can be useful. The principle of such methods is based on perturbing a catalytic system working under steady state conditions by changing one of the parameters that has an effect on the state/concentration of active species (reagent concentration, temperature etc.). The signal of the chemical species affected by the change will show concentration/spectral changes. To deconvolute pure component spectra, a second-order chemometric tool for

studying dynamics of complex systems, MCR, was applied here [4]. Thus, temporal evolution of components, i.e. active species and intermediates can be obtained and insights into the catalytic mechanism could be addressed.

In this chapter we investigate the interaction of reagents, urea and 2-HC, with the surface of single and mixed metal oxides by performing static and transient experiments monitored by *in situ* ATR-IR spectroscopy and subsequent MCR analysis in order to understand the activation of both reagents and propose activation/reaction mechanisms.

7.2 Experimental section

7.2.1 Catalyst and experimental setup

Interactions of urea and 2-HC with single and mixed metal oxides were investigated by *in situ* time-resolved ATR-IR spectroscopy using a flow-through cell. As an internal reflection element (IRE) 45° trapezoidal ZnSe crystal with the dimension of 80×10×4 mm³ was used. The gap between the polished surface of an aluminum cover of the cell and the IRE was 1.5 mm and the cell sealed by a Viton O-ring. The length and width of the exposed area of the IRE was ca 76x6 mm², respectively. The edges of the exposed area were rounded off to avoid stagnant regions of the flowing liquid. The total volume of the cell was 684 μL. The flow-through cell can be heated and cooled by means of a thermostat. The static experiment was performed at room temperature and the transient experiment was performed at 373 K.

Mixed oxides with the general formula M_b²⁺-M_t³⁺ containing Mg²⁺/Zn²⁺ as bivalent cation (M_b²⁺) and Al³⁺/Fe³⁺ as trivalent cation (M_t³⁺) with a constant molar ratio M_b²⁺/M_t³⁺=3 were synthesized by the co-precipitation method described in Chapter 2. The synthesis of metal oxide materials (ZnO, Al₂O₃, MgO, Fe₂O₃), followed the same synthesis protocol.

5 mg of catalyst powder were dispersed in 10 mL of ethanol. The slurry was dropped on one side of IRE using a micropipette and obtained catalyst layer was dried at room temperature overnight. After drying the crystal was placed in ATR flow-through cell.

After assembling, the cell was mounted onto an ATR attachment (PIKE Technologies) within the Fourier transform IR spectrometer (Bruker, Tensor 27). The bench of the spectrometer was continuously purged with nitrogen to eliminate CO₂ and water vapor contributions to the spectra. Spectra were recorded at 4 cm⁻¹ resolution. Liquid solution was passed from two separate glass bottles over the sample by means of a peristaltic pump (ISMATEC Reglo) situated after the cell. The source of liquid flow, thus the selection of the two tanks, was controlled by a pneumatically actuated three way Teflon valve (PARKER PV-1-2324). Teflon tubing was used throughout. A schematic drawing of the ATR-IR system is shown in Figure 7.1.

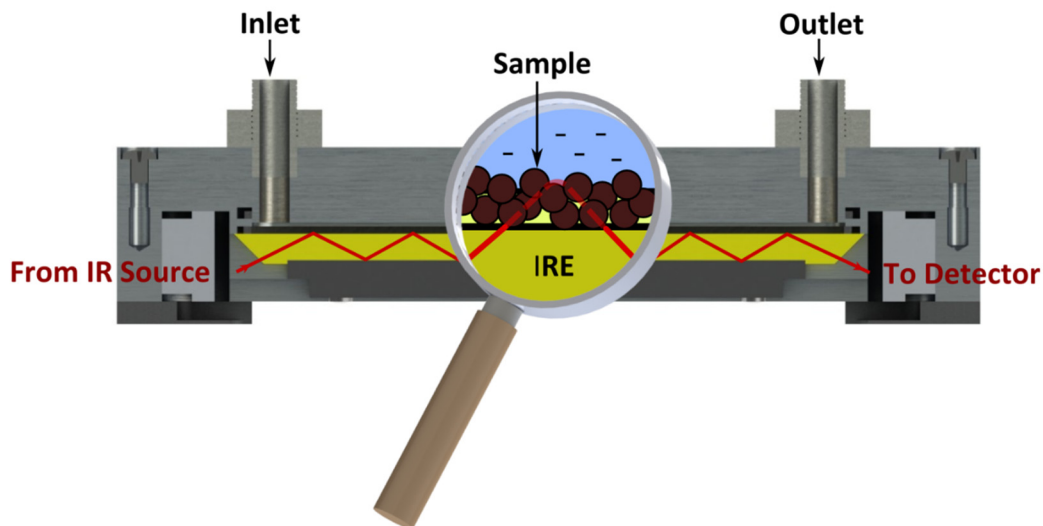


Figure 7.1. ATR-IR flow-through cell for static and transient experiments.

7.2.2 *In situ* static experiment

Interaction of urea and 2-HC with the catalyst surface was studied by using respective solution in acetonitrile (ACN) at a concentration of 0.06 M. Prior to each experiment pure ACN was passed through the cell with a catalyst deposited on the IRE and a background spectrum was acquired. Solution of urea or 2-HC was pumped over the catalyst until no changes over time were observed in the spectra. After the spectral changes were stabilized, the liquid flow was switched back to ACN and kept pumping until urea or 2-HC was completely removed from the cell and signal was stabilized. Then the spectra of the adsorbed reagents were collected subsequently.

7.2.3 *In situ* transient experiment

Behavior of active species and intermediates was monitored by *in situ* transient experiments performed at 373 K using 0.03 M solutions of urea or 2-HC in EG and pure EG. Preliminarily, pure EG was passed through the cell over the catalyst and a background spectrum was recorded. After the stabilization of the spectrum, a solution of the reagent (urea or 2-HC) was passed over the catalyst until the signal was stabilized. Transient experiment was then started by periodically pumping solution with the reagent against pure EG at the flow rate of 0.17 mL·min⁻¹. 60 spectra were collected over one period at the speed of 20 spectra per sample. Normally, 6-12 periods were studied for one transient experiment.

7.2.4 Data treatment

The spectra of transient experiment were read into and processed in MATLAB [5]. The experimental data were arranged in matrices, where the rows were the recorded spectra and the columns were the absorbance values at

different wavenumbers. The data containing multiple cycles were averaged into one period to improve signal-to-noise and baseline correction was performed.

Obtained time-resolved spectra were analyzed in Unscrambler [6] applying MCR-ALS method, described in Chapter 2. Resulting absorbance spectra of pure components were scaled in a way that the corresponding concentration profiles normalized with respect to the maximum concentration taken from corresponding concentration profiles.

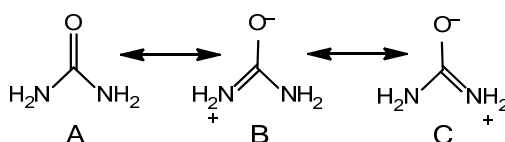
7.3 Results and discussion

7.3.1 Urea activation

7.3.1.1 *In situ* static experiment: Urea adsorption over single and mixed metal oxides

Urea is considered as a basic molecule that has several possibilities to react with surface of metal oxides. Depending on the nature of metal cation in metal oxides urea molecule forms coordination bond either with oxygen or nitrogen. These coordination bonds result in changes of electron distribution in the urea molecule which can be observed by IR.

The structure of urea involves resonance between the following three forms:



When urea forms a coordination bond to a metal through O atom, the contribution of structure A will decrease and this will result in more double bond character for the C-N bond and more single bond character for the C-O bond. The results in a decrease in the C-O frequency and an increase in the C-N stretching frequency, with unaltered N-H stretching frequency [7]. On the other

hand, coordination with metal ions through the nitrogen atom may occur according to Penland et al. [8]. In this case the contributions of structures B and C will decrease, resulting in an increase of C-O stretching frequency and a decrease of N-C and N-H stretching frequencies with the presence of two N-H and two N-C-N deformation bands due to the free and coordinated CNH_2 groups of the same coordinated urea molecule.

Taking this background into account we have measured spectra of urea over single and mixed metal oxides and compared the spectra with pure urea spectrum in liquid phase. Spectra are presented in Figure 7.2.

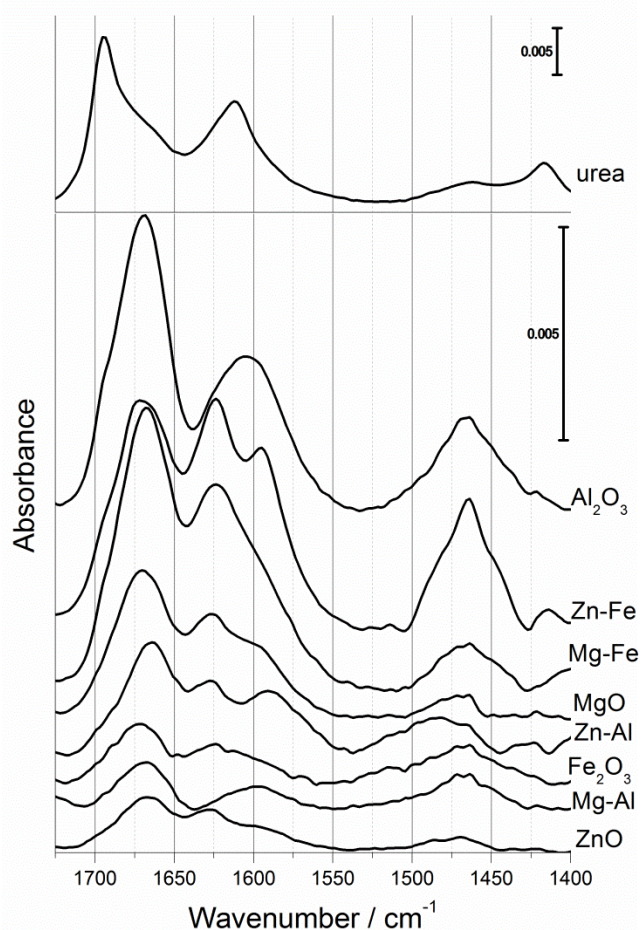


Figure 7.2. ATR-IR spectra of urea in solution and adsorbed on metal and mixed oxides.

In the region of 1400-1700 cm^{-1} four IR bands are expected: $\nu(\text{CO})$, $\nu_{\text{as}}(\text{CN})$, and symmetrical and asymmetrical NH_2 -deformation (or bending, $\delta(\text{NH}_2)$) vibrations. However, in the literature there are contradictions and uncertainties regarding the position of these bands.

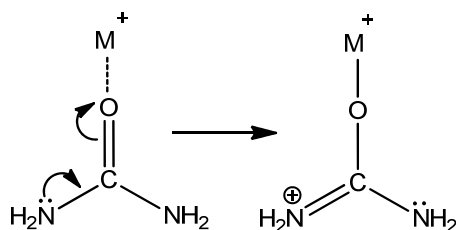
The reference spectrum of urea in solution (Figure 7.2, top) shows three strong bands characteristic of vibrational modes of urea. The sharp intense peak at 1695 cm^{-1} corresponds to CO stretching vibrational mode $\nu(\text{CO})$, the second strong peak at 1612 cm^{-1} is the bending vibrations of $\delta(\text{NH}_2)$ and the third less intense peak at 1416 cm^{-1} is attributed to asymmetrical CN stretching vibration $\nu_{\text{as}}(\text{CN})$, according to Hadzi and Stewart [9]. There is no agreement in the literature about the relative position of the $\nu(\text{CO})$ and the $\delta_{\text{s}}(\text{NH}_2)$ vibrations. Some authors claim that there is considerable coupling of both $\nu(\text{CO})$ and $\delta_{\text{s}}(\text{NH}_2)$ [10]. According to some calculations and IR and Raman analysis [10a, 11], the band at 1683 cm^{-1} has minor contribution of $\nu(\text{CO})$, whereas the band around 1601 cm^{-1} has more $\nu(\text{CO})$ character. Moreover in agreement with the literature [12] the bands of $\delta_{\text{as}}(\text{NH}_2)$ and $\nu_{\text{as}}(\text{CN})$, are expected to be observed at 1625 and 1466 cm^{-1} , respectively. These contradictions and uncertainties originated from the fact that the interpretation was made based on gas phase theoretical calculations for a urea sample measured in a solid form due to strong packing and intermolecular interactions in molecular solids. The most relevant study of urea in ACN solution is that of Hadzi et al. [9a], although their assignment is limited to only in-plane vibrations. The IR band assignments and positions are listed in Table 7.1, where they are compared with IR data of our study.

Table 7.1. Band assignments and positions of urea adsorbed on single and mixed metal oxides.

Assign.	Urea [9a]	Urea (exp)	A ₂ O ₃	MgO	Mg-Al	ZnO	Mg-Fe	Zn-Fe	Zn-Al	Fe ₂ O ₃
$\nu(\text{CO})$	1695	1695	1669	1670	1672	1668	1668	1669	1664	1672
$\delta_s(\text{NH}_2)$	1614	1612	1593	1593	1593	1593	1593	1593	1593	1593
$\delta_{as}(\text{NH}_2)$	1614	1612	1622	1631	1622	1628	1625	1626	1628	1626
$\nu_{as}(\text{CN})$	1419	1416	1466	1469	1464	1469	1467	1464	1487	1467

The region of 1550–1700 cm^{-1} where three bands are observed causes difficulty in differentiating the $\nu(\text{CO})$ from the two $\delta(\text{NH}_2)$ deformation bands. The strong bands at 1664–1672 cm^{-1} are assigned to $\nu(\text{CO})$. Observed red-shift of $\nu(\text{CO})$ (as compared with urea in ACN) indicates an interaction of carbonyl group with metal cation of single and mixed metal oxides and/or weakening of the bond by the interaction. Due to the formation of metal-oxygen bonds (or strong interaction), the coupling between the bands of the $\nu(\text{CO})$ stretching and $\delta(\text{NH}_2)$ bending decreases, causing them to be more separated. Therefore, $\delta_{as}(\text{NH}_2)$ can be attributed to the band appearing around 1625 cm^{-1} , and $\delta_s(\text{NH}_2)$ to the band around 1593 cm^{-1} . Besides, the bands located at 1464–1487 cm^{-1} correspond to $\nu_{as}(\text{CN})$, which are blue-shifted due to the strengthened C-N bonds by the oxygen coordination to the metal sites.

The IR study of urea adsorption (Table 7.1) clearly indicates that urea coordinates to the surface metal atoms of metal oxides via the carbonyl oxygen, forming a chemical bond or resulting in a strong interaction inducing changes in the distribution of electrons in the urea molecule. As the results, the C-N bond is strengthened as illustrated by the scheme below.



7.3.1.2 *In situ* transient experiment: Urea activation over single and mixed metal oxides

Activation of urea requires elevated temperature. It is known that urea starts to decompose above 425 K, forming ammonia, cyanic acid (HNCO) and ammonium cyanate (NH₄NCO) [2, 13]. According to an IR study of urea decomposition [2], NCO⁻ formation was observed at the temperature close to the melting point of urea (406 K). Such species are reported to be reactive in transesterification of urea with alcohols [1, 14]. Moreover, some amphoteric and Zn-containing metal oxides are prone to produce NCO⁻ species and thus, improve urea conversion.

To study urea activation and formation of active species during the reaction over the catalyst surface, transient *in situ* ATR-IR spectroscopic experiments were performed at 373 K close to the temperature of the catalytic tests by passing alternatingly urea in EG and only EG solvent. The obtained and averaged time-resolved spectra were processed by MCR, separately for two regions 1500–1750 cm⁻¹ and 2100–2300 cm⁻¹. The most representative component spectra are presented in Figure 7.4.

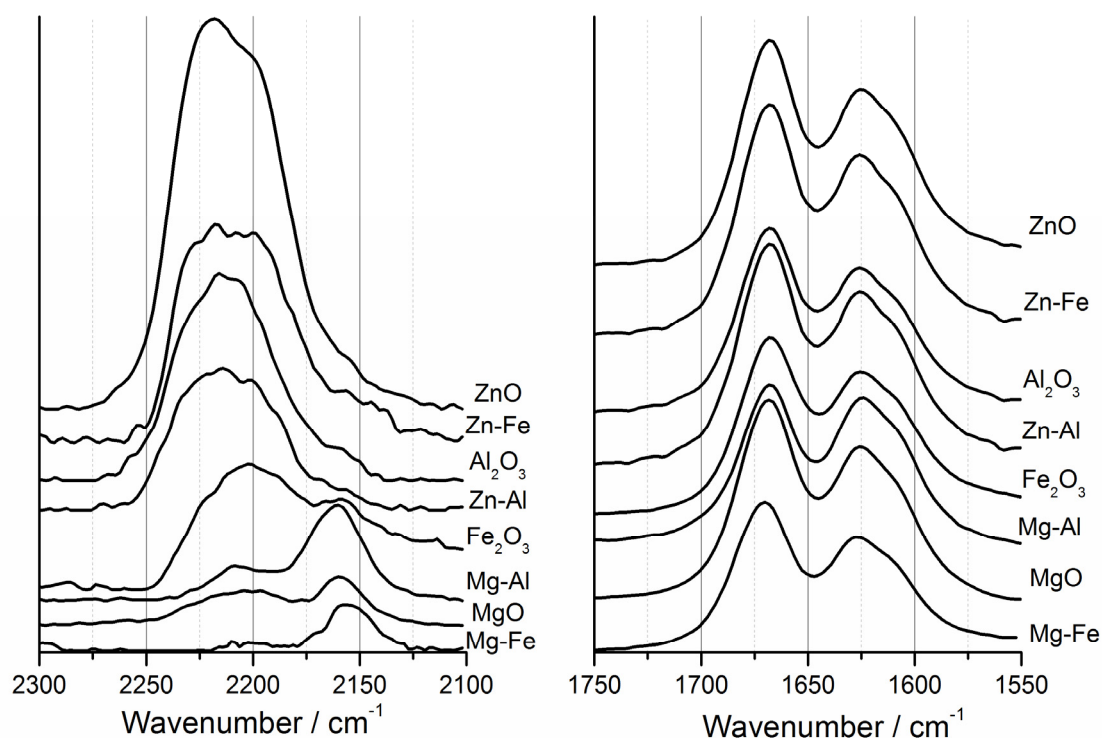
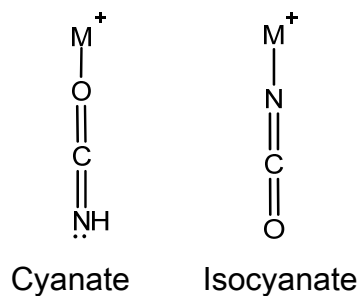


Figure 7.3. The major component spectra obtained by MCR with the spectra of transient *in situ* ATR-IR experiments by alternatingly passing urea in EG and only EG over single and mixed metal oxides at 373 K.

The region of 1550–1750 cm^{-1} shows almost identical spectral features, suggesting the chemical component to be urea in EG solution. The bands at 1669 cm^{-1} and 1625 cm^{-1} are attributed to the $\nu(\text{CO})$ and $\delta(\text{NH}_2)$ modes of urea, respectively. The spectral features are similar to those of the urea in ACN solution (Figure 7.2) but with some differences. The differences indicate that the bands of urea extracted by MCR are mostly urea in solution which is, on average, interacting with the metal oxide surfaces or reversibly adsorbing/desorbing over the surface.

The region of 2100–2300 cm^{-1} presents the second chemical component with new spectral features that were not observed in the static room temperature measurements. Two bands were found in this region for all samples, which may be originated from different species or from the same chemical species. For some materials such as Al_2O_3 , Fe_2O_3 and Zn-containing metal oxides, the band at 2212

cm^{-1} is more pronounced, whereas in case of Mg-containing oxides peak at 2161 cm^{-1} is more intense than the band at 2212 cm^{-1} . According to the study of Paul et al. [15] the band at 2212 cm^{-1} could be preliminary assigned to asymmetric stretching vibrations of cyanate coordinating to metal cation through oxygen (NCO-M), whereas position of the band at 2161 cm^{-1} is probably attributed to nitrogen-coordinated cyanate (M-NCO):



To check whether the new component is indeed active species and does not belong to urea in solution or solvent, the concentration profiles of the two components (shown in Figure 7.3) are presented in Figure 7.4, taking ZnO as an example. The concentration of the species showing peaks at $2100\text{--}2300 \text{ cm}^{-1}$ is changing periodically and has a delay of 7-10 min compared with that assigned to "urea in solution". This confirms that the formation of the new component depends on concentration profile of urea and its formation requires time. It is also important to note that the surface species disappears with delay when urea concentration decreases. Therefore, the new component can be classified as active species forming from urea at elevated temperatures.

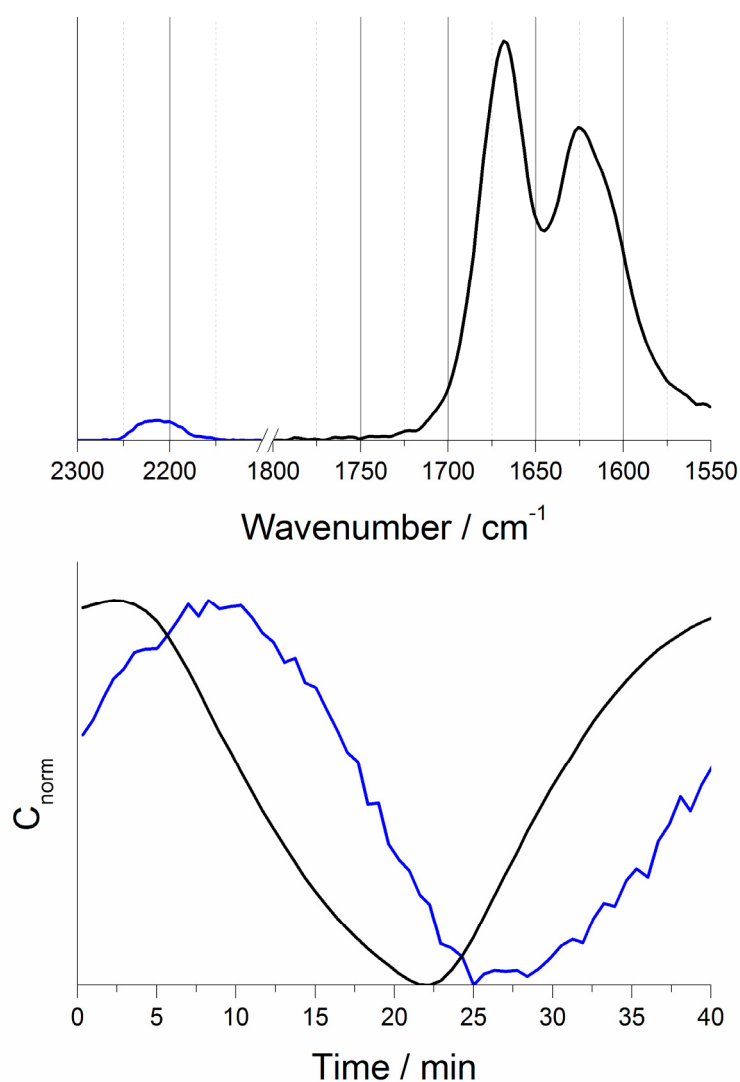


Figure 7.4. (top) Component spectra and (bottom) component concentrations obtained by MCR from the spectra of transient *in situ* ATR-IR experiment of urea over ZnO.

To identify the nature of active species, the identical experiments using urea isotopomers labelled with ¹³C and ¹⁵N were performed. As representing samples facilitating the formation of the species with the bands at 2212 cm⁻¹ and 2161 cm⁻¹, two materials giving most pronounced signal for one of the bands were selected: Al₂O₃ to monitor the band at 2212 cm⁻¹ and Mg-Al to monitor the band at 2161 cm⁻¹. The spectra using urea isotopomers after MCR analysis for the region of 2050–2300 cm⁻¹ are shown in Figure 7.5.

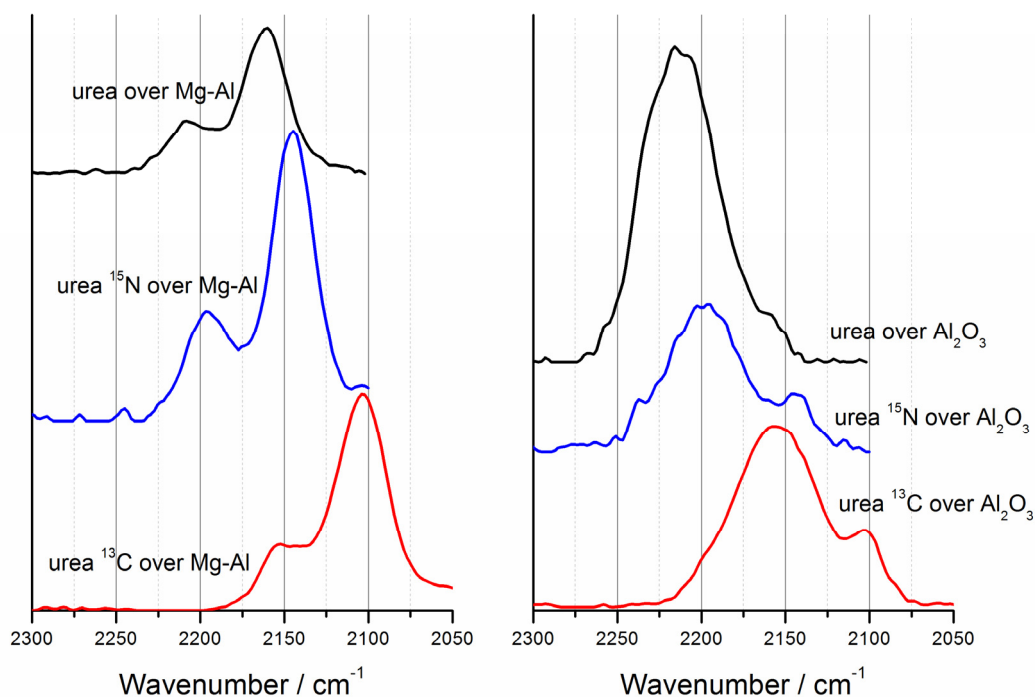


Figure 7.5. The major component spectra obtained by MCR from the spectra of transient *in situ* ATR-IR experiment using urea isotopomers over Al_2O_3 and Mg-Al in the region of 2050-2300 cm^{-1} .

For both Al_2O_3 and Mg-Al, substitution of nitrogen in urea by ^{15}N causes red-shift by 16-17 cm^{-1} for both bands. When carbon atom in urea is substituted by ^{13}C , a prominent red-shift by 57-58 cm^{-1} was observed. The band positions are summarized in Table 7.2. The observed red-shifts of both bands clearly point out the presence of both C and N atoms in the structure of active species, which is in a good agreement with previous assignment of bands 2212 cm^{-1} and 2161 cm^{-1} to cyanate (oxygen-coordinated NCO-M) and isocyanate (nitrogen-coordinated OCN-M), respectively [15].

Table 7.2. Band position of transient surface species formed by urea (and urea isotopomers) adsorption over Al₂O₃ and Mg-Al.

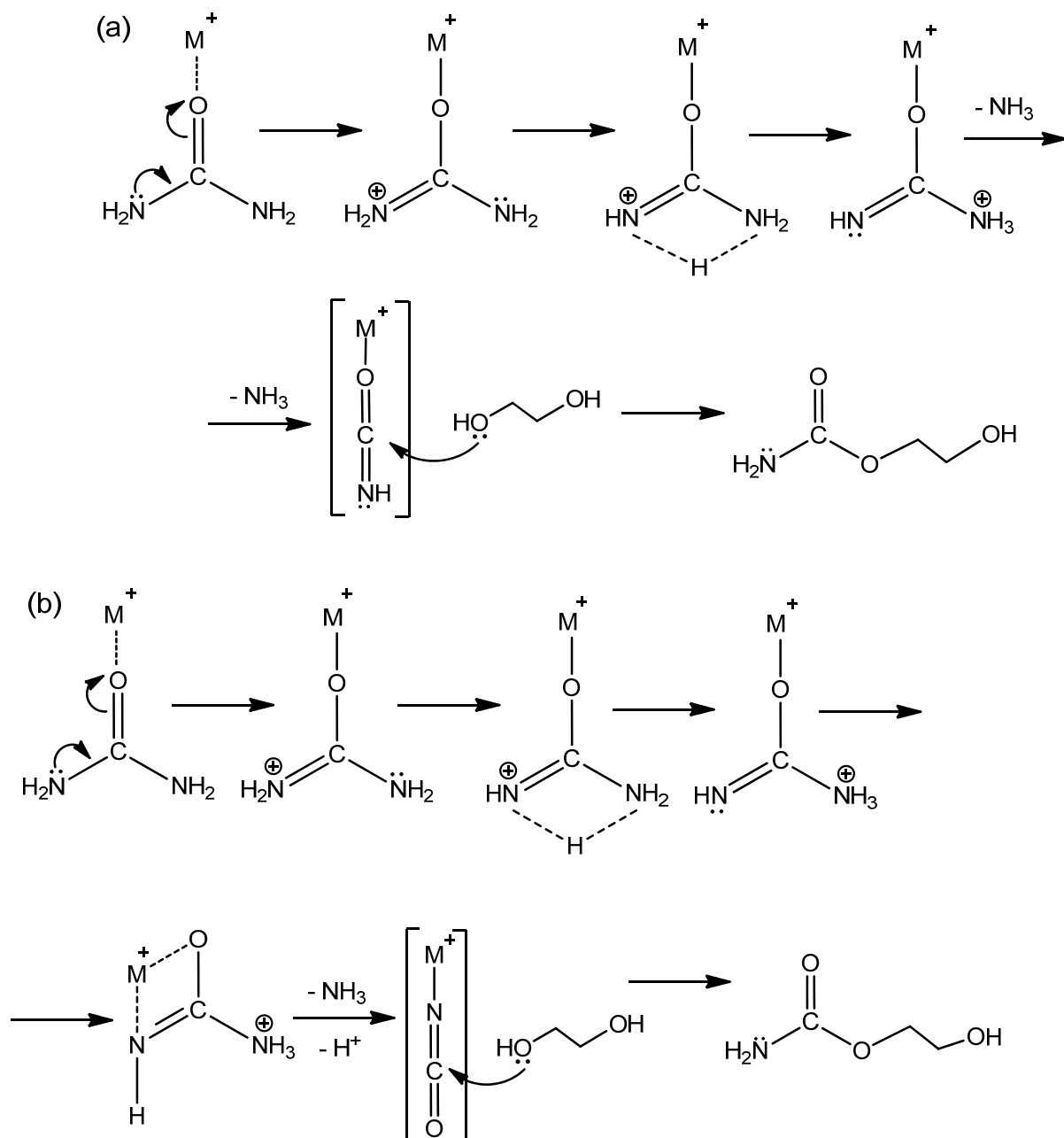
Mg-Al / cm ⁻¹			Al ₂ O ₃ / cm ⁻¹		
Urea	2212	2161	Urea	2212	2161
Urea ¹⁵ N	2196	2144	Urea ¹⁵ N	2196	2146
Urea ¹³ C	2154	2104	Urea ¹³ C	2156	2104

On the basis of the findings mechanism of urea activation with formation of two types of active species can be suggested.

7.3.1.3 Mechanism of urea activation

In situ static and transient IR experiments of urea interaction with the metal oxides indicate that urea molecule coordinates to metal cations through oxygen of carbonyl group and upon heating two types of active species are formed depending on the nature of metal oxides. Zn-containing mixed oxides, ZnO, Al₂O₃ and Fe₂O₃ were prone to form oxygen-coordinated cyanate species, whereas interaction of urea with Mg-containing oxides results in nitrogen-coordinated isocyanate species (Scheme 7.1 a and b).

Urea molecule, coordinating through oxygen with electrophilic metal cation, undergoes proton transfers at elevated temperatures. Afterwards in case of Zn-containing oxides metal – OCN complex is formed by elimination of one ammonia molecule and can be further attacked by oxygen of –OH group in EG, producing 2-HC (Scheme 7.1a)



Scheme 7.1. Mechanism of urea activation and reaction with EG over (a) Al₂O₃, Fe₂O₃ and Zn-containing oxides, (b) Mg-containing oxides.

In case of Mg-containing oxides after proton transfer, nitrogen atom that possesses lone electron pair coordinates to metal cation, forming metal–NCO complex after ammonia elimination. EG molecule subsequently attacks carbon atom of the new fragment resulting in 2-HC (Scheme 7.1b).

In both suggested mechanisms, formation of active species with different coordination to metal cation (either M-NCO or M-OCN) does not influence reaction outcome since only one possible product – 2-HC – is obtained by nucleophilic attack of oxygen in EG on carbon. According to the schemes, it is a prerequisite to activate urea by ammonia removal and make it available for EG attack. In Chapter 4, mildly acidic materials were efficient in urea activation. These materials are those forming cyanate where oxygen is coordinated. It may be possible that the urea activation path via oxygen coordination (Scheme 7.1a) is more facile than nitrogen coordination (Scheme 7.1b) because the latter requires oxygen as well as nitrogen activation at one step whereas the former requires only oxygen coordination.

7.3.2 2-HC activation

7.3.2.1 *In situ* static experiment: 2-HC adsorption over single and mixed metal oxides

2-HC molecule has carbonyl group as in urea and one amino group with a lone electron pair. In the spectral region of 1500-1800 cm^{-1} , two characteristic IR bands are expected: CO stretching vibration $\nu(\text{CO})$ at higher frequencies (1732 cm^{-1}) than that of in urea and NH_2 bending vibration $\delta(\text{NH}_2)$ (1604 cm^{-1}). Similar to urea molecule, when 2-HC coordinates via oxygen to the metal sites, it is expected to enhance double bond character for C-N and C-O bond will have more single-bond character. In this case, red-shift of $\nu(\text{CO})$ is expected as discussed above. When 2-HC interacts with metal cation through nitrogen atom, C-O stretching frequency will increase (i.e. blue-shift) due to the transfer of electron density towards oxygen.

Figure 7.6 shows the spectra of static *in situ* ATR-IR spectroscopic experiment of 2-HC adsorption over single and mixed metal oxides.

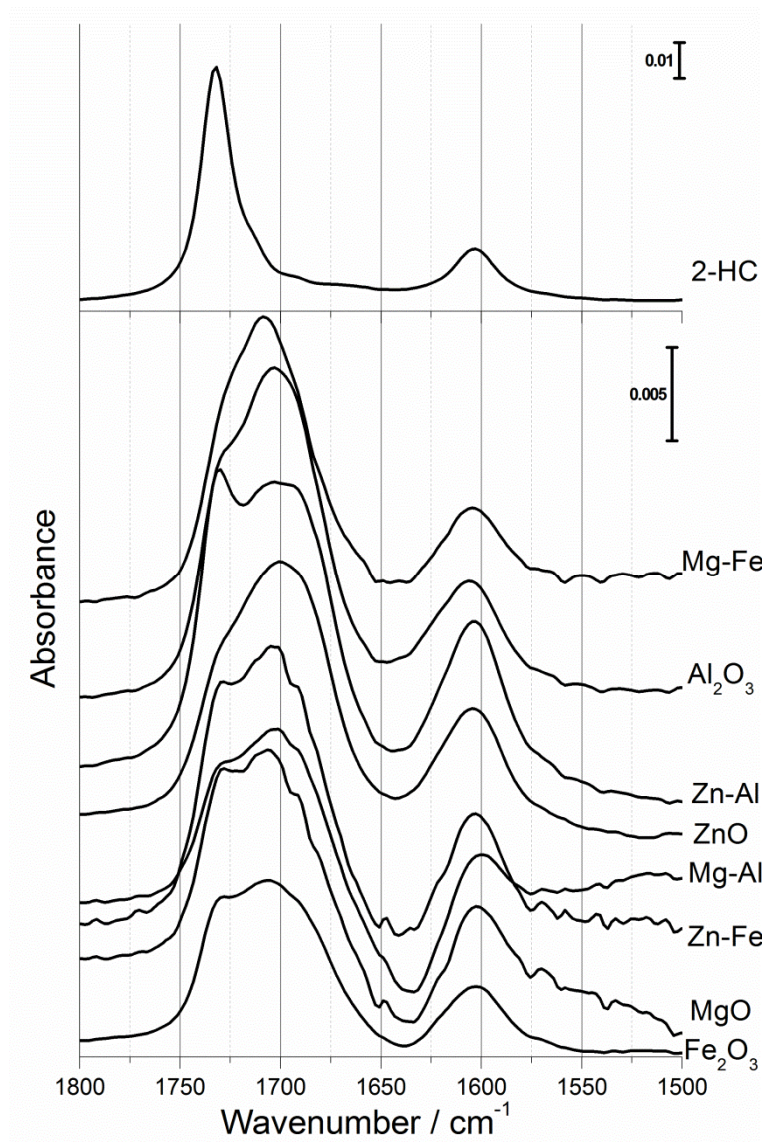
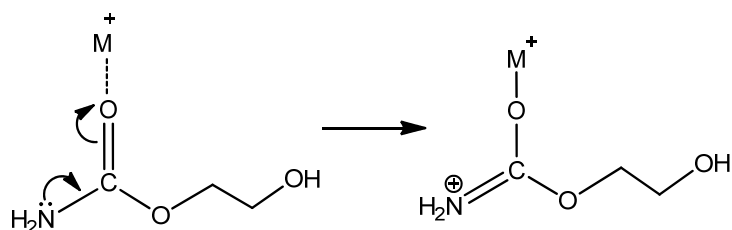


Figure 7.6. ATR-IR spectra of 2-HC in ACN and 2-HC adsorbed over single and mixed metal oxides.

Upon 2-HC adsorption, the band of $\nu(\text{CO})$ was red-shifted to around 1700–1708 cm^{-1} . The band at 1732 cm^{-1} is attributed to residual 2-HC in solution, which was difficult to remove completely. No bands at higher frequencies were found, indicating that 2-HC interacts with all metal oxides in the same manner as urea molecule, i.e. by coordination of oxygen with metal cation.



7.3.2.2 *In situ* transient experiment: 2-HC activation over single and mixed metal oxides

In the same manner as in the transient urea activation study, dynamically varying spectral components over the catalysts induced by the change in 2-HC concentration was studied by transient experiments at 373 K. The major spectra obtained by MCR for the ranges of 2100-2300 cm^{-1} and 1500–1800 cm^{-1} are presented in Figure 7.7 a and b, respectively.

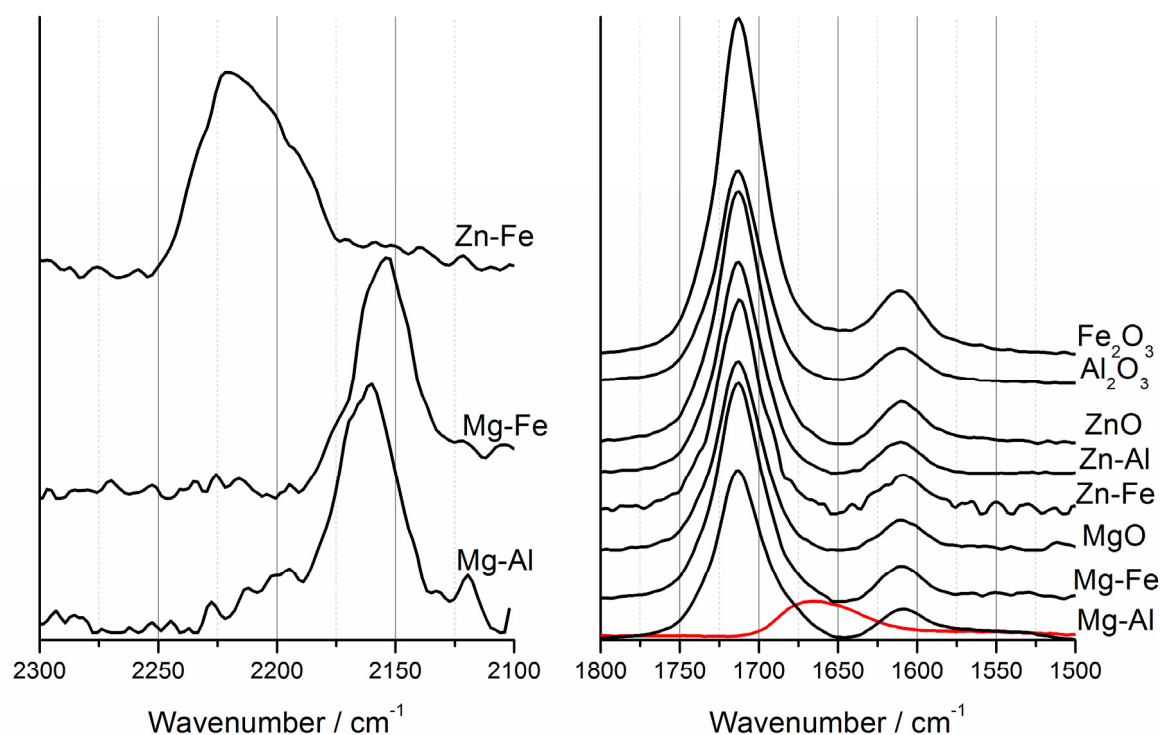


Figure 7.7. The major component spectra obtained by MCR from the transient IR study by alternately passing 2-HC in EG and only EG over single and mixed metal oxides at 373 K.

In the region of 1500–1800 cm^{-1} all samples except Mg-Al displayed characteristic peaks of 2-HC in solution, which is due to simple convectional exchange of 2-HC in the IR cell. Interestingly, Mg-Al presents an additional strong band at around 1673 cm^{-1} . Furthermore, other new spectral features were also found in the region of 2000–2300 cm^{-1} over Mg-Al, Mg-Fe and Zn-Fe. Zn-Fe showed a broad band at ca. 2212 cm^{-1} , whereas Mg-Al and Mg-Fe displayed a sharp band at around 2161 cm^{-1} . The frequency region of the bands is similar to that observed in the transient experiment using urea solution. Therefore, it may be possible that the same species are produced, i.e. oxygen-coordinated cyanate M-OCN over e.g. Zn-containing materials and nitrogen-coordinated M-NCO over Mg-containing materials. However only the few catalysts were able to form these species under the experimental conditions. This may imply that the reaction of 2-HC proceeds much slower than urea conversion (thus consequent low concentration change of the surface species).

To make sure that observed species are indeed the same as in urea activation and to learn more about the new species with band at 1673 cm^{-1} we investigated the component spectra and concentration profiles for Mg-Al and Zn-Fe and the results are presented in Figure 7.8.

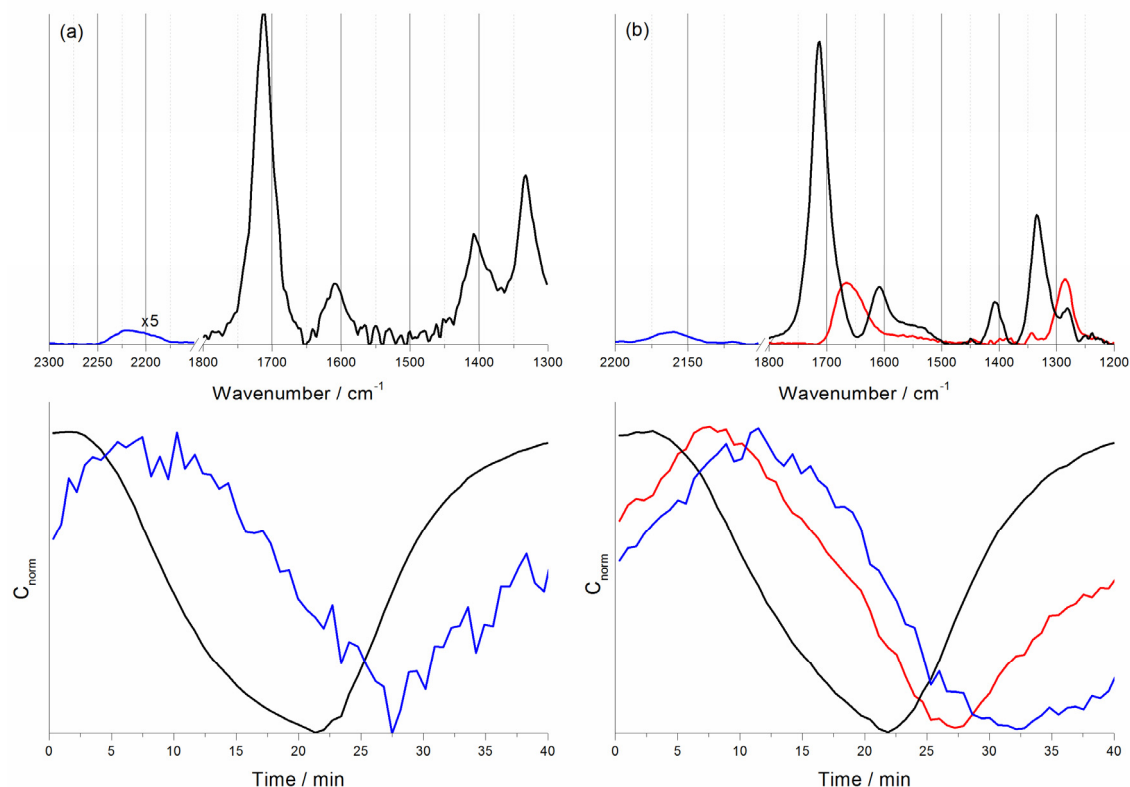
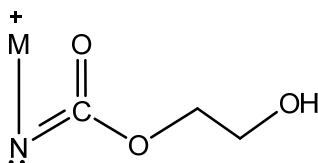


Figure 7.8. MCR processed component spectra and component concentrations extracted from transient *in situ* ATR-IR experiment of 2-HC activation over (a) Zn-Fe and (b) Mg-Al.

When 2-HC is passed over the Zn-Fe surface with periodic concentration change (Figure 7.8, black line (below) with corresponding 2-HC spectrum in black (top)), the broad band at 2212 cm⁻¹ is observed with the delay with respect to 2-HC as it was expected for cyanates species. Hence it is confirmed that 2-HC over Zn-containing oxides can be activated in the same manner as urea, i.e. via carbonyl oxygen coordination to the metal sites, forming cyanate surface species.

A similar delay was observed by passing 2-HC over Mg-Al for the band at 2161 cm⁻¹ which is characteristic of isocyanate species. MCR analysis clarified another chemical component with the band at 1673 cm⁻¹ that was observed only over Mg-Al (Figure 7.8b). It showed a periodic concentration change similar to 2-HC but responding more quickly than that of the isocyanate species. Assuming that initially 2-HC coordinates to the metal sites of the catalyst through oxygen

and that isocyanate species are nitrogen-coordinated, the chemical specie could be an intermediate coordinated either with O or N atom. The vibrational frequency of ca. 1673 cm^{-1} is typically found for carbonyl group of tertiary carbamates [16]. Hence we suggest that the intermediate is N-coordinated and has carbonyl group that gives spectral band at 1673 cm^{-1} as shown below.



It is reasonable that this is the intermediate to form surface isocyanate species. Based on the spectral interpretations given above, possible activation mechanisms of 2-HC over different metal oxides are discussed below.

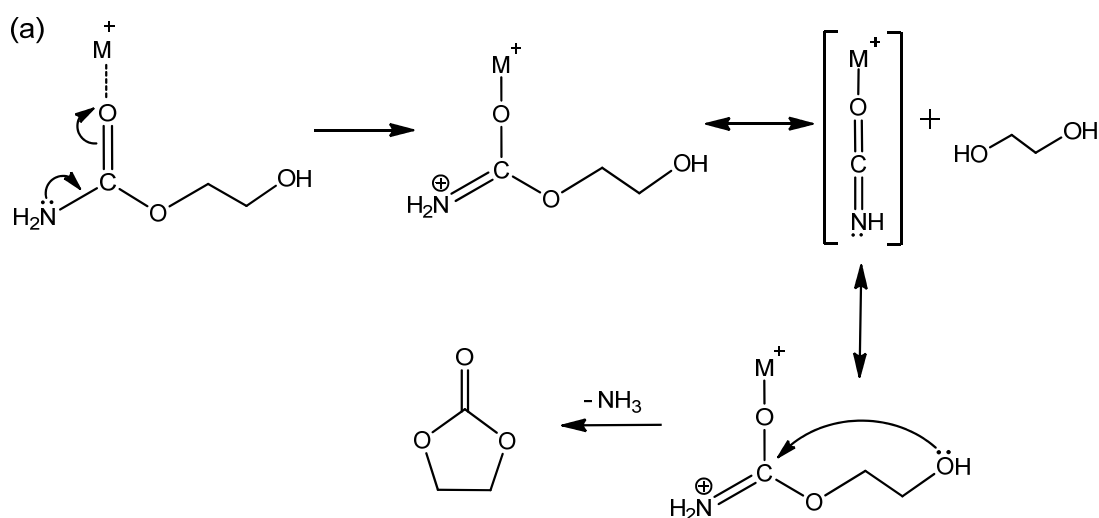
7.3.2.3 Mechanism of 2-HC activation and correlation with acid-base properties of catalyst

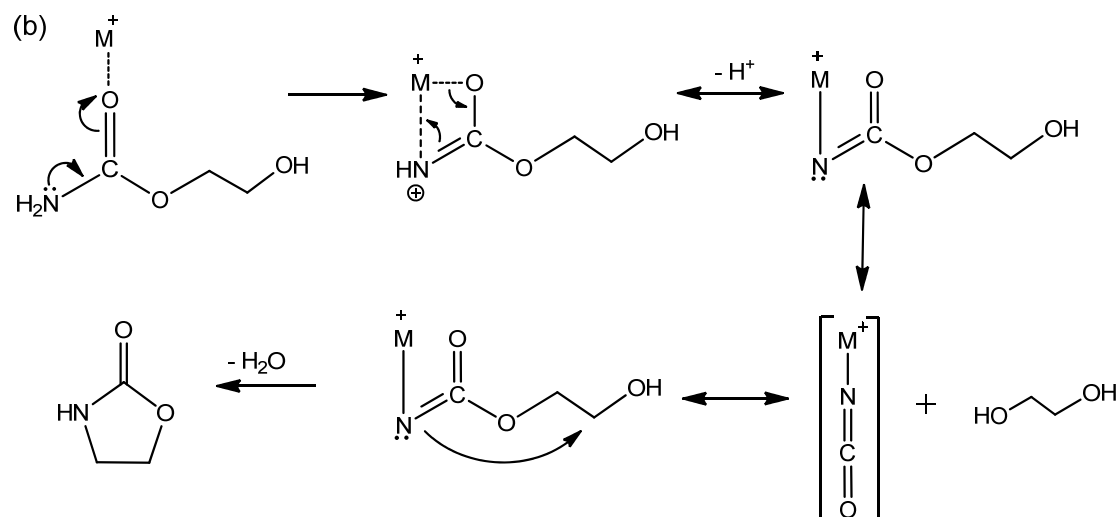
As reported in literature [17] and in Chapter 4, 2-HC reacts over the catalysts to produce two products, EC and 2-Ox, and selectivity of product is dependent on the nature of the catalyst. Basic sites promote the formation of 2-Ox, whereas EC selectivity was higher in the presence of the catalysts with higher acidity.

Static and transient IR experiments of 2-HC interaction with the catalysts revealed that two types of species are formed over the metal oxides of different “families”: O-coordinated cyanates over Zn-Fe, and N-coordinated isocyanates over Mg-Al. Additionally N-coordinated carbamate intermediate was formed over Mg-Al before isocyanate. It is important to highlight that Zn-Fe and Mg-Al are the materials with extremely opposite acid-base properties as evidenced by the EC yield and product selectivity (Chapter 3 and 4). In the presence of Zn-Fe, EC yield was found to be the highest among all catalysts evaluated, whereas Mg-Al showed the lowest EC yield and, notably, almost 50% selectivity to 2-Ox.

Therefore, two favored reaction mechanisms of 2-HC leading to EC over Zn-Fe and leading to 2-Ox over Mg-Al can be proposed (Scheme 7.3 a, b).

The mechanism of 2-HC conversion into EC involves carbonyl oxygen coordination to the metal cation and polarization of electron density causing a positive charge on the nitrogen atom. The obtained fragment is unstable and dissociates into O-coordinated cyanate, which is observed by the transient IR experiment, and EG molecule. The dissociation most likely occurs due to our experimental conditions. That is, in order to favor the fragment conversion, ammonia should be intensively removed to shift the reaction equilibrium towards EC, which is hardly achievable in the transient liquid-flow experiments where there is not gas outlet in the cell. When reaction conditions are favorable for ammonia removal the ring is closed by the nucleophilic attack of oxygen with its lone pair onto the carbon in the carbonyl group, resulting in EC formation.





Scheme 7.3. Mechanism of 2-HC reaction over Zn-Fe mixed oxide (a) and Mg-Al mixed oxide.

2-HC molecule undergoes a different pathway when it interacts with the Mg-Al surface. At the first step oxygen of carbonyl group coordinates to the metal cation causing positive charge on nitrogen. Afterwards due to the high basicity of metal oxide additional bond is formed between cation and positively charged nitrogen. Thus obtained complex appears on the experimental spectra as N-coordinated carbamate. As in case of Zn-Fe, the obtained fragment is equilibrium sensitive and when it is not shifted towards the product (2-Ox) it dissociates to yield isocyanate species that we have observed experimentally. Under the ordinary reaction conditions, the nitrogen atom with lone electron pair would attack carbon connected to the -OH group and close carbon ring by elimination of water to give 2-Ox.

7.4 Conclusions

In situ static and transient ATR-IR study of urea and 2-HC adsorption/activation over single and mixed metal oxides coupled with MCR analysis was performed to investigate activation of the two molecules, produced active species and intermediate fragments, and their dynamic behavior.

Combining ATR-IR spectroscopy and MCR analysis facilitates detection of species directly involved in the reaction, improving signal-to-noise ratio and selectively separates components having different kinetic profiles.

The results of *in situ* ATR-IR static experiments indicate that, upon adsorption over the metal oxide surface, urea and 2-HC form coordination bond through oxygen of carbonyl group to the surface metal sites. Transient *in situ* ATR-IR experiments demonstrated that, depending on the nature of metal oxides, urea decomposes into different active species (O-coordinated cyanate M-OCN and nitrogen coordinated isocyanate M-NCO) that can further react with EG to produce 2-HC.

For the conversion of 2-HC, acid-base properties of catalyst play crucial role since different species were observed for samples with opposite acid-base character. Two possible pathways were suggested for 2-HC reaction. Over mildly acidic Zn-Fe, the reaction leads to the formation of O-coordinated intermediate carbamate and, after nucleophilic attack of oxygen of -OH group and expulsion of ammonia, carbon ring closes with formation of EC. Efficiency of Zn-Fe for EC synthesis is supported by catalytic studies of previous chapters – the highest EC yield is reached in the presence of Zn-Fe. Over basic Mg-Al material, 2-HC undergoes a series of transformation to form N-coordinated intermediate carbamate where nitrogen with lone electron pair closes ring to give 2-Ox and water. The mechanistic insights gained by the ATR-IR spectroscopic study are in excellent agreement with the catalytic studies, giving plausible explanations for the high EC selectivity of Zn-Fe and high 2-Ox selectivity of Mg-Al.

References

1. (a) Fujita, S.-i.; Yamanishi, Y.; Arai, M., *J. Catal.* 2013, 297 (0), 137-141; (b) Li, Q.; Zhao, N.; Wei, W.; Sun, Y., *J. Mol. Catal. A: Chem.* 2007, 270 (1-2), 44-49.
2. Schaber, P. A.; Colson, J.; Higgins, S.; Thielen, D.; Anspach, B.; Brauer, J., *Thermochim. Acta* 2004, 424 (1-2), 131-142.
3. Buergi, T.; Baiker, A., Attenuated total reflection infrared spectroscopy of solid catalysts functioning in the presence of liquid-phase reactants. In *Advances in Catalysis*, 2006; 50, 227-283.
4. Tauler, R., *Chemometr. Intell. Lab.* 1995, 30 (1), 133-146.
5. Mathworks *MATLAB Version 7.10 (R2010a)*.
6. Camo *Unscrambler 10.2*, 2012.
7. Rao, C. N. R., *Chemical Applications of Infrared Spectroscopy*. Academic Press, New York: London, 1964; 577.
8. Penland, R. B.; Mizushima, S.; Curran, C.; Quagliano, J. V., *J. Am. Chem. Soc.* 1957, 79 (7), 1575-1578.
9. (a) Hadži, D.; Kidrič, J.; Knežević, Ž. V.; Barlič, B., *Spectrochim. Acta Mol. Biomol. Spectrosc.* 1976, 32 (4), 693-704; (b) Stewart, J. E., *J. Chem. Phys* 1957, 26 (2), 248-254.
10. (a) Yamaguchi, A.; Miyazawa, T.; Shimanouchi, T.; Mizushima, S., *Spectrochim. Acta* 1957, 10 (2), 170-178; (b) Keuleers, R.; Desseyn, H. O.; Rousseau, B.; Van Alsenoy, C., *J. Phys. Chem. A* 1999, 103 (24), 4621-4630.
11. (a) Laulicht, I.; Pinchas, S.; Petreanu, E.; Samuel, D., *Spectrochim. Acta* 1965, 21 (9), 1487-&; (b) Arenas, J.; Parellad, R., *J. Mol. Struct.* 1971, 10 (2), 253-&; (c) Duncan, J. L., *Spectrochim. Acta Mol. Biomol. Spectrosc.* 1971, A 27 (7), 1197-&; (d) Saito, Y.; Machida, K.; Uno, T., *Spectrochim. Acta Mol. Biomol. Spectrosc.* 1971, A 27 (7), 991-&; (e) Diaz, G.; Campos, M., *Spectrosc. Lett.* 1981, 14 (5), 365-377.

12. (a) Vijay, A.; Sathyanarayana, D. N., *J. Mol. Struct.* 1993, 295, 245-258;
(b) Dixon, D. A.; Matsuzawa, N., *J. Phys. Chem.* 1994, 98 (15), 3967-3977; (c) Spoliti, M.; Pieretti, A.; Bencivenni, L.; Sanna, N., *Electron. J. Theor. Ch.* 1997, 2 (1), 149-159.
13. (a) Stradella, L.; Argentero, M., *Thermochim. Acta* 1993, 219, 315-323;
(b) Chen, J. P.; Isa, K., *J Mass Spectrom Soc Jpn* 1998, 46 (4), 299-303.
14. Zhao, W.; Peng, W.; Wang, D.; Zhao, N.; Li, J.; Xiao, F.; Wei, W.; Sun, Y., *Catal. Commun.* 2009, 10 (5), 655-658.
15. Paul, D. K.; McKee, M. L.; Worley, S. D.; Hoffman, N. W.; Ash, D. H.; Gautney, J., *J. Phys. Chem. A* 1989, 93 (11), 4598-4603.
16. Pinchas, S.; Ben-Ishai, D., *J. Am. Chem. Soc.* 1957, 79 (15), 4099-4104.
17. Li, Q.; Zhang, W.; Zhao, N.; Wei, W.; Sun, Y., *Catal. Today* 2006, 115 (1-4), 111-116.

Chapter 8

Summary and Outlook

8.1 Summary

A series of single and mixed metal oxides, mostly derived from hydrotalcite precursors, consisting of four metal cations (Zn, Mg, Al, Fe) were synthesized with the aim to fine-tune the acid-base properties. These materials were tested in urea transesterification with ethylene glycol (EG) and in every comprising reaction pathway identified in this work. The concentration profiles of the reactants/products and kinetics parameters were obtained by means of IR monitoring using a dip-in ATR-IR probe with subsequent multivariate analysis (MCR). The roles of acidity and basicity at each reaction step have been unambiguously clarified from the relations between acidity and basicity of the materials and the reaction performance or the kinetic information (reaction rate constants).

We could generalize that the reactions accompanying NH_3 release are acid-catalyzed and those accompanying CO_2 or H_2O release are base-catalyzed. The target product (ethylene carbonate, EC) can be formed selectively over acidic sites; however the surface reactivity is hindered when the acidity is too strong by urea adsorption (i.e. site-blocking). The formation of undesired products is catalyzed by basic sites. For these reasons, well balanced amounts of acidic and basic sites are critical in achieving high EC yield with high EC selectivity. Among all the materials tested, Zn-Fe material with 3:1 atomic ratio, showed the best overall performance towards EC production.

Further material optimization showed that increased Fe content in Zn-Fe mixed oxides can enhance EC yield, however EC selectivity decreased due to promoted EC decomposition. Another material science approach attempted to improve EC synthesis was the use of Y-zeolites as support and deposit metal oxide (here ZnO) by the impregnation method. As a result of the acidic nature of zeolites and their high surface area, high EC selectivity was achieved using NaY

supported ZnO catalyst compared to pure ZnO (and also NaY) at similarly high EC yield.

Mechanistic insights into the adsorption and activation processes of urea to produce the intermediate (2-hydroxyethyl carbamate, 2-HC) and of subsequent conversion of 2-HC to EC or the major side product (2-oxazolidone, 2-Ox) over single and mixed metal oxides were gained by static and transient *in situ* ATR-IR spectroscopic study. Urea is activated via the coordination of oxygen of the carbonyl group to the surface metal atom, resulting in distinct active species (cyanate or isocyanate species), depending on the nature of metal oxides. The active species further react with EG to give 2-HC. A similar activation path is possible for 2-HC. Coordination via carbonyl oxygen or via nitrogen of 2-HC to the surface metal sites determines the selectivity to the desired product (EC) or the undesired one (2-Ox). Correlations between the reaction mechanisms and the role of acidity and basicity of the catalysts were identified.

Furthermore, a statistical approach (DoE) was used to optimize the conditions of the reaction where a number of experimental parameters influence the final quantify of interest in a very complex and dependent manner. This study demonstrated the usefulness and effectiveness of DoE for this reaction and suggested the same for complex acid-base catalyzed reactions in general. The DoE approach successfully identified the experimental conditions under which EC productivity and selectivity can be maximized. In summary, this study shows a holistic approach aiming to improve catalytic performance of a complex acid-base reaction based on the combination of rational (using structure-activity relationship) and statistical approaches efficiently maximizing the yield of desired products.

8.2 Outlook

This study clearly shows that both rational (i.e. based on tuning catalyst materials with the feedback of surface active species, acid-base properties and reaction kinetics) and statistical approaches are extremely valuable to improve the yield of desired chemical products in a complex acid-base catalytic reaction. This holistic approach is expected to be usefully applied to other acid-base catalyzed reactions to selectively produce target products at high reaction rates. For urea transesterification of EG, the key factors influencing the reaction in terms of acid-base properties and reaction conditions have been elucidated and the information should be exploited further to find novel catalyst materials giving better yield of EC.

Another important aspect influencing the reaction performance is reaction engineering / reactor design, which has been out of the scope of this thesis work. Since the reactor type may have a strong influence on products distribution, some suggestions are made along this direction.

It was confirmed that urea transesterification with EG consists of two reaction steps, involving first the transesterification reaction to 2-HC, followed by further transesterification to EC with possible formation of side products like 2-Ox. Bearing in mind the stoichiometry of reaction, it is noticed that for 1 mol of EC 2 mols of NH_3 are formed, whereas in the course of 2-Ox production only 1 mol of NH_3 is released. It is therefore expected that formed NH_3 must be efficiently removed in order to shift chemical equilibrium and achieve maximum EC selectivity.

When transesterification of urea with EG is undergone in a closed (no N_2 purging) batch reactor without catalyst, the selectivity to EC falls from 100% to 47% after 6 h of the reaction and 2-Ox selectivity increased up to 37.5%. The EC selectivity in a system with continuous N_2 purging was 86.5%, showing the

importance of NH_3 removal. Figure 8.1 illustrates the reaction performance at 423 K without catalyst in the closed batch reactor.

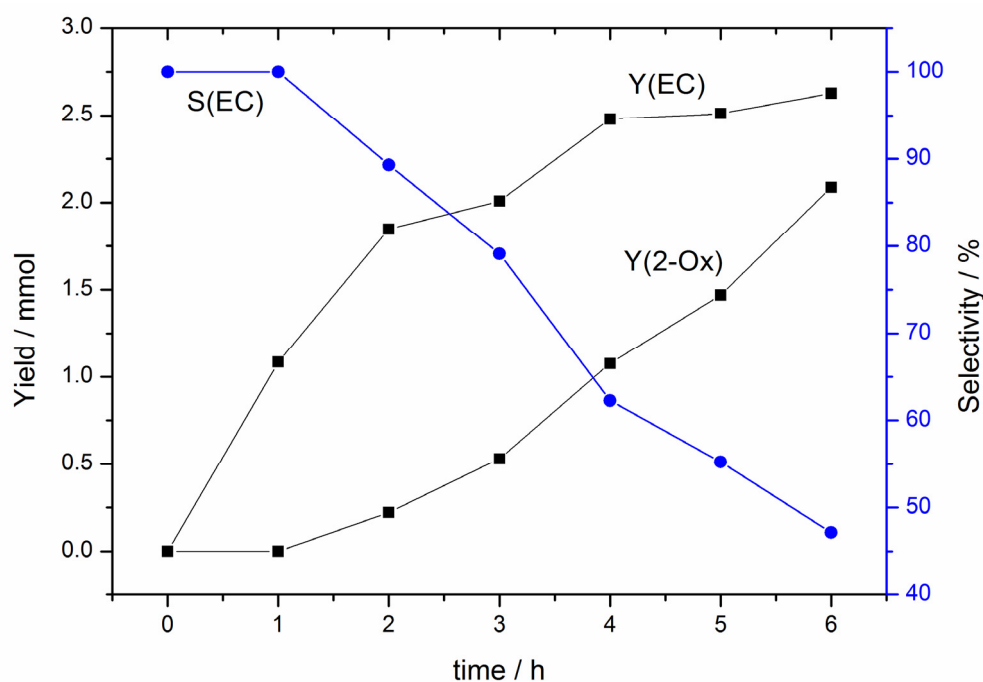


Figure 8.1. Transesterification of urea with EG in an unpurged batch reactor without catalyst.

For reversible reactions continuous removal of products increases the net reaction rate by slowing down the reverse reaction, thereby driving the reaction in a direction that favours a higher yield of product. In this case the semi-batch mode of operation is desirable, since one of the reactants is a gas of limited solubility [1]. It involves the use of a purge stream of inert gas to continuously remove one or more of the products of a reversible reaction. However, semi-batch processes are among the most difficult to analyse from the viewpoint of reactor design because one must deal with an open system operating under non-steady-state conditions. Hence, the mathematical formulation involving differential equations describing dynamic regime is more complex than it would be for the same reaction carried out batchwise.

Another approach to increase reaction efficiency is to employ either several individual tanks in series (battery) or units containing multiple stages

within a single shell (see Figure 8.2). Tanks in series are more expensive but provide more flexibility in use, since they are more readily altered if process requirements change [2].

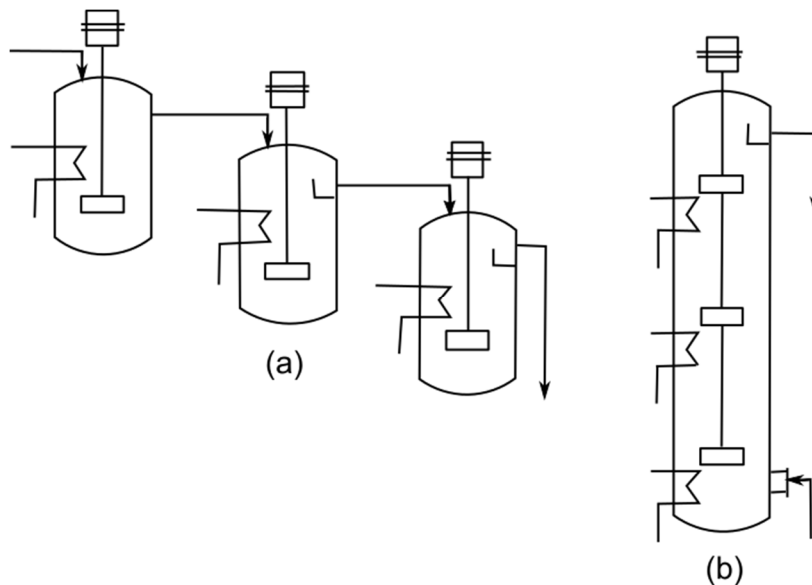


Figure 8.2. Types of CSTRs: (a) three-stage continuous stirred tank reactor battery, (b) three-stage continuous stirred tank battery in a single shell. Adapted from [3].

The main advantage of the continuous stirred-tank reactors is the possibility to improve selectivity to a desired product. They are preferred if a reaction (network) consists of several steps including parallel formation of target and by-products. In our case the consecutive urea transesterification with EG could be divided into two steps. Each step can be performed in a separated tank reactor containing different catalytic materials as shown in Figure 8.3.

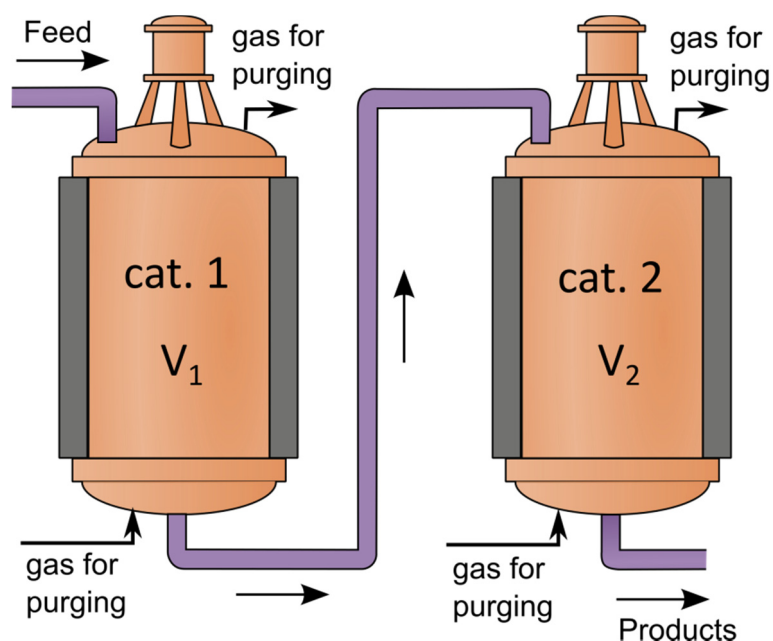


Figure 8.3. 2-step process of transesterification of urea with EG performed in CSTR.

In the first reactor, formation of the intermediate (2-HC) takes place, after that reaction mixture is fed to the second tank where the desired product (EC) is produced. The choice of catalytic materials is important in every step to achieve maximum selectivity and yield of target product as well as intermediate compound. This configuration can become effective once we know the factors influencing the selectivities to produce 2-HC and to produce EC from 2-HC since only an effective catalyst for the particular step can be employed.

During preliminary catalyst screening, we observed that in the presence of zirconium oxide, the reaction intermediate product 2-HC was formed with highest yield and selectivity after 6 h, whereas EC yield was low (which is attributed to blockage of active acid sites as discussed earlier in Chapters 4 and 7). After the reaction, the solution was cooled down, filtered and loaded in the reactor containing Zn-Fe mixed oxide. After carrying out the reaction with Zn-Fe under the same conditions, impressive yield of EC ($47.7 \text{ mmol} \cdot \text{g}_{\text{cat}}^{-1}$) was obtained. This value is almost twice of that obtained in one step-reaction with Zn-Fe ($25.9 \text{ mmol} \cdot \text{g}_{\text{cat}}^{-1}$). We also tested the physical mixture of both Zn-Fe and ZrO_2 in the single

reactor for 12 h. Obtained EC yield was actually notably high but still lower than the case performed in two-steps with ZrO_2 and Zn-Fe separately. The catalytic results are summarized in Table 8.1.

Table 8.1. Catalytic performance of urea transesterification performed in two steps in the presence of ZrO_2 in the first step reaction, Zn-Fe in the second step and in one tank containing the physical mixture of both catalysts.

Catalyst	$Y_{EC} / \text{mmol} \cdot \text{g}_{\text{cat}}^{-1}$	$Y_{2-HC} / \text{mmol} \cdot \text{g}_{\text{cat}}^{-1}$	$S_{EC} / \%$
ZrO_2 - 1st step (6 h)	8.9	41.2	94.5
Zn_3-Fe_1 after ZrO_2 - 2nd step (6 h)	47.7	28.7	88.7
Zn_3-Fe_1 and ZrO_2 – one step (12 h)	30.3	6.9	88.5

Additionally, since the volume of reaction mixture decreases by releasing ammonia, second reactor could be designed accordingly in order to minimize capital costs.

References

1. (a) Mojet, B. L.; Ebbesen, S. D.; Lefferts, L., *Chem. Soc. Rev.* 2010, 39 (12), 4643-4655; (b) Davis, M. E.; Davis, R. J., *Fundamentals of Chemical Reaction Engineering*. Dover Publications: 2013.
2. Hill, C. G., *An introduction to chemical engineering kinetics & reactor design*. Wiley: 1977.
3. Couper, J. R.; Penney, W. R.; Fair, J. R.; Walas, S. M., *Chemical Process Equipment (Revised Second Edition)* Elsevier: 2010.

Appendix

Supplementary Information of Chapter 4

Kintaic modelling of urea transesterification with EG

Commonly, time-dependent concentration profiles of a chemical reaction can be modeled by a set of time-dependent ordinary differential equations in the form of $\sum_i \frac{d}{dt} C_i(t) = f(t, C_i(t), k)$ where $C_i(t)$ represents the concentrations of chemical species i at time t .

Assuming the consecutive and parallel character of urea transesterification reaction and the above kinetic studies, we have set up a set of the rate equations (A1-A4):

$$\frac{dC_{\text{urea}}}{dt} = -k_{\text{urea}} \cdot C_{\text{urea}}^2 \quad (\text{A1})$$

$$\frac{dC_{2\text{-HC}}}{dt} = k_{\text{urea}} \cdot C_{\text{urea}}^2 - k_{2\text{-HC}} \cdot C_{2\text{-HC}} \quad (\text{A2})$$

$$\frac{dC_{\text{EC}}}{dt} = k_{2\text{-HC} \rightarrow \text{EC}} \cdot C_{2\text{-HC}} - k_{\text{EC}} \cdot C_{\text{EC}} \quad (\text{A3})$$

$$\frac{dC_{2\text{-Ox}}}{dt} = k_{2\text{-HC} \rightarrow 2\text{-Ox}} \cdot C_{2\text{-HC}} - k_{2\text{-Ox}} \cdot C_{2\text{-Ox}} \quad (\text{A4})$$

After solving the differential equations simultaneously, concentration profiles of all four species can be obtained. An example of the solution for Zn-Fe (using the obtained k values obtained from the above studies) using the above equations is shown in Figure A1.

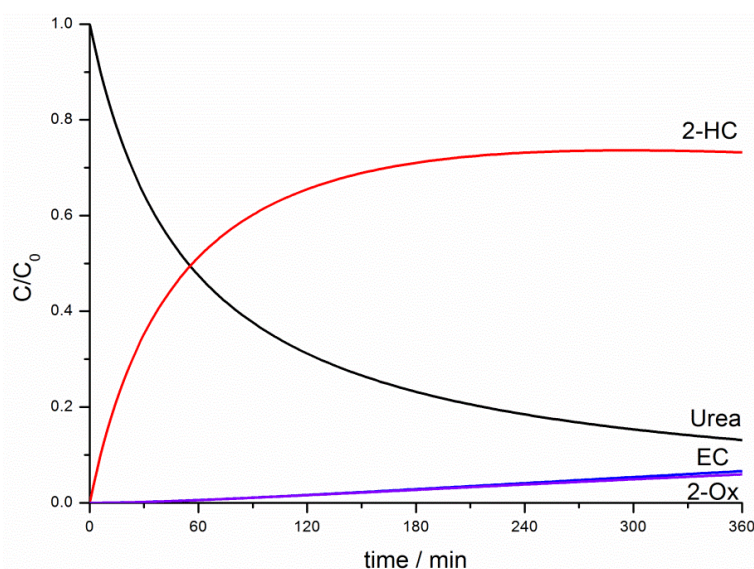


Figure A1. Calculated concentration profiles in urea transesterification for Zn-Fe based on k values obtained (Chapter 4) from the comprising reactions.

Based on the set of differential equations, the kinetic rate constants can be fitted to the concentration profiles observed experimentally. We minimized the sum of squared errors to find rate constants from obtained kinetic model.

Prior to fitting, urea concentration was normalized by the initial concentration; $C_{\text{urea},n} = \frac{C_{\text{urea}}}{C_{\text{urea},0}}$. Concentrations of EC and 2-Ox obtained after MCR analysis were normalized using the final experimental concentrations (Formula A5):

$$C(t)_{i,n} = \frac{C(t)_i}{C_{i,\text{final}}} \cdot \frac{C_{i,\text{final}}^{\text{exp}}}{\sum C_{i,\text{final}}^{\text{exp}}} (1 - C_{\text{urea},n}^{\text{final}}) \quad (\text{A5})$$

where

$$\sum C_{i,\text{final}}^{\text{exp}} = C_{2\text{-HC},\text{final}}^{\text{exp}} + C_{\text{EC},\text{final}}^{\text{exp}} + C_{2\text{-Ox},\text{final}}^{\text{exp}} + C_{\text{DEG},\text{final}}^{\text{exp}} + C_{\text{TEA},\text{final}}^{\text{exp}} + C_{3\text{-(2-EtOH)-2-Ox},\text{final}}^{\text{exp}}$$

The concentration profile of 2-HC was calculated by subtracting normalized concentrations of other products found in the IR monitoring (Formula A6):

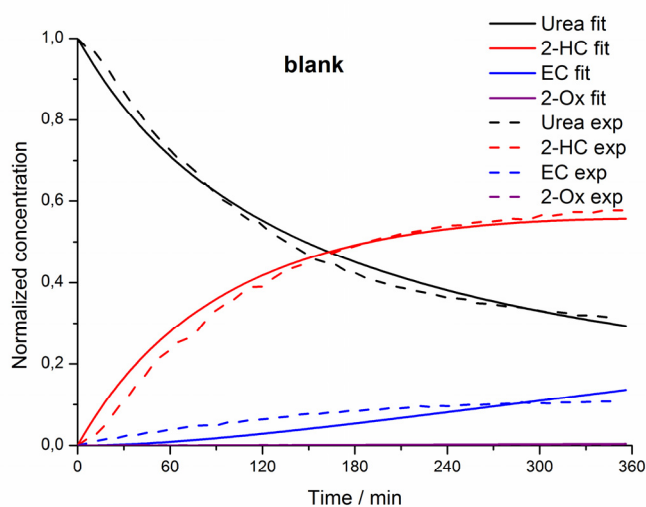
$$C_{2\text{-HC},n} = 1 - C_{\text{urea},n} - C_{\text{EC},n} - C_{2\text{-Ox},n}. \quad (\text{A6})$$

Thus obtained reaction rate constants of overall reactions (i.e. by means of fitting) are compared with the rate constants obtained from the kinetic studies of reaction steps ("single reaction", Table A1). The major differences were observed for the k values of the reaction of 2-HC. This implies that the reaction rate of 2-HC is significantly different when the reaction is initiated with 2-HC itself or starting from urea. The results have been interpreted as selective blocking of acidic sites by urea and promoted conversion of 2-HC by basic sites. The latter can lead to higher rate in conversion, but this does not necessarily impact the catalytic performance positively depending on promoted reaction pathways as discussed in the main text.

Table A1. Comparison of reaction rate constants. The rate constants obtained by fitting are shown with the range of 95% confidence interval.

Catalyst	$k'_{\text{urea}} \cdot 10^{-3}/\text{min}^{-1}$		$k_{2\text{-HC}} \cdot 10^{-3}/\text{min}^{-1}$		$k_{\text{EC}} \cdot 10^{-3}/\text{min}^{-1}$		$k_{2\text{-Ox}} \cdot 10^{-3}/\text{min}^{-1}$	
	Single reaction	Overall reaction	Single reaction	Overall reaction	Single reaction	Overall reaction	Single reaction	Overall reaction
blank	7.5	6.7±0.1	0.2	1.0±0.1	0.3	0.5±0.3	0.4	0
Al ₂ O ₃	8.9	8.6±0.2	0.4	1.1±0.1	0.5	0	0.5	0
ZnO	14.6	10.5±0.4	1.3	13.9±0.8	0.5	1.6±0.3	0.7	3.2±1.1
MgO	15.4	13.6±0.4	2.4	7.1±0.2	1.6	1.0±0.1	0.8	4.0±1.7
Fe ₂ O ₃	10.8	9.8±0.1	0.5	1.1±0.1	2.4	2.2±0.5	1.5	0
Zn-Al	16.9	13.5±0.5	0.8	8.2±0.3	0.4	1.5±0.2	0.7	4.0±2.0
Zn-Fe	18.4	14.8±0.5	0.6	10.4±0.4	0.4	1.6±0.2	0.7	0
Mg-Al	14.4	11.7±0.7	2.4	6.2±0.4	2.3	6.7±2.3	0.8	0.7±0.5
Mg-Fe	19.4	17.9±0.8	2.4	18.2±1.1	1.7	1.5±0.2	0.6	2.6±0.8

The normalized concentration profiles obtained by MCR analysis and fitted profiles are compared in Figure A2.



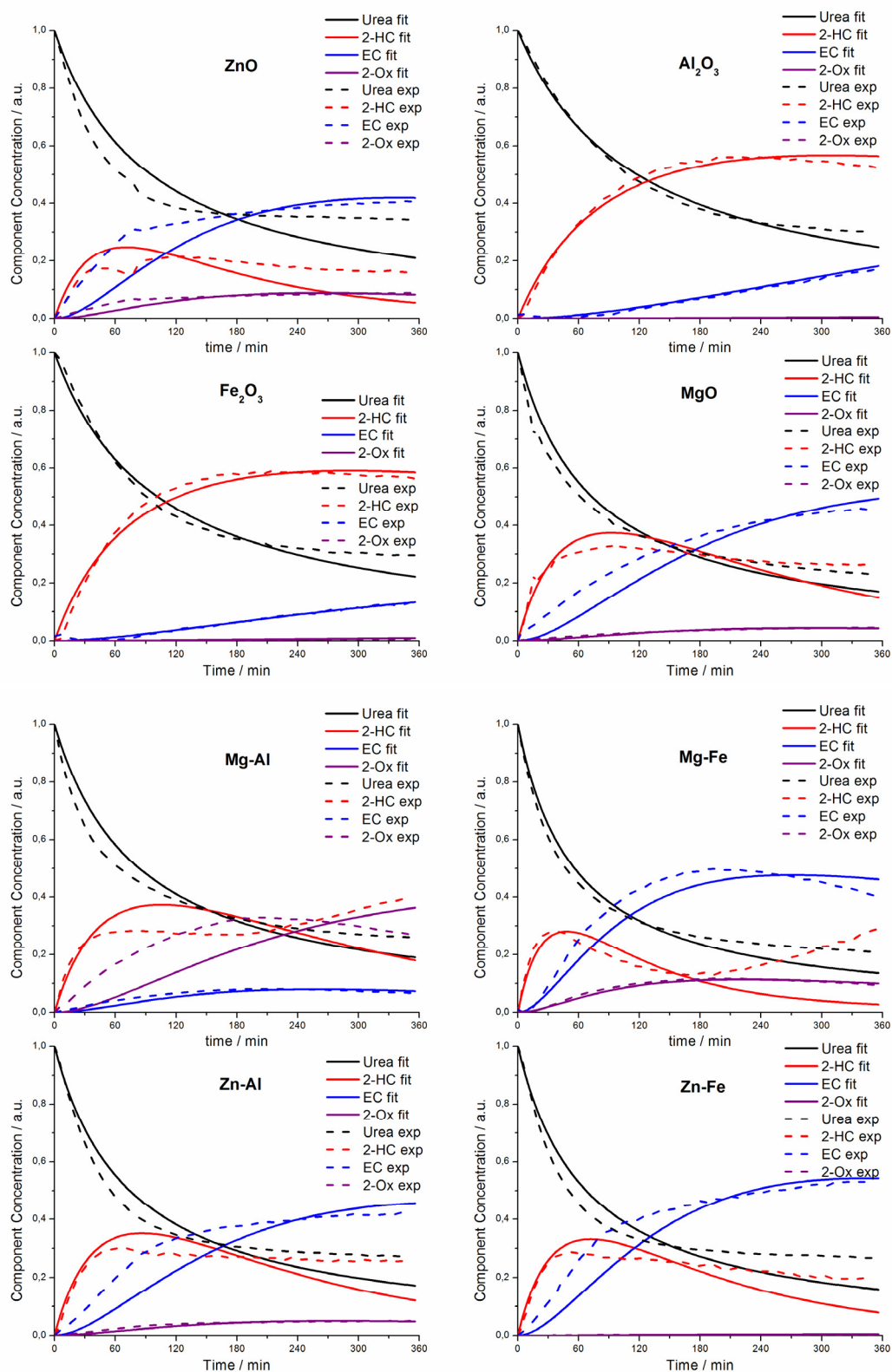


Figure A2. Comparison of experimental and fitted concentration profiles.

Publications and Conference Contributions

Journal publications

Rational and Statistical Approaches in Enhancing the Yield of Ethylene Carbonate in Urea Transesterification with Ethylene Glycol over Metal Oxides

Dina Fakhrnasova, Ricardo J. Chimentão, Francisco Medina, and Atsushi Urakawa

ACS Catalysis, 2015, 5, pp 6284–6295

Static and Transient *In situ* ATR-IR Study of Catalytic Activation Mechanisms in Urea Transesterification with Ethylene Glycol

Manuscript in preparation

Dina Fakhrnasova, Francisco Medina, and Atsushi Urakawa

Conference contributions

7th International Conference on Environmental Catalysis, Lyon (France), 2-6 September 2012

Oral presentation contribution: *“Transesterification of urea with ethylene glycol to ethylene carbonate over mixed oxides derived from hydrotalcites”*

D. Fakhrnasova, R. J. Chimentão, A. Urakawa, F. Medina

The Seventh Tokyo Conference on Advanced Catalytic Science and Technology (TOCAT7), Kyoto, Japan, 1-6 June 2014

Poster contribution: *“In situ spectroscopic and kinetic elucidation of the function of acid-base sites in urea transesterification with ethylene glycol over mixed oxides”*

Dina Fakhrnasova, Ricardo Chimentão, Francisco Medina, Atsushi Urakawa

Curriculum Vitae

Dina Fakhnasova

E-mail	d.fahnasova@gmail.com
Date of birth	October 3, 1987
Place of birth	Glazov, Russia
Nationality	Russian

Education

02.2011 – 02.2016	PhD in Chemical Engineering Institute of Chemical Research of Catalonia (ICIQ) / Chemical Engineering Department, University Rovira i Virgili, Tarragona, Spain <u>PhD topic:</u> <i>Rational and statistical approaches in enhancing yield of ethylene carbonate in urea transesterification with ethylene glycol</i>
09.2004 – 02.2010	Diploma Engineer D. Mendeleev University of Chemical Technology of Russia, Moscow, Russia Department of Technology of Organic Substances and Chemical Pharmaceutical Compounds Specialty – Chemical Technology of Natural Energy Sources and Carbon Materials <u>Diploma work:</u> <i>Preparation of catalytic membranes for dehydrogenation of propane by sol-gel method</i>

Research Activities

- 09.2008 – 06.2009 Research work: *Mixed Conducting Ceramic Membranes for Oxygen Separation*
A. A. Baikov Institute of Metallurgy and Material Science (IMET), Russian Academy of Science (RAS)
- 09.2007 – 06.2008 Research work: *Laboratory methods for analysis of gaseous products of coking*
Moscow Coke and Gas Plant (Mechel group)

Work Experience

- 04.2010 – 02.2011 **Lead Development Sales Manager**
Department of Raw Materials for Household Chemicals
Unived LTD. Moscow, Russia
- 07.2015 - Current **Lead Process Engineer**
Department of Engineering Solutions
The Dow Chemical Company, Schkopau, Germany

UNIVERSITAT ROVIRA I VIRGILI
Rational and Statistical Approaches in Enhancing Yield
Of Ethylene Carbonate in Urea Transesterification with Ethylene Glycol
Dina Fakhrnasova